Summer 2001

Transverse Variability of the Flow and Density in Inlets of Southern Chile

Mario Arturo Cáceres Muñoz
Old Dominion University

TRANSVERSE VARIABILITY OF THE FLOW AND DENSITY IN

INLETS OF SOUTHERN CHILE

by

Mario Arturo Cáceres Muñoz
B.S. Dec. 1982, Naval Polytechnical Academy, Chile
M.S. Oceanography, Dec. 1989, University of Concepcion, Chile.

A Dissertation submitted to the Faculty of
Old Dominion University in Partial Fulfillment of the
Requirement for the Degree of

DOCTOR OF PHILOSOPHY

OCEANOGRAPHY

OLD DOMINION UNIVERSITY
August 2001

Approved by :

Arnoldo Valle-Levinson (Director)

Larry P. Atkinson (Member)

Thomas C. Royer (Member)

Kuo-Chuin Wong (Member)

ABSTRACT

TRANSVERSE VARIABILITY OF THE FLOW AND DENSITY IN INLETS OF
SOUTHERN CHILE

Mario A. Cáceres
Old Dominion University, 2001
Director: Dr. Arnoldo Valle-Levinson

Measurements of velocity and density profiles were made to describe the flow transverse structure in three inlets of southern Chile. The inlets show marked differences in their transverse dynamics in response to external forcing. In Aysen Fjord (45.2° S) the mean flow showed a three layer structure that was consistent with up-fjord wind-induced exchange, while in Chacao Channel (41.8° S), the mean flow exhibited predominantly a lateral structure that featured sharp velocity shears. In both cases, a bank in the center of the sections seemed to play an important role in shaping the mean flows. In Ventisquero Sound (44.4° S), the presence of a sill/contraction combination determined differences in the residual circulation on both sides of the contraction. The subtidal transverse momentum balance in Aysen alternates from quasigeostrophic during calm winds to a frictional layer and quasigeostrophic interior during periods of wind forcing. In Chacao, both advective accelerations and friction seem to play a major role in the transverse dynamics. In Ventisquero Sound, advective accelerations were dominant to the north of the contraction and over the sill. Typical nondimensional groups such as Rossby number, Ekman number, Reynolds number and Richardson number revealed dynamic similarities and differences among the different systems.

To my wife María Teresa Sánchez, with love

ACKNOWLEDGMENTS

There are many people to whom I owe thanks for their support, guidance and friendship during this endeavor. This project contains the contributions of my family, academic associates, research partners and Chilean Navy shipmates. First, I am very grateful to my wife María Teresa. Her support, understanding and encouragement, along with the inspirations from María Fernanda, José Tomás, María Jesús and Javier Ignacio, truly sustained this project. I cannot express in words the heartfelt gratitude I have for all the love, help and comfort that María Teresa has given me during the hard and good times. I am also most thankful to my advisor, Dr. Arnoldo Valle-Levinson, for introducing me to the field of physics of estuaries, for his guidance, patience and flexibility, and for making me feel like a colleague and a friend. I also thank my committee members, Drs. Larry Atkinson, Tom Royer and Kuo Wong for their help and comments. I would like to specially thank Larry Atkinson for his guidance, support and encouragement in this project. I am also thankful to the members of the faculty and staff for their support and help. I would like to give special thanks to the former Directors of the Hydrographic and Oceanographic Service of the Chilean Navy, Captains Rafael Mackay and Hugo Gorziglia, for supporting and believing in my success. Special thanks to Commander Rodrigo Núñez, who had an interest in my education at the Center for Coastal Physical Oceanography. Without his help and encouragement, this achievement would not have been possible. I want to thank my friends and classmates that brought me smiles and gave me moral support along the way.

TABLE OF CONTENTS

Section

LIST OF TABLES

LIST OF FIGURES

LIST OF FIGURES (continued)

LIST OF FIGURES (continued)

LIST OF FIGURES (continued)

LIST OF FIGURES (continued)

INTRODUCTION

1.1 Background

Fjords are high latitude estuaries that are usually long relative to their width, relatively steep sided and deep, normally possess one or more sills, and usually feature a river discharging at their most upstream reaches (their head). The study of fjords and inland seas is challenging because of the different forcings that affect their hydrodynamics. The variability of their coastline geometry, the amount and location of the freshwater inflow, the external conditions of wind and tide and also the frequent influence of the nonlinear processes complicate the understanding of these systems. In addition, the presence of sills and bumps plays a relevant role in many fjord problems. In the fjords and Inland Sea of southern Chile, basic knowledge such as the dynamic balance that determines the flows remains undescribed. As in other types of estuaries, studies in fjords have focused particularly on the understanding of the longitudinal and vertical variability of the flow, while the transverse distributions have received relatively little attention. The works of *Freeland et al.* [1980] and *Farmer and Freeland* [1983] provide extensive reviews and abundant references about the circulation in fjords, confirming that the preferential interest has been given to the longitudinal and vertical dimensions.

The hydrodynamics of fjords are usually assumed to have an along-fjord momentum balance in which the pressure gradient is balanced by friction or advective accelerations (in constrictions), and a lateral geostrophic balance, i.e., between Coriolis accelerations and pressure gradient accelerations [*Dyer*, 1997].

The *Journal of Geophysical Research* was used as the Journal model

Modifications to the geostrophic lateral balance in a shallow estuary have been demonstrated by *Dyer* [1977], when centrifugal forces and wind stresses have become be important. In fjords, the geostrophic approximation has been demonstrated to be valid in fjords of British Columbia [*Cameron*, 1951] and in Juan de Fuca Strait [*Tully*, 1958], but more intensive and extensive work is required to understand the mechanisms modifying this balance in deep estuaries. The purpose of this study is to describe the basic properties of the transverse variability of flow in three regions of the Chilean Inland Sea. The relative contribution of the terms in the across-channel momentum balance is assessed in the cross-sections. Typical nondimensional groups such as Rossby number, Ekman number, Reynolds number and Richardson number are used to establish dynamic similarities and differences among the different systems.

1.2 Geographical area of interest

The general area of interest includes the coastal ocean, fjord and inlets of southern Chile between 41° S and 47° S (Figure 1). The tidal regime throughout the Inland Sea is mixed, predominantly semidiurnal. The tidal range in this area is variable. On the adjacent continental shelf and in the Inland Sea to the south of Guafo Mouth tidal ranges may reach ~2 m, but in the Gulf of Ancud and Reloncavi Sound tidal ranges are about ~6.5 m. The reason for this amplification is still under investigation, but it may be partially explained by resonant effects on the tide that enters through Guafo Mouth and propagates northward, along the east side of Chiloe Island up to Ancud Gulf. This hypothesis is supported by tidal gauge records showing a continuous increase of tidal ranges from Guafo Mouth (~2 m) to Ancud Gulf (~7 m).
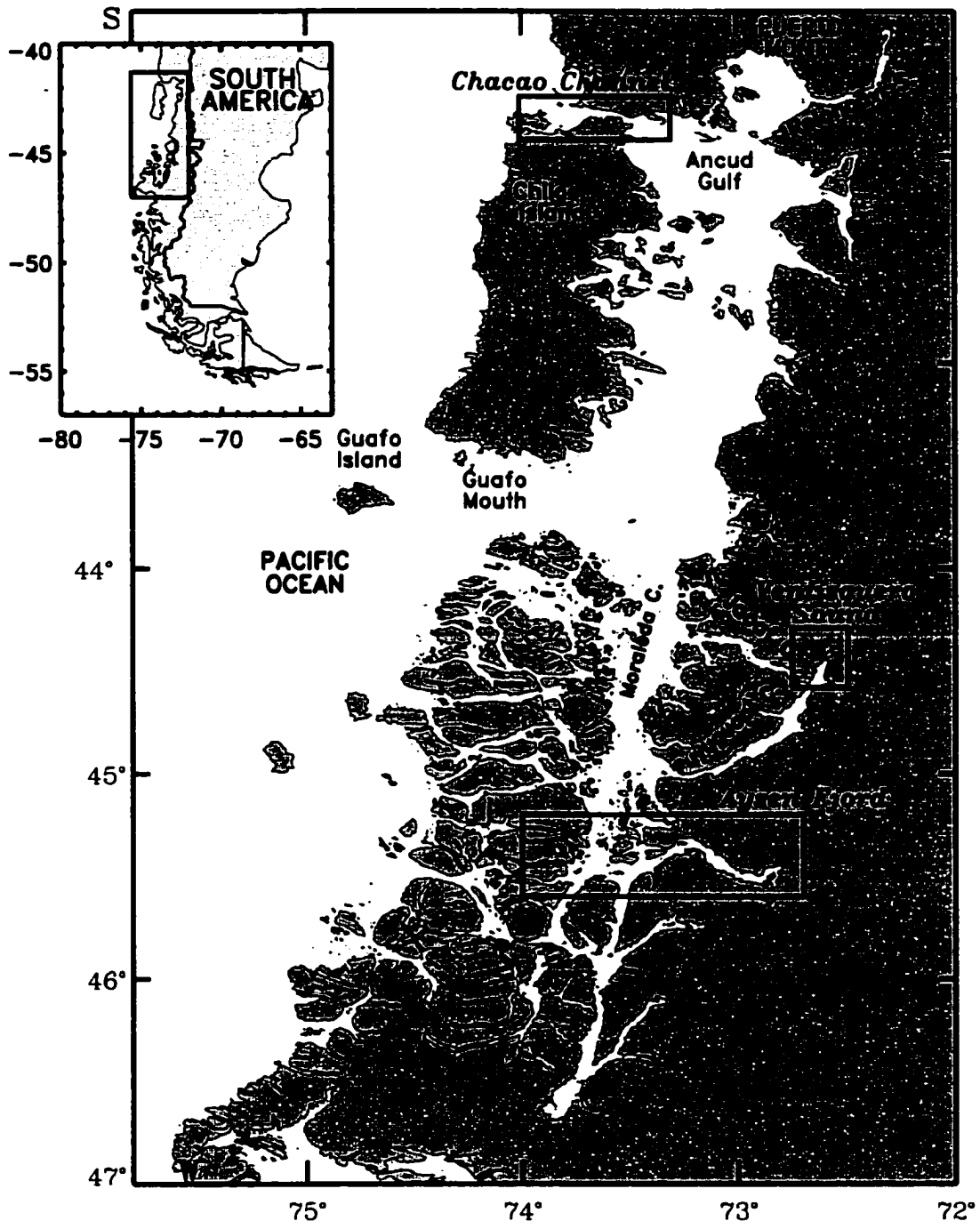
Figure 1. General study area. Boxes indicate regions of interest: Chacao Channel, Ventisquero Sound and Aysen Fjord

Fresh water inputs are provided by many rivers entering the Inland Sea along the eastern coast where they drain from the Andes mountain range. According to *Niemeyer and Cereceda* [1984], the largest average annual discharges in the region have been reported for rivers feeding to Reloncavi Fjord (~900 m^3/s) and Aysen Fjord (~620 m^3/s). The annual regime of freshwater discharges in the region exhibits two annual peaks corresponding to the autumn increase in precipitation (April-June) and the summer melting of snow (October-February). The typical depths in the Inland Sea range from 100 to 200 m. Most of the western border of the archipelago between 45° S to 47° S (south of Guafo Mouth) exhibits a moraine of about 60 m depth, which limits the exchange of estuarine waters with saline waters from the shelf. Hence the two main locations for exchanges between saline and estuarine waters are the Guafo Mouth and Chacao Channel. Owing to the effect of the freshwater inputs in the eastern side, there is a well defined pycnocline shallower than 15 m in most of the fjords with a river in its head [*Silva et al.*, 1995, *Silva et al.*, 1997].

On the basis of data obtained at Guafo Island (Figure 1a) by the Meteorological Service of the Chilean Navy (SMA), the wind regime for this region of the Inland Sea is dominated by southerly and southwesterly winds during spring and summer (Oct-Mar), and northerly and northwesterly winds during fall and winter (April-Sept). The mean total annual precipitation (1968-1999) for stations around the study area fluctuates between 1100 and 2100 mm (SMA, pers. comm.)

The first systematic study of the hydrography of the deep Chilean estuaries and fjords was done by *Pickard* [1971]. He described a survey that consisted of 175 stations in 32

inlets (fjords) and the adjacent outside passages. Sampling was done in March 1970 (early

Fall). His main conclusion was that owing to the lack of shallow sills no stagnant waters

were observed. He recommended investigations on seasonal variability, river runoff, and

precipitation. More than 20 years later, during October 1995, a similar oceanographic

cruise (named Cimar Fiordo 1) was carried out by the Chilean Oceanographic Committee,

in the inland water between Puerto Montt and San Rafael Lagoon. A circulation pattern

based on hydrographic casts was hypothesized. During 1998 a second cruise with similar

characteristics, named Cimar Fiordo 4, was carried out in the region. Its findings provided

a better understanding of the Cimar Fiordo 1 results.

1.3 Specific regions of interest

Three regions of the Inland Sea have been explored in joint CCPO (Center for

Coastal Physical Oceanography)-Chilean Institution field work. The information derived

from these efforts shall be essential to the objectives of this study. The first region is

Aysen Sound, the second region is Chacao Channel, at the northern communication

between the Inland Sea and the continental shelf, and the third one is Ventisquero Sound

(Figure 1). These three regions were chosen separately, for different reasons, at the time

of sampling, bu are put into a similar context in this work.

Region 1: Aysen Sound

Aysen Sound is a fjord-like inlet with a length of about 65 km measured between its

mouth and its head, and an average width of about 6.5 km. Its average depth is 217 m,

and exhibits a sill of about 125 m depth in the region of its mouth. The orientation of the

fjord in its first 30 km from the mouth is in the SW-NE direction. The orientation changes

in the following 25 km to the NW-SE direction, and to the SW-NE direction in the last 10

km (toward the head). As Aysen Sound is glacially carved and has a fjord-like

morphology, henceforth it will be referred to as Aysen Fjord. The main forcing agents in

the vicinity of the mouth of the fjord are postulated to be tidal forcing, local wind stress

and river discharge. Mean tidal ranges are about 2.5 m in the region of the mouth [*Fierro*

et al., 1999] and 2.2 m inside Aysen Fjord [*SHOA*, 1993b].

Region 2: Chacao Channel

Located at the northernmost part of the region of fjords in the Chilean Inland Sea,

this channel represents one of the two direct openings between the ocean and the Inland

Sea, the other being Guafo Mouth. Chacao Channel connects the open ocean with the

Gulf of Ancud in the east-west direction and is approximately 40 km long with an

average width of 4 km. Tidal currents of about 4 m/s are customarily observed in this

channel. At its narrowest portion (2.2 km) the bathymetry exhibits a prominent pinnacle

of 20 m depth placed at the center. This pinnacle separates the flow in two branches. One

over the northern and deeper area (120 m), and the other one over the southern and

shallower area (70 m). Flow measurements have confirmed the presence of enhanced

quarter-diurnal and sixth-diurnal overtides over the southern branch, while CTD

(Conductivity, Temperature and Depth) casts have shown a mixed water column. The

differences in tidal ranges reported from tidal gauge records in both extremes of the

channel [*SHOA*,1993a], ~2 m over the adjacent shelf region and 5-7 m in the Gulf of

Ancud, explain the strong tidal currents observed.

Region 3: Ventisquero Sound

Ventisquero Sound is a fjord-like inlet located in the region of the Chilean Inland

Sea, and it is part of the northernmost end of Puyuguapi Channel (Figure 1). Typical tidal

ranges are around 1 m [*Valle-Levinson et al.*, 2001a]. The geomorphology in Galvarino

Pass, a pass connecting the northern and southern regions of Ventisquero Sound,

represents a coastline contraction of about 90%, decreasing from 2000 m to 200 m in just

1500 m in the along-channel direction [*Valle-Levinson et al.*, 2001a]. Depth varies from

40 m on the norhtern side of the pass to 10 m at the shallowest portion of the sill to 80 m

south of the pass. The bottom slopes by roughly 30%. Freshwater inputs to Ventisquero

Sound are provided mainly by two ungauged small streams discharging in the northern

side of the contraction. The interaction of the tidal currents with the sill/contraction

combination in the region of the pass should make advective accelerations important for

the momentum balance.

1.4 Data availability

Current measurements and vertical profiles of temperature and salinity already

obtained in the three regions indicated above provides the basis for the analysis of the

research questions indicated below. In the three systems the current data collection was

made using an Acoustical Doppler Profiler (ADCP) and a Global Positioning System

(GPS) interfaced to a laptop computer. The ADCP was mounted on a catamaran ~1.2 m

long, which was towed from the starboard side of a local boat at speeds between 2 and 2.5

m/s. Velocity profiles obtained in this way traversed the inlets under study for at least 8

times during one complete semidiurnal tidal cycle.

The semidiurnal tide is separated from the subtidal signal of the observed flow components using sinusoidal least squares regression analysis. After determining the subtidal flow, the relative magnitude of the terms reliably estimated in the across-channel and along channel momentum balance will be scaled to assess their relative contribution to the corresponding momentum balance. Dimensionless analysis will be used to assess dynamic similarities among the three systems.

1.5 Research questions

The transverse dimension

In analytic studies of estuarine systems, it has been common practice to assume that lateral variations in the flow are small. Estuarine investigations have typically focused on longitudinal and vertical features of the circulation and parameter distribution. It has been only recently that cross-sectional variabilities have shown to be equally significant [Wong, 1994]. The idea that flows are not constant across the cross-section, and that this is likely to be the norm rather than the exception is becoming prevalent. Thus the laterally homogeneous assumption is not realistic since the magnitude of the circulation may be unevenly distributed across the estuary [*Dyer*, 1977, 1997].

The importance of the transverse dimension is exemplified by the fact that lateral density gradients may maintain net across-channel flow, and across-channel differences in velocity and dissolved/suspended material concentrations may have a large effect on material longitudinal fluxes [*Kjerfve et al.*, 1981]

In this study I explore the relative contribution with the terms in the across-estuary momentum balance, making some comparison with the terms in the along-estuary

momentum balance. The terms in the across and along-channel momentum balance that may be reliably estimated from the sectional distributions will be identified. These estimates are oriented to answer the following questions

- What are the contributions of the terms in the across-channel momentum balance to the lateral dynamics?

- Are the magnitudes of the terms in the along-estuary momentum balance comparable to those of the across-estuary channel momentum balance?

In order to further explore the latter question, I also make a comparison of the subtidal velocities in the component along-estuary with those of the across-estuary dimension.

In Aysen Sound, the across-channel dynamics could be simplified by geostrophy, but the effects of the wind and bathymetry might be important to the lateral balance. In Chacao Channel, strong tidal currents interacting with rough bathymetry should cause flow nonlinearities that might enhance the advective and frictional terms. In the case of Ventisquero Sound, the sill/contraction combination should make advective terms important in the dynamics.

Once I identify the important terms in the dynamics, I should also be able to assess the main forcing determining the balance. Circulation in estuaries is generally produced by density gradients, tidal forcing, wind stress, river discharge, and coastal sea level

fluctuations. Bathymetry and the earth's rotation may also influence the flow. In fjords, as in some estuaries, tidally induced and density-driven flows should be the major components of the subtidal flow [*Li et al.*, 1998]. In the case of Aysen Fjord and Ventisquero Sound, we should expect both baroclinic and barotropic components competing, with transient influences of wind-induced flow, and tidal mixing by the effect of the sill/contraction in the case of Ventisquero Sound. In the case of Chacao Channel barotropic pressure gradients should be balanced by friction, as the main sources of fresh water are located far from the tidal excursion region.

Subtidal flows

Residual currents are the net direction and amplitude of water movement after the semidiurnal or shorter sinusoidal tidal currents have been removed. They can be generated by wind, density gradients, or rectification of the sinusoidal tidal currents. Concerning the latter mechanism, tides may generate residual currents through: 1) nonlinear bottom friction, 2) the nonlinear terms in the continuity equation, and 3) the nonlinear advective terms in the momentum equation. Residual flows are important in a broad range of estuarine phenomena including dispersion of salt, turbidity maxima generation, phytoplankton dispersion, and pollutant and suspended sediment transport [*Jay and Smith*, 1990].

For the purposes of this study, the concept of 'mean flow' occurring in a semidiurnal tidal cycle will be used interchangeably with 'residual current'. As flow and bathymetry differ in these systems, I should expect differences in the corresponding sectional structures of flow. Then the specific main questions would be

- What are the main features of the lateral structure of the along-channel mean flow in the three systems under study?

- What are the magnitudes and lateral distribution of the semidiurnal tidal flows?

As most of the estuarine flux variability occurs in response to tidal currents, the understanding of the tidal amplitude distributions in the cross-section constitutes a key issue to be addressed. The main properties of mean flow in the lateral direction should be a result of the main forcing in the cross-section. An understanding of the properties of the flow should arise from the analysis of the across-estuary distribution of the mean along-estuary flow.

Topographic effects

Subtidal flows may also be affected by bottom topography. Tides interacting with the topography of the water body, transfer energy from the short period (of the order of one day or less) to long term residual motion. When this occurs, the role of advective terms in tidally generated residual circulation becomes important to the momentum balance [*Murty et al.*, 1980]. The specific question to be addressed is

- What are the effects of the bottom topography on the cross-sectional distributions of subtidal flows and momentum balance terms?

Theoretical approaches to a basin with a rectangular cross-section [*Ianniello*, 1977,

1979, 1981] have described tidally induced mean flow to be landward on the surface and

seaward below. This is opposite to the results of *Pritchard* [1956] and *Hansen and*

Rattray [1965], which exhibit typical gravitational circulation with seaward flow in the

upper layer and landward below. More realistic approximations to natural systems using

nonrectangular cross-sections [*Wong*, 1994], have shown that lateral variations of depth

cause lateral variations of turbulence and bottom friction, which result in a tilt of the

gravitational circulation. Under this scenario, lateral shears would become important in

the transverse dimension. The landward flow thus tends to be located in the channel, and a

seaward flow on the shoals, as shown by *Wong* [1994], *Li and O'Donnell* [1997] and

Valle-Levinson and Lwiza [1997]. Making use of simple qualitative estimations, *Kjerfve*

[1978] has shown that in well mixed, high salinity estuaries net circulation experiences

ebb-directed flow in the deeper channel and flood directed flood in the shallower channel.

As the three systems have different bottom profiles and coastline morphology, we should

expect different effects in the flow. Chacao Channel exhibits a high aspect ratio pinnacle

in the center of the cross-section; Aysen Fjord also has a bank of low aspect ratio in the

center of the section; cross-sections in the north and the south of Ventisquero Sound

exhibit almost rectangular sections, and the sill/contraction dominates the bottom profile

in the along-fjord direction.

Dynamic similarity

The three systems will be analyzed separately in terms of their cross-section

properties and the scaling of the terms in the momentum balance. The specific question

to be addressed is

- Are the three systems under study similar among them from the point of view of their dynamics?

We know that two flows having different values of length scales, flow speeds, or fluid properties can be apparently different, but still "dynamically similar". Making use of nondimensional analysis, I explore the dynamic similarity among the flows in the cross-sections. The idea of dimensionless products is intimately associated with the concept of similarity. For example, flows having similar values of Reynolds number may be dynamically similar. For this particular case, I use nondimensional numbers like the Rossby number, Ekman number (horizontal and vertical), Reynolds number (horizontal and vertical), and Richardson number, in order to establish similarities and differences among flows in the three systems. The depth to tidal range ratio is also used as a nondimensional number involving a geometric characteristic of the cross-sections.

1.5 Significance of the research

In spite of its ecological importance, the region of the Chilean Inland Sea indicated in Figure 1 has received little attention. From the point of view of the physical oceanography, understanding of basic processes, such as the main characteristics of its circulation, still remain unsolved. The understanding of the mechanisms controlling circulation is still rudimentary. The present study shall contribute to the understanding of the main features of the circulation in the Chilean Inland Sea.

The few field efforts carried out so far in the region have been biased toward the longitudinal and vertical dimension previously observed in other estuaries. Making use of

field efforts that used towed ADCP measurements in fjords of southern Chile, this study favors the across-estuary dimension. In doing this, it is expected to effectively advance the understanding of the transverse variability of flows in the region.

The proposed study should also contribute to advance the general knowledge on: 1) Dynamic balances in fjords, and 2) Effects of the bathymetry and coastline geometry on the flow characteristics.

The following sections present the individual results obtained in Aysen Fjord (Section 2), Chacao Channel (Section 3) and Ventisquero Sound (Section 4). A study about dynamic similarities among the three systems is performed in Section 5.

REGION OF AYSEN FJORD

2.1 Introduction

As indicated previously, the hydrodynamics of fjords are usually assumed to have

lateral geostrophic balance, i.e., between Coriolis accelerations and pressure gradient

accelerations [*Dyer*,1997]. The geostrophic approximation has been demonstrated to be

valid in fjords of British Columbia [*Cameron*,1951] and in Juan de Fuca Strait [*Tully*,

1958]. However, wind stress may frequently become relevant to the lateral dynamics.

Wind stress may also reverse the classical mean vertical velocity profile in estuarine

systems . For instance, year-long series of current measurements in a coastal-plain estuary

have shown that, at least during 21% of the time, inflow was observed on the surface and

outflow near the bed [*Elliot*, 1978]. This effect may not be very different in fjords. Their

steep coastal walls may confine the wind flow, thus enhancing the along-fjord intensity of

wind and hence the wind-induced flow. The reversal of the surface layer flow by up-fjord

winds has been well documented in British Columbia [*Pickard and Rodgers*, 1959;

Farmer, 1976; *Farmer and Osborn*, 1976] and Norway [*Svendsen and Thompson*, 1978;

Svendsen, 1980]. In some cases wind has been postulated to be one of the main forcing

agents for deep water renewal [*Gade*, 1973; *Gade and Edwards*, 1980]. Some efforts

have been made to model the wind-driven circulation in fjords [*Klinck et al.*, 1981;

Krauss and Brugge, 1991]. The across-fjord variations of the flow, nevertheless, are still

a matter that requires more scrutiny. The objective of this study is to document the lateral

structure of the flow and density fields near the mouth of a Chilean fjord. The objective is

pursued with measurements of velocity and density profiles obtained at a cross-fjord

transect over a bank located near the mouth of Aysen Sound in southern Chile, South America.

2.2 Study area

Aysen Sound (Figure 2b) is a fjord-like inlet with a length of about 65 km measured between its mouth (station C in Figure 2) and its head (Station J in Figure 2), and an average width of about 6.5 km. The average depth in the longitudinal section (Stations A-J in Figure 2) is 217 m, with maximum values of 360 m in the outer basin at the mouth (C) and 350 m in the inner basin (H-I). It has a sill of about 125 m depth located to the west and east-southeast of Colorada Island (station E in Figure 2), and banks of 60, 90 and 90 m at stations F, G and H, respectively (Figure 2). The orientation of the fjord in its first 30 km from the mouth is in the SW-NE direction. The orientation changes in the following 25 km to the NW-SE direction, and to the SW-NE direction in the last 10 km (toward the head).

Waters of oceanic origin reach the fjord chiefly from the north through the Meninea constriction (Figure 2b). Modified Subantarctic waters of salinity 32.0 may fill the deep basin (210 m deep, letter A in Figures 2b and 2c) to the south of the Meninea constriction according to Silva et al. [1995]. Because of this constriction, along with the shoalings (~50 m) at Middle Passage(B) and to the south of Elisa Peninsula in Figure 2b, and also because of the narrow channels that connect the study area with the ocean 50 km to the west, the estuarine circulation in Aysen Fjord is believed to be little affected by remote forcing generated on the continental shelf (outside the Inland Sea). To the south of Costa Channel the system receives fresh water inputs from small rivers and glaciers and its
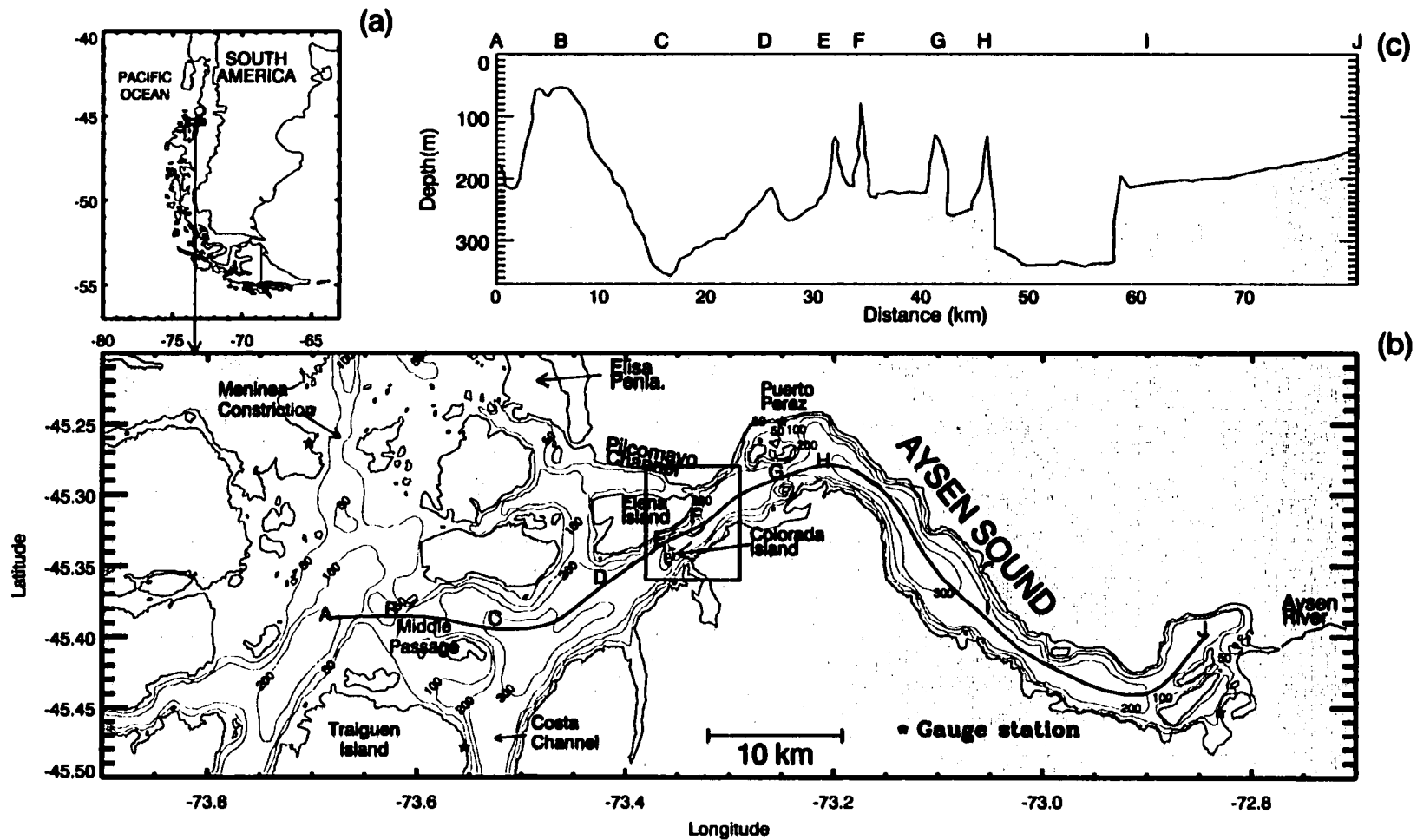
Figure 2. (a) Study area on the southern coast of Chile. (b) The measurements obtained during this experiment were made in the box shown to the south of Elena Island. The Pacific Ocean is about 50 km to the west of the left edge of the lower panel. Isobaths shown: 50, 100, 200, and 300 m. (c) Bottom profile in the longitudinal transect A-J.

exchanges with the open ocean are strongly reduced by the presence of narrow (<1 km width) and shallow (~50 m) channels. Owing to this insulating morphology, the main forcing agents in the vicinity of the mouth of the Aysen Fjord are postulated to be tidal forcing from the coastal ocean, local wind stress, and river discharge. The main characteristics of these forces in the region are outlined below.

The tidal regime throughout the Inland Sea is mixed, predominantly semidiurnal. Outside of Aysen Fjord, four months of sea level measurements made during spring 1998 in the vicinity of Meninea constriction and at the entrance to Costa Channel, have shown M_2 tidal amplitudes of 76.33 cm and 81.67 cm, respectively, for these locations [*Fierro et al.*, 1999]. They have also revealed mean tidal ranges during spring tides of 2.46 m and 2.64 m at the same locations. Inside Aysen Fjord, similar ranges of 2.2 m in Puerto Pérez and 2.7 m at the head of the fjord (C, Figure 2b) also have been reported for this region [*SHOA*, 1993b]. Following *Stigebrandt* [1977], the amplitude of the tidal current *(u)* in the bank region should be about 0.12 m/s, using $u=aYw/A$, where w is the frequency of the semidiurnal tide (2π/12.42h.), a is the mean amplitude in water level at Puerto Pérez, Y is the horizontal area of the fjord (350 km²), and A is the cross sectional area at the bank (0.5 km²). As confirmed by this study, tidal currents were in the range of 0.1 to 0.2 m/s. These are similar to the wind-induced currents in the fjord.

The wind regime in this region of the Inland Sea is dominated by southerly and southwesterly winds during spring and summer (Oct-Mar), and northerly and northwesterly winds during fall and winter (April-Sept). Westerly and southwesterly winds may favor wind-driven, up-fjord surface circulation at the mouth and in the outer

half of the fjord, which would decelerate the surface layer mean outflow. North and northwesterly winds could be important for wind-driven circulation in the inner half of the fjord, as the low land profile at the northern region of Puerto Perez may favor winds coming from that direction.

The main source of fresh water to the fjord is provided by Aysen River (Figure 2). Similarly to many other Andean and trans-Andean rivers, Aysen River exhibits two annual peaks of discharges at the head corresponding to the autumn increase in precipitation (April-June) and the summer melting of snow. Sampling for this study was carried out in October, close to the snow melting peak in November. The mean annual river discharge is estimated to be 620 m³/s [*Niemeyer and Cereceda*, 1984] and the mean total annual precipitation (1968-1999) for stations around the study area fluctuates between 1100 and 2100 mm (SMA, pers. comm.)

In the transition zone at the mouth between C and E (Figure 2), a strong horizontal salinity gradient at the surface (~12.5 /10 km) has been observed in March [*Silva et al.*,1995], September [*Muñoz et al.*, 1992] and November [*Silva et al.*, 1997]. This feature suggests the presence of a tidal intrusion front in the region of confluence between the brackish layer coming from the fjord and the intrusion of salty water from the west. As salinity is representative of the density field in this region, this will be used hereafter when describing density patterns. A satellite image obtained in February 1993 (Figure 3), also suggests the shape of the front, which might represent the tidal intrusion going into the fjord on the northern side and the brackish water tending to leave the fjord on the south.

This study concentrated on the bank near the mouth located in the box marked F in Figure 2b, and had the objective of examining the transverse variability of the flow associated with this bathymetric feature. The working hypothesis was that the transverse dynamics would reflect geostrophic conditions: inflow of saltier water on the northern side and outflow of fresher water on the southern side, as suggested by *Muñoz et al.* [1992] and also by the satellite image in Figure 3.

2.3 Data collection and processing

Current velocity and density measurements were obtained between October 14-17, 1998 in the vicinity of the mouth of Aysen Fjord, in order to describe the transverse structure of density and flows in that region. Current profiles were obtained along a ~3-km long cross-fjord transect (Figure 4) using a RD Instruments 307.2 kHz towed Acoustic Doppler Current Profiler (ADCP) during a complete semidiurnal tidal cycle on October 16. The across-fjord transect was traversed 20 times during the 11 hours of data collection. The sampling began at 13.00 h and had a time interval of ~33 min between repetitions. The ADCP was mounted looking downward on a catamaran 1.2 m in length, which was towed at approximately 2.5 m/s on the starboard side of the local boat "Cordillera I" on October 16. The ADCP recorded ensembles of 8 pings averaged over 30 seconds. Bin size was 4 m and the first velocity bin was centered at ~8 m depth. The standard deviation of the current measurements was then <3 cm/s. The depth limit of the ADCP profiles was 100 m. Navigation was carried out using a Trimble Global Positioning System (GPS). The repetitions of the cross-fjord transect were made over a bank of ca. 65 m depth placed 1 km southeast of Elena Island (Figure 4). The ADCP
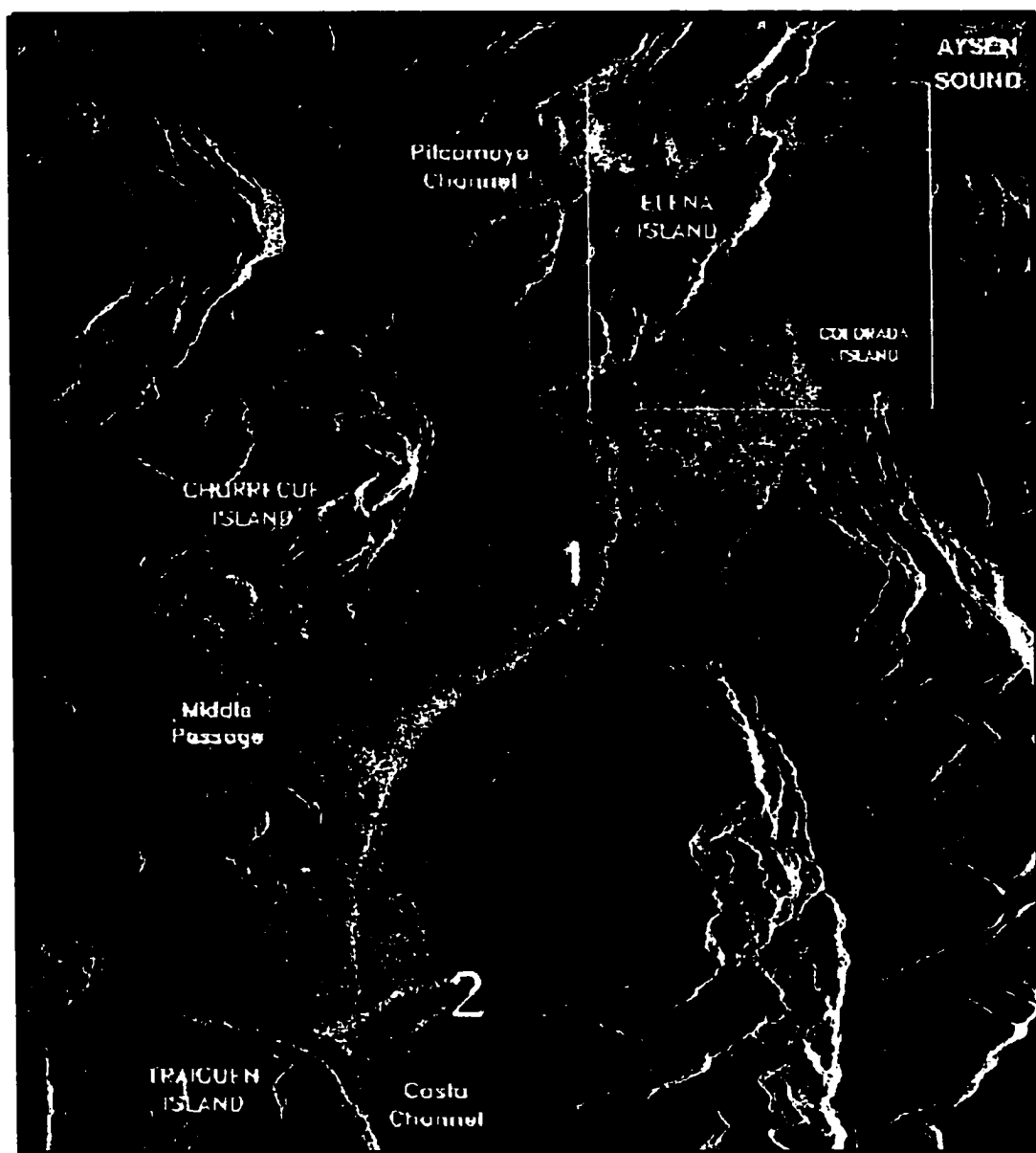
Figure 3. ERS-1 (European Research Satellite) radar satellite image from the study area obtained on February 3, 1993. The surface roughness suggests the position of a frontal zone (1) extending from the south of Elena Island to the north of Traiguén Island. A train of internal waves (2) at the entrance of Costa Channel is also suggested in the image.
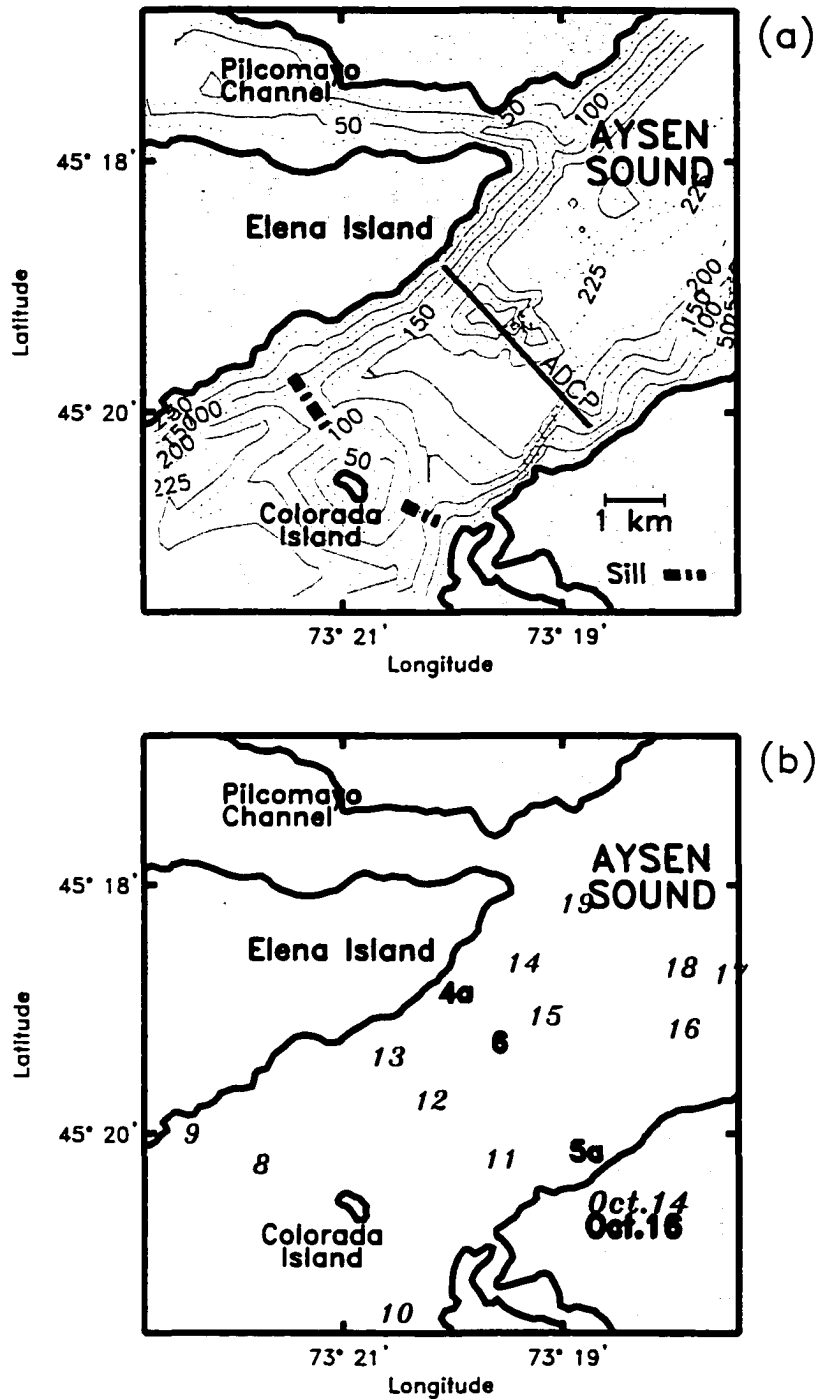
Figure 4. (a) Position of the ADCP transect on October 16 (~3 km length). Locations of sills referred to in the text are pointed out with the segmented line. Depth in meters. (b) Position of CTD stations. Stations 4a, 6 and 5a were made in conjunction with the ADCP sampling.

compass data were calibrated following *Joyce* [1989] and erroneous velocity data were

removed following the procedure explained by *Valle-Levinson and Atkinson* [1999].

The semidiurnal tidal signal (represented by the M_2 constituent with a period of

12.42 hours) was separated from the subtidal signal of the observed flow components

using sinusoidal least- squares regression analysis [e.g. *Lwiza et al.*, 1991]. The subtidal

signal represented the mean over the 12 hours of observation. The current measurements

were complemented with density profiles obtained with a Sea-Bird SBE-19 conductivity-

temperature-depth (CTD) recorder from the Chilean Navy patrol craft "Rano Kau" on

October 14. Data processing was followed according to the manufacturer's software. The

pressure, temperature and conductivity measurements were aligned, data with pressure

reversals were removed and the data were averaged to 1 m bins. Profiles were measured

at the end of each transect repetition and over the bank in the center of the transect

(Figure 4a). Maximum depth of CTD profiles was 50 m owing to restrictions of the

CTD's pressure sensor. On October 14, two days prior to the ADCP sampling, twelve

CTD stations (numbered 9 to 19, Figure 4b) were sampled during ~3 hours of flood. The

CTD sampling on October 14 provided a general idea of the horizontal distribution of the

density field in the vicinity of the bank. This is explained in the context of the velocity

profiles in the next section.

The closest meteorological stations to the study area were Guafo Island and Raper

Cape, located in the coastal region at 225 km to the northwest and 250 km to the

southwest, respectively. Owing to this long distance and to the orography in the fjord

region, they were not representative of the wind conditions in the study area. Wind data

were collected onboard during the period of sampling. Winds were calm during the first three hours of sampling, and then they started to increase reaching maximum values of about 8 m/s in the up-fjord direction (southwesterly winds) at the end of the sampling. A right handed coordinate system was adopted for which y was positive to the north and x was positive to the east. It follows that the along-fjord and across-fjord components of the velocity were given by u and v, respectively. The data were rotated counter clockwise 60° to an along- (u-flow) and across- (v-flow) channel coordinate system. This angle was oriented to the direction of greatest variability of the tidal currents and of weakest across-channel tidal flows. It follows that the x and y axis were oriented toward 030° and 300° true, respectively.

2.4 Results

This section presents the across-fjord distribution of the subtidal and tidal flows for the observation period. It also describes the horizontal salinity distribution, time series of salinity profiles, time evolution of the near-surface salinity across the fjord, and the time evolution of vertical sections of salinity across the fjord. These salinity representations help explain the observed subtidal flow patterns discussed below.

Subtidal and tidal flows

The along-fjord mean u-flow over the period of observations (Figure 5) suggests a three layer structure that included a thin (< 8m) surface weak outflow close to the surface (not entirely resolved by the ADCP measurements), a region of net inflow immediately underneath and a compensatory outflow farther below. Vertical profiles of current velocities at selected sites of the transect showed that the average outflow within a layer

Along-channel mean u-flow (cm/s)
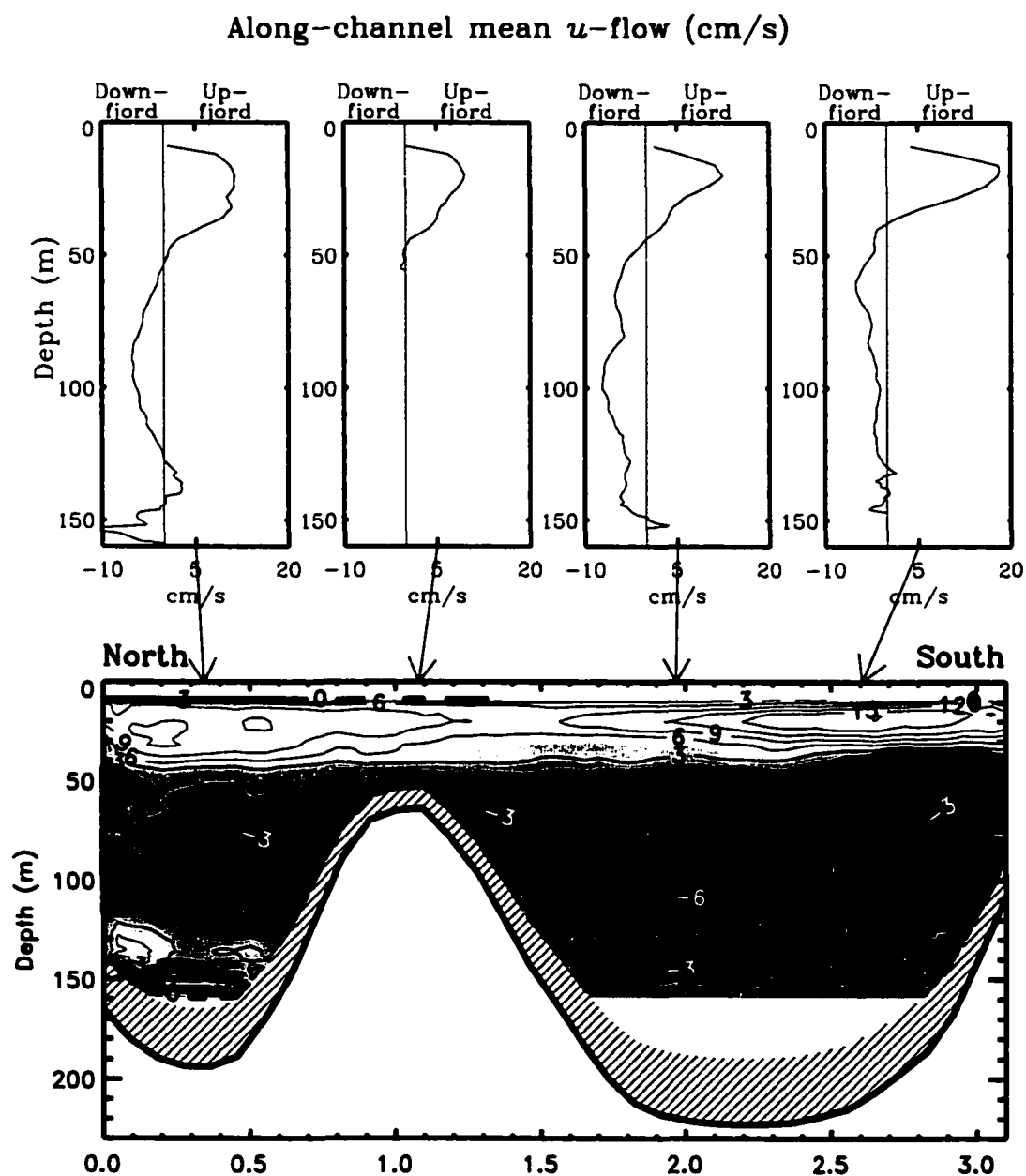
Figure 5. Across-fjord distribution of the mean flow (looking up-fjord).The mean flow suggested a surface (8 m) outflow on the northern side (black contour). It also showed a near-surface inflow and an interior outflow (dark tones). Contour interval is 3 cm/s. Vertical profiles of current velocities at selected sites of the transect are shown in the upper region of the figure. Data in the shaded region near the bottom were not considered in the analysis due to side lobe effects. White region near the bottom was out of the profiling range of the ADCP

extrapolated to the surface from ~8 m depth was 0.03 m/s. Below this unresolved outflow, a 30-40 m thick layer showed up-fjord velocities of 0.1 m/s, most likely due to the dominant southwesterly winds during the experiment. The interior outflow layer of 60-100 m thickness had typical velocities of 0.05 m/s and was most likely a compensatory flow from the pressure gradient set up by the wind in the along estuary direction.

The along-fjord mean flow exhibited transverse variability related to the bathymetry. Upper layer current magnitudes were weaker over the channel to the north of the bank than to the south. This might be attributed to the fact that the northern channel is shallower and narrower than the southern channel. Over the bank, frictional effects were evident in the decreasing magnitudes of the mean current relative to that on either side and by the fact that most of the water column showed up-fjord net flow, i.e., the near-bottom compensatory outflow was not developed in this region of the cross-section. The effects of the steep bottom also showed that horizontal friction might be playing a role in the dynamics, as the greatest outflow magnitudes were observed in the center of both channels at mid-depth. Throughout the section, the zero isotach at about 50 m exhibited downward slope toward the north, which was contrary to that expected from a geostrophic balance in a two-layered density driven flow, where the zero isotach would slope upward toward the north. The sign of the slope of the zero isotach indicated that the lateral momentum balance in the mean flow could not be explained by geostrophy. Below 50 m, nevertheless, where the flow was westward, the current was forced to the left by the Coriolis effect, resulting in a thicker layer at the south, i.e. the zero isotach was higher in the water column at the south. The observed slope suggested then that the compensatory

flow below 50 m was consistent with geostrophy. It appears then that the observed distribution consisted of a frictional surface layer and a quasigeostrophic interior.

The transverse flows (Figure 6a) were directed northward above ~50 m and throughout the northern channel, and southward only within the southern channel. The interaction of the flow going toward the north and toward the south over the bank, suggested recirculations over this feature. On both sidewalls of the bank, flow tended to travel away from the bank. Thus, the transverse circulation indicated that effects of advection could be important around the bank. The strongest northward flow was located at the surface over the southern channel, far from the effects of the frictional effects of the sidewalls. Even though the velocities were in the range of the standard deviation (± 3 cm/s), the distribution could not be dismissed as it showed a coherent pattern throughout the section. The mean flow is depicted by flow vectors in Figure 6b, which shows the tendency of the vectors to follow the bathymetry around the bank. This figure also shows the uppermost (8m) layer going down-fjord on the northern side, and up-fjord on the southern side.

The amplitude of the semidiurnal along-fjord current (Figure 7) also showed transverse variability that featured maximum tidal currents of ~0.2 m/s over the bank. This distribution contrasted those in coastal plain estuaries where bottom friction causes the greatest magnitudes to appear in the deepest part of the cross-section [Li and Valle-Levinson, 1999]. Nonetheless, the transverse distribution observed in the Aysen Fjord was consistent with observations of greatest flows over sills or constrictions in response to the Bernoulli effect [e.g. Farmer and Armi, 1999], where bottom friction plays a secondary

North   **Across-channel mean** v**-flow (cm/s)**   **South**

(a)

North   **Mean flow (cm/s)**

10 cm/s

(b)
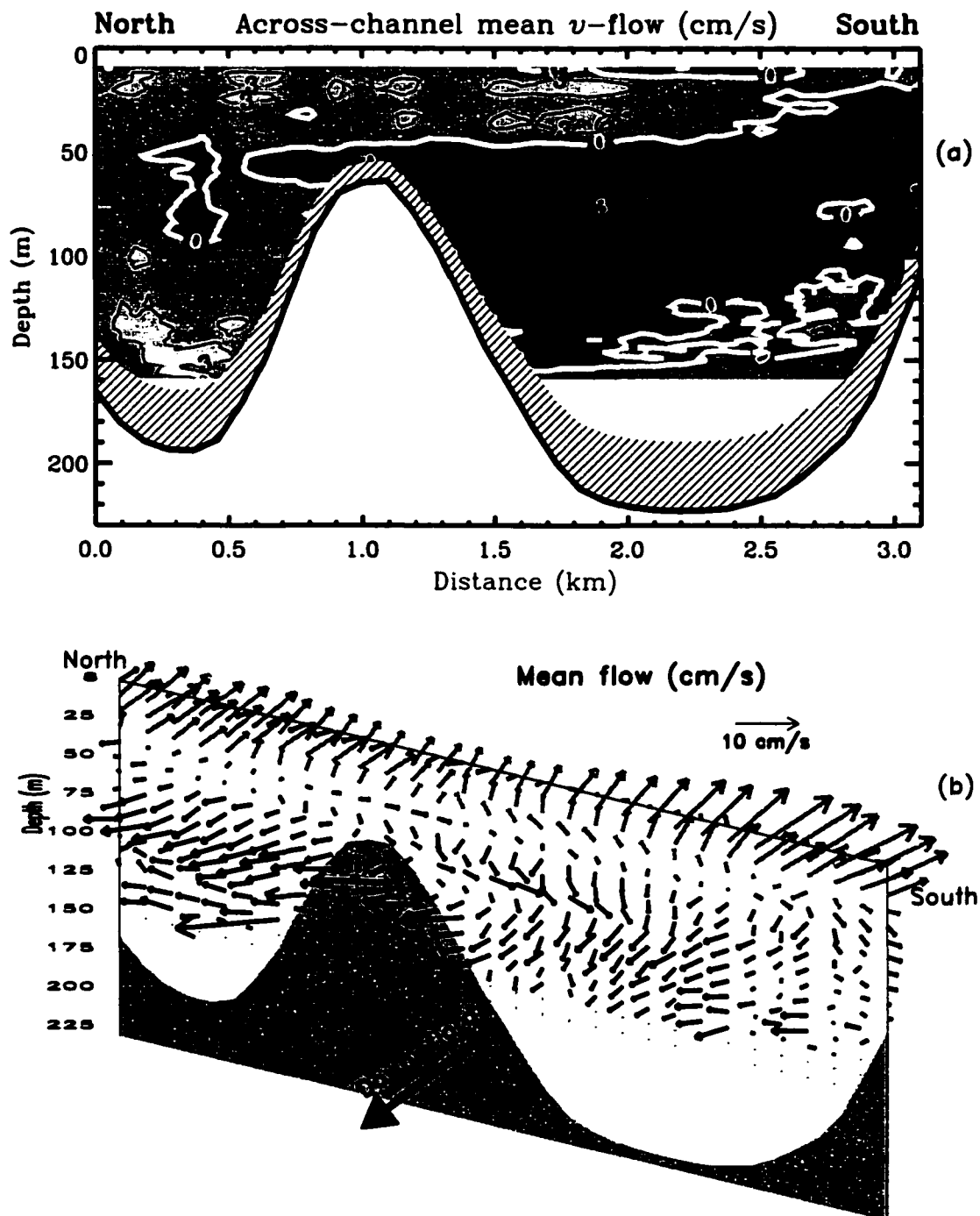
South

Figure 6. (a) Across-fjord distribution of the lateral mean flow. Darker tones denote flow to the south and lighter tones flow to the north. Recirculation over the bank and advection away from the sidewalls of the bank are suggested in the figure. Data in the shaded region near the bottom were not considered in the analysis due to side lobe effects. White region near the bottom was out of the profiling range of the ADCP. (b) Vectorial representation of the mean flow. Vectors are drawn at 10 m intervals starting at 8 m (black), 18 and 28 m , (gray) and 38 to 158 m (black).
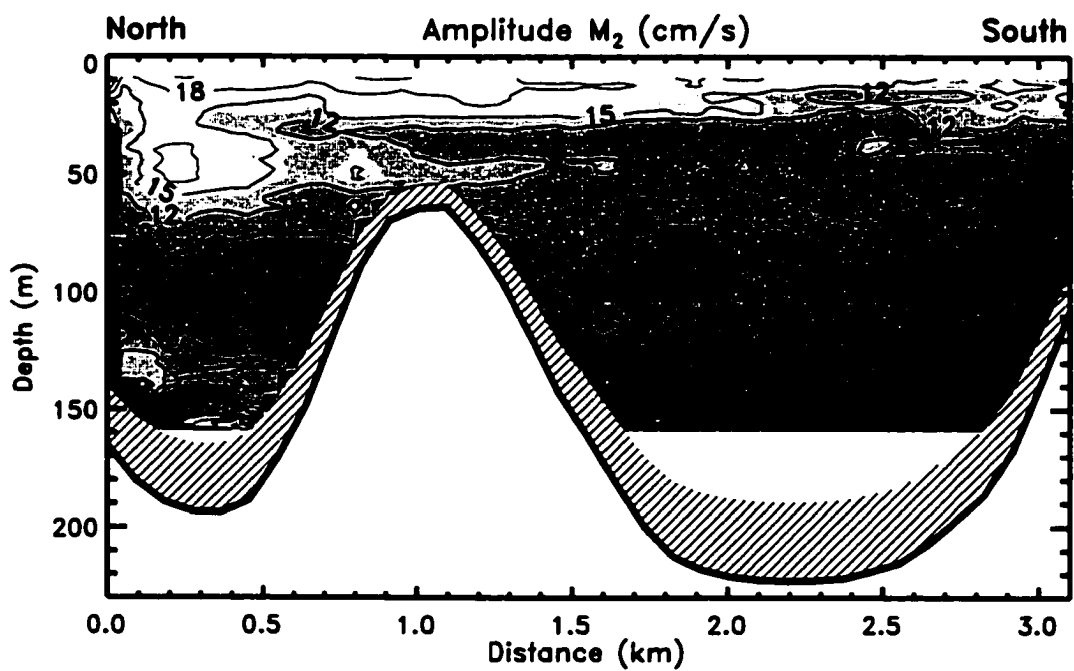
Figure 7.- Across-fjord distribution of the M_2 tidal current amplitude obtained from the ADCP current measurements. Highest amplitudes were observed over the bank. Contour interval is 2 cm/s. Data in the shaded region near the bottom were not considered in the analysis due to side lobe effects. White region near the bottom was out of the profiling range of the ADCP.

role in shaping the flows. Therefore, the tidal flows in this area should be mostly responding to pressure gradient induced by tidal elevations and advective accelerations produced by the abrupt changes in morphology.

Tidal and subtidal salinity

In general, both density and salinity profiles showed a pycnocline in the first ~8 m depth with typical salinities between 15 and 25 in the surface layer and 30 in the deeper layer through 50 m depth, which was the maximum depth of CTD casts. Other observations in this area [*Silva et al.*, 1995 and 1997] showed consistent distributions with those observed here and salinities that increased up to 31.2 in the deepest part of the fjord. Figure 8 shows the horizontal salinity distributions from stations 8 to 19 near the surface and 15 m depth on October 14, two days before the ADCP measurements. The time between the first and last station was about 2.7 hours. Above the pycnocline (at 1 m), a fresh water tongue was evident over the northern side, while saline water intruded from the northern channel into the center of the fjord. Horizontal salinity gradients across the fjord seemed to be at least as large as along-fjord gradients in this particular instance. Below the pycnocline (at 15 m), where the horizontal and vertical salinity gradients were greatly reduced, the horizontal salinity distribution showed fresh water over the northern side and salty water on the southwest. This distribution also suggested the influence of wind-induced upwelling before the ADCP measurements, because the greatest salinities were found along the southern side. Also noteworthy is the separation of the flow suggested by the shape of the 29.30 isohaline around the bank in station 15 (Figure 8), where salty water bifurcated around this feature (based on just three points across the
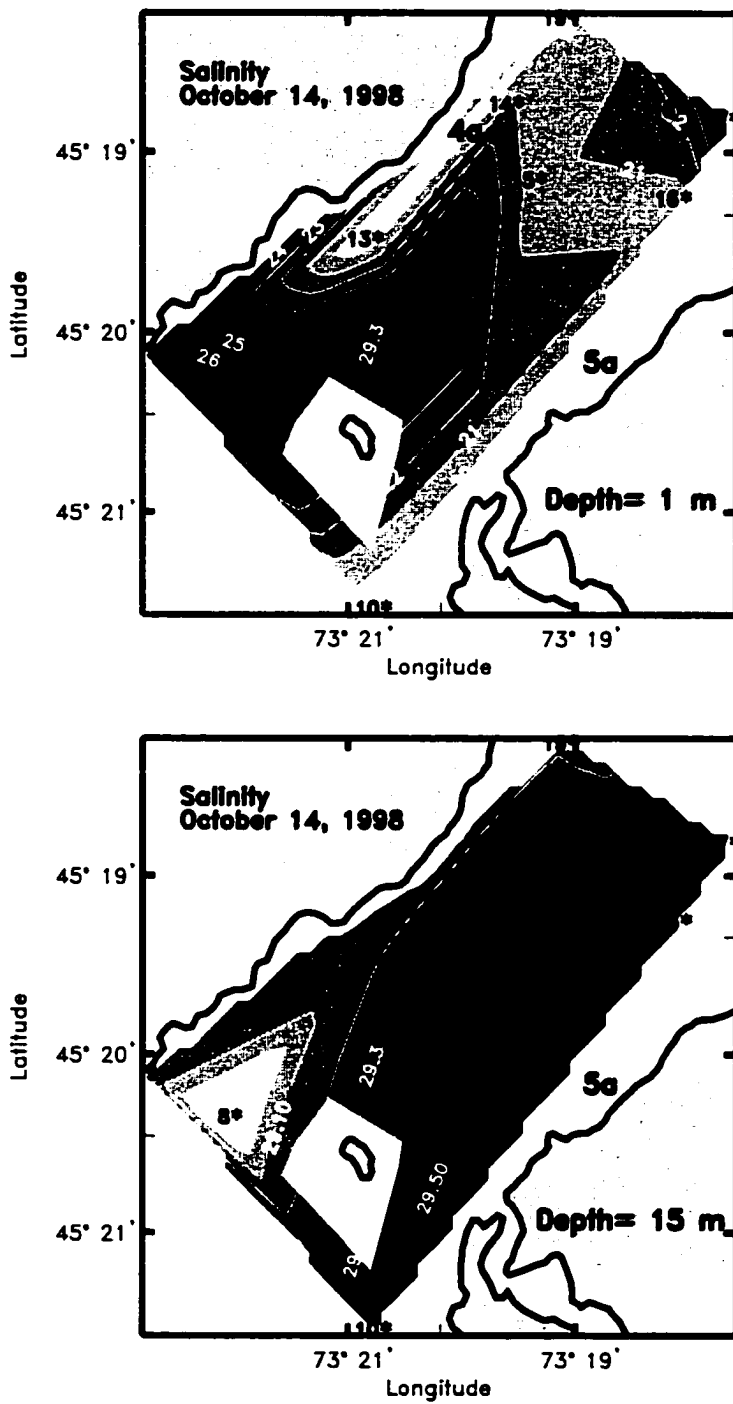
Figure 8. Horizontal salinity distribution from stations 8 to 19 at surface and 15 m depth on October 14. Isohalines are drawn in white and station positions are printed in black. Positions of CTD stations made on October 16 (4a, 6, 5a) are also drawn for reference. The area around of Colorada Island has been masked because of lack of measurements there.

fjord). This provided further evidence of the influence of the bank in modifying the flow.

Evidence of fresher surface water on the northern side relative to the southern side was

also suggested by time series of vertical salinity profiles at stations 4a, 6 and 5a (Figure

3) taken during the ADCP measurements (Figure 9). In this case, the surface salinity was

lower over the northern side than on the southern side. This distribution was contrary to

that expected from the earth's rotation influence but could be related to local upwelling

over the southern coastline of the fjord, as is also suggested by the across-fjord tilt of the

zero isotach (Figure 5) and the across-fjord flow (Figure 6). Also worth noting is the

change in the depth of the 28 isohaline during the tidal cycle, which is associated with the

along-fjord velocity changes during this period. Below 8 m, the depth resolved by the

measurements, velocities may be attributed to the combined effect of tide and wind. In the

southern station, the down-fjord flow is less dominant than in stations in the center and

north, probably attributed to the combined effect of up-fjord wind (Figure 5) and low tidal

amplitude shown in that side (Figure 7). Some tidal straining effects are apparent in the

three stations in the sense that the buoyant layer thickens during ebb and thins during

flood.

The transverse structure of the near-surface salinity field throughout the tidal cycle

(Figure 10) showed that, as wind started to blow from the southwest at about 17:30 h and

persisted during the rest of the experiment, high salinity waters began to appear over the

southern portion of the section, another suggestion of upwelling. In accordance with the

effect of the earth's rotation, the salty water due to inflow at that depth was expected to

be located over the northern side of the fjord as observed between 14 h and 17:30 h. As

Salinity (contours) and u-velocities (arrows)   October 16, 1998

15 cm/s

Station 4a (north)

14   Flood   Ebb   Flood 24

Station 6 (center)

14   Flood   Ebb   Flood 24

Station 5a (south)

14   Flood   16   18   Time (h)   20 Ebb   22   Flood 24
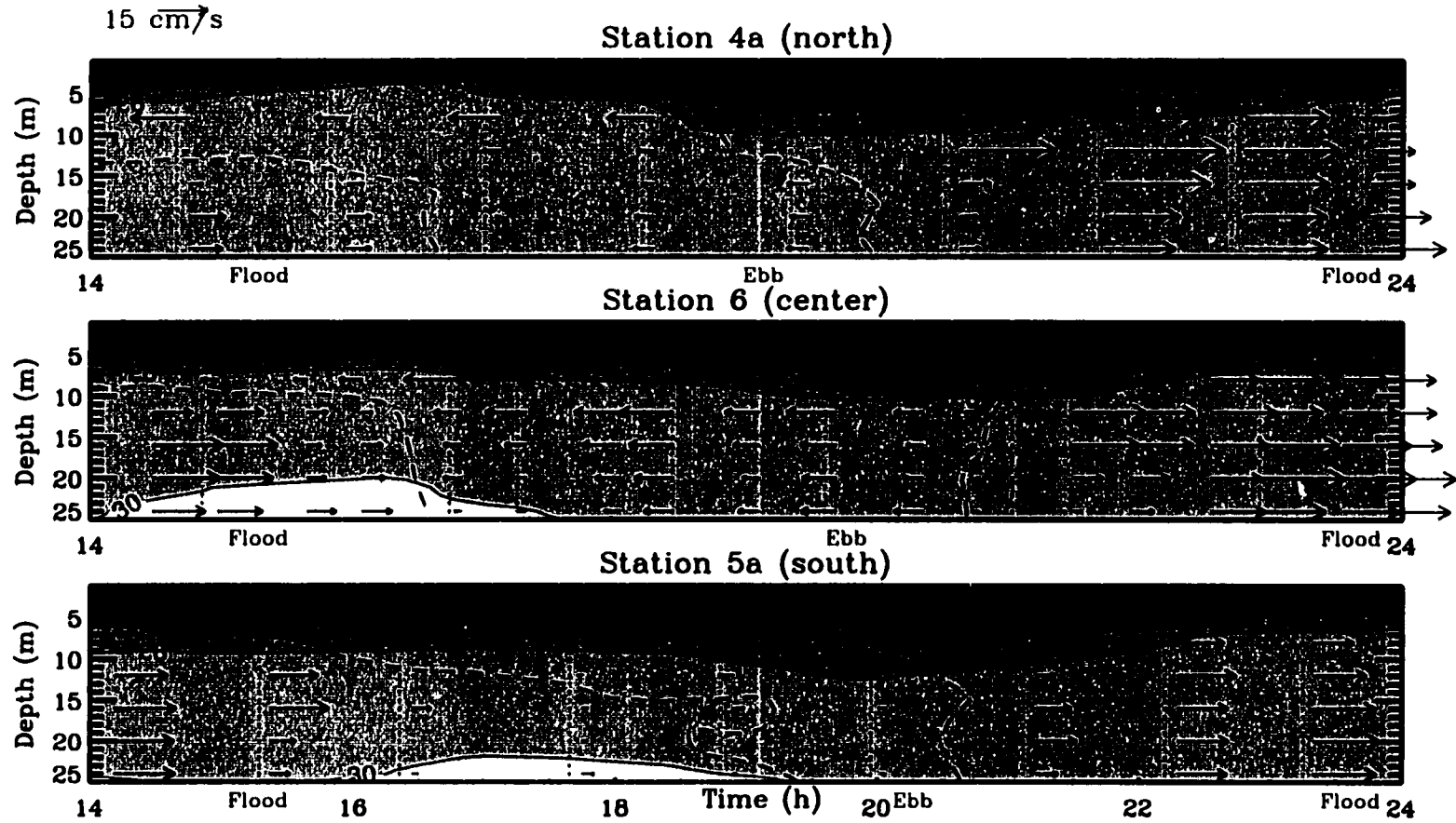
Figure 9. Temporal variability of the salinity (contours) and flow profiles (vectors) from stations 4a, 6 and 5a on October 16. Along-fjord ADCP measurements for those stations are overplotted. Broken line corresponds to the zero ADCP velocity contour.

33

October 16, 1998   Salinity   Depth = 2 m
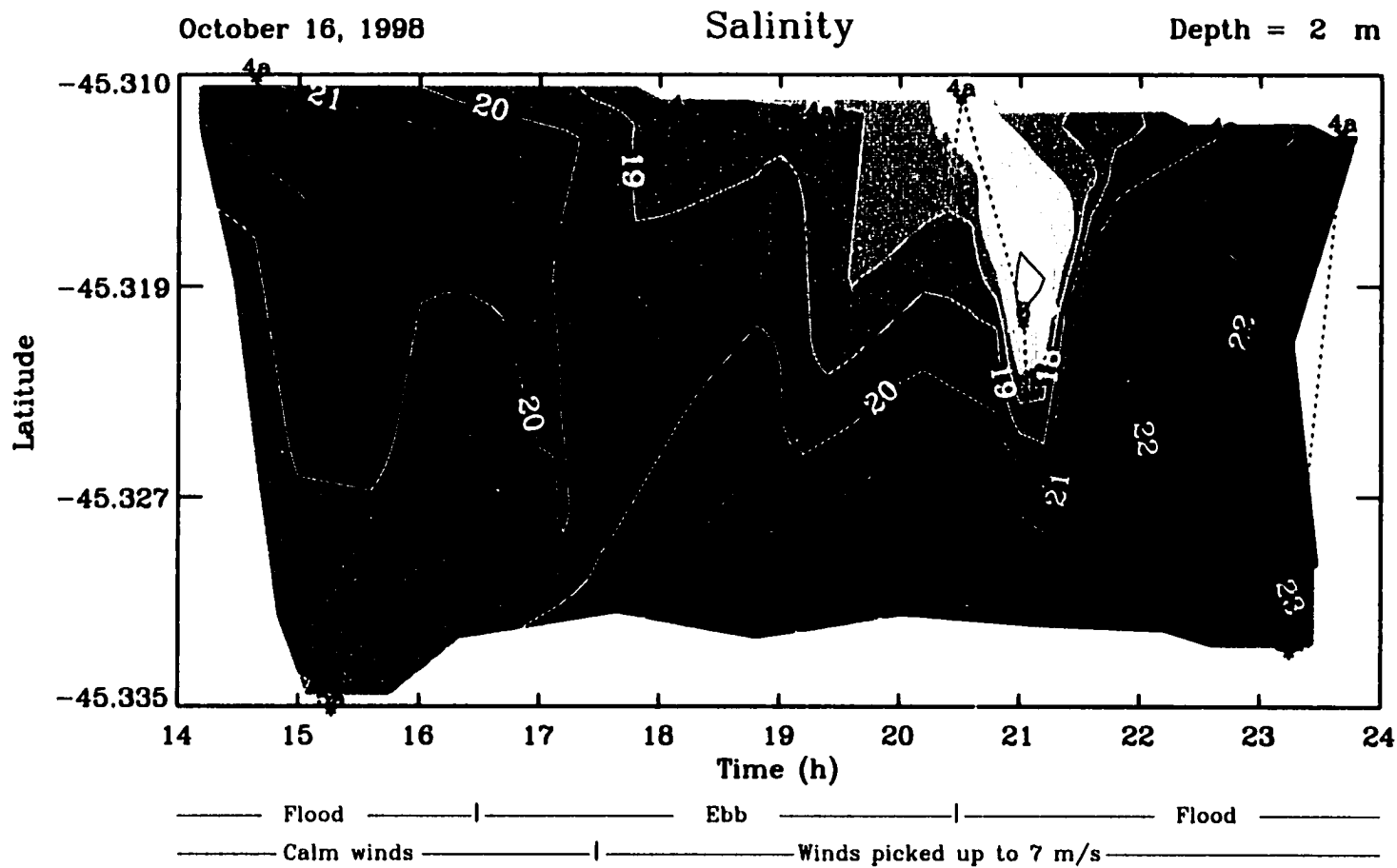
Figure 10. Horizontal across-fjord salinity distribution from stations 4a, 6 and 5a plotted in time. Dotted lines correspond to the ship track. Wind started blowing steadily at 17:30 h and caused upwelling on the southern side.

southwesterly winds persisted, high salinity waters covered the whole width of the fjord

at 24 h. Low salinities observed over the bank at about 21 h were probably due to the

effect of fresh water convergence at 2 m depth, by the combined effect of up-fjord wind

and starting of flood. The effect of the wind was also appreciable in the vertical sections

of the CTD stations 4a, 6 and 5a (Figure 11) on the first 3 repetitions, where all isohalines

tilted down toward the south side during calm wind, as expected from a typical

geostrophic balance in the transverse direction for down-fjord flow. As winds picked up

during the fourth repetition, isohalines of 22, 24, 26 and 28 rose progressively in

repetitions 4, 5, 7 and 8, respectively. During repetition 8 every isohaline lower than 29 in

the surface layer was higher on the southern side than on the northern side. Between 20

and 50 m (the maximum depth of CTD casts), isohalines greater than 29 were higher in

the south at every repetition (not plotted here). The slope of the 29 isohaline, lower in the

south, could not be explained by the measurements. It follows that, according to the

salinity mesurements, effects of the upwelling were noticeable in the first 50 m.

The salinity distributions discussed in this subsection showed a consistent message.

Southwesterly winds in the lower Aysen Fjord seem to produce upwelling along the

southern coast and downwelling along the northern coast above 50 m depth, which

transiently invalidates the geostrophic approximation for the transverse dynamics. Also

during these wind episodes, the saline intrusion shifts from the northern to the southern

side.

2.5 Discussion

Wind forcing seemed to be the main driving mechanism of the mean flow during the
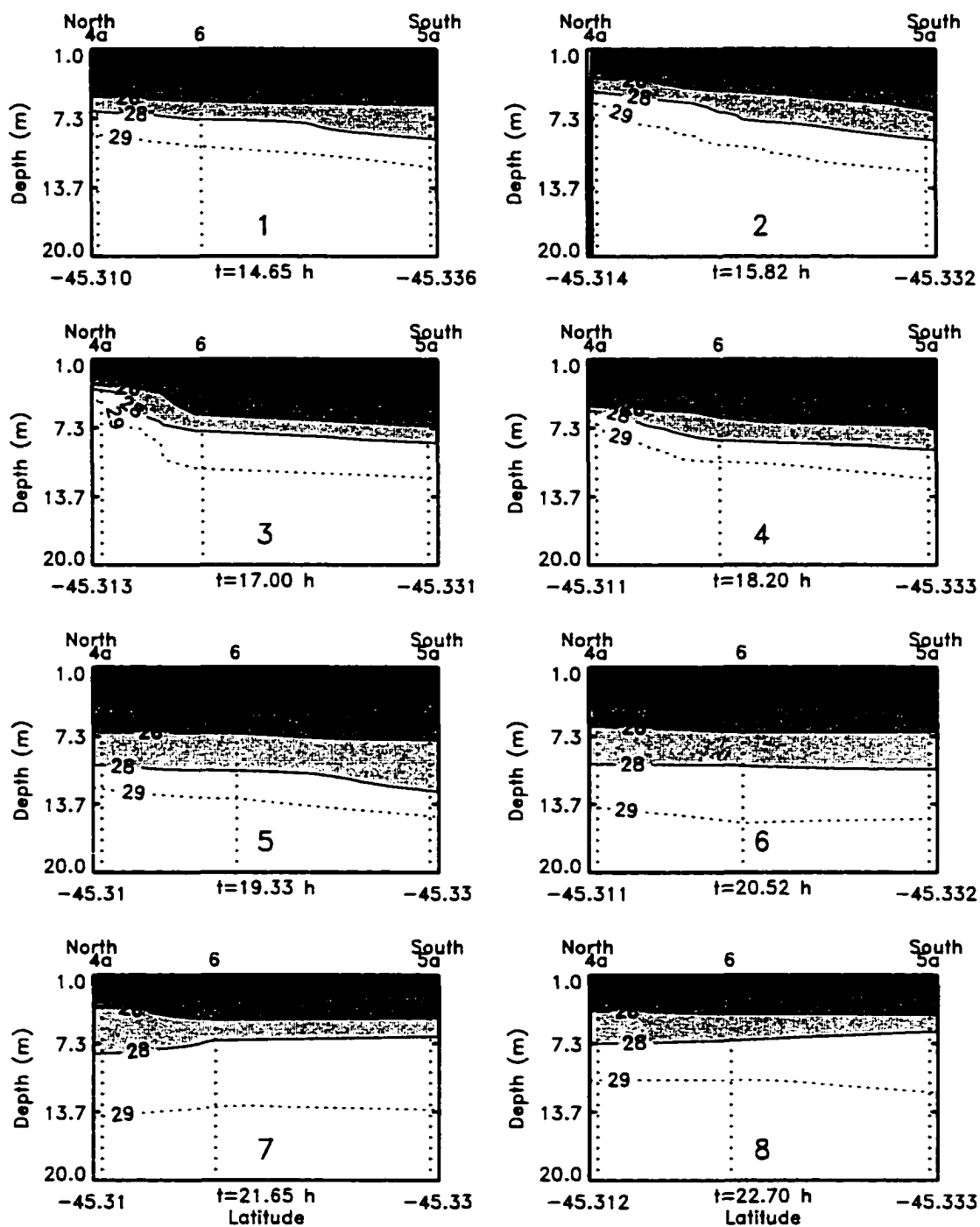
Figure 11. Cross-fjord vertical salinity sections at different times (looking into the fjord). Persistent southwesterly winds starting after repetition 3 induced upwelling, as reflected by the progressive rise of the isohalines on the southern side. Time corresponds to the beginning of each repetition. Maximum depth plotted is 20 m, which was where the most appreciable changes appeared.

sampling period as the mean flow was up-fjord near the surface, below 8 m depth.

Similar profiles to those presented in Figure 4, resulting from up-fjord wind driven

circulation, have been observed in the fjords of Norway [*Svendsen and Thompson*,1978;

Svendsen, 1980] and British Columbia [*Farmer*, 1976]. This wind episode also may have

induced upwelling, as suggested by the zero isotach and the pycnocline both tilting

downward toward the north, and by the presence of more saline water in the south than in

the north. Evidence of fresher water on the northern side than on the southern side could

be a transient wind-induced phenomenon, as salinity horizontal fields observed in the

region of Colorada Island by *Muñoz et al.* [1991] showed more saline water over the

northern side during calm winds. This was also observed during calm winds at the

beginning of our experiment.

The bank affected the across-channel distribution of subtidal flow as it shifted the

location of both the strongest near-surface inflow and the strongest mid-depth outflow to

the channels. It also masked the three-layer mean flow that was observed in the channels.

Evidences of flow bifurcation induced by the bank were observed in the horizontal

salinity distribution below the pycnoline. The effect of the bank in shaping the flows was

also observed in the secondary circulation patterns, as flow tended to travel away of the

sidewalls and suggested recirculations over the summit. These effects induced by the

bank suggest that advective accelerations and friction could be important for the across-

fjord momentum balance during strong wind episodes.

In order to establish the relative contribution of advection and friction to the across

momentum balance, the Coriolis term and advective and friction (vertical and horizontal)

terms were compared. In the across-channel direction, the subtidal momentum balance

can be given by

$$<v(\partial v/\partial y)> + <fu> = - <1/\rho\ (\partial p/\partial y)> + <A_z(\partial^2 v/\partial z^2)> + <A_h(\partial^2 v/\partial y^2)> \qquad (2.1)$$

where $v(\partial v/\partial y)$ represents the advective terms (the other two could not be evalutated), fu

is the Coriolis term (f= 1.03 x10^{-4}), $1/\rho\ (\partial p/\partial y)$ is the pressure gradient term, where p is

the seawater density, $A_z(\partial^2 v/\partial z^2)$ is the vertical frictional term, $A_h(\partial^2 v/\partial y^2)$ is the horizontal

frictional terms and brackets ($<\ >$) denote tidal averages. The coefficients A_z and A_h

denote the vertical and horizontal eddy viscosities. These were the terms of the complete

momentum balance that could be reliably approximated, with exception of the pressure

gradient term.

For the vertical eddy viscosity, A_z, we first consider wind stresses of the order of

0.03 Pa, for an average wind of 2.5 m/s during the tidal cycle. If $\tau=\rho A_z\partial u/\partial z$ then A_z may

be given by $A_z=\tau/(\rho\ \partial u/\partial z)$. Considering ρ=1024 kg/m^3 (the average of the full set of

density data) and $\partial u/\partial z$ = 3.5 x10^{-3} s^{-1} (averaged from distribution of Figure 5), an

estimate of A_z from wind stresses will be 0.0027 m^2/s. The relationship proposed by

Csanady [1975], $A_z= u_*^2 / 200 f$ for estuaries of large depth, where u_* is the frictional

velocity $(\tau/\rho)^{1/2}$, provides an estimate of A_z produced by bottom friction. This solution

gives typical values in the order of A_z=0.0004 m^2/s. Subtracting this from 0.0027 (as

shown by Wong [1994] and Csanady [1975]) gives A_z=0.0023 m^2/s. Therefore, we used a

constant eddy viscosity coefficient of 0.002 m^2/s. As expected, bottom friction played a

secondary role in the dynamics and most of the vertical friction was attributed to the wind stress.

Similar empirically derived forms of the magnitude of the horizontal eddy viscosity in tidal channels are less widely used. *Tee* [1976] used a value of A_h =100 m²/s for an energetic tidal channel (currents of ~5 m/s), *Ianniello* [1979] used estimates ranging from 1 to 10 m²/s for tidal channels, and *Jones and Elliot* [1996] used estimates of 0.5 to 10 m²/s in the parametrization of friction in rivers. Following the method proposed by *Ianniello* [1979] to estimate the width of the channel that makes A_h important to the momentum balance, we used an estimate of A_h =1 m²/s, according to the velocities and horizontal lengths observed in this system.

The absolute value of the ratios $<v(\partial v/\partial y)>/<fu>$, $<A_z(\partial^2 v/\partial z^2)>/<fu>$ and $<A_h(\partial^2 v/\partial y^2)>/<fu>$ is shown in Figure 12. These ratios showed that the non linear accelerations, vertical friction term and horizontal friction term were comparable to Coriolis accelerations during the sampling period, as most of the magnitudes of the sectional means were about 1. The distributions showed that values >1 were located around the bank and close to the sidewalls and bottom, where advective and frictional terms were expected to be larger than the Coriolis term. There was also a thin layer of values >1 at about 50 m depth across the entire fjord, which may be explained by the position of the zero velocity in Figure 5, which made the Coriolis term to tend to zero. Analogously, the along-fjord momentum balance appears to transition from a balance between pressure gradient and advection during calm conditions, reminiscent of a
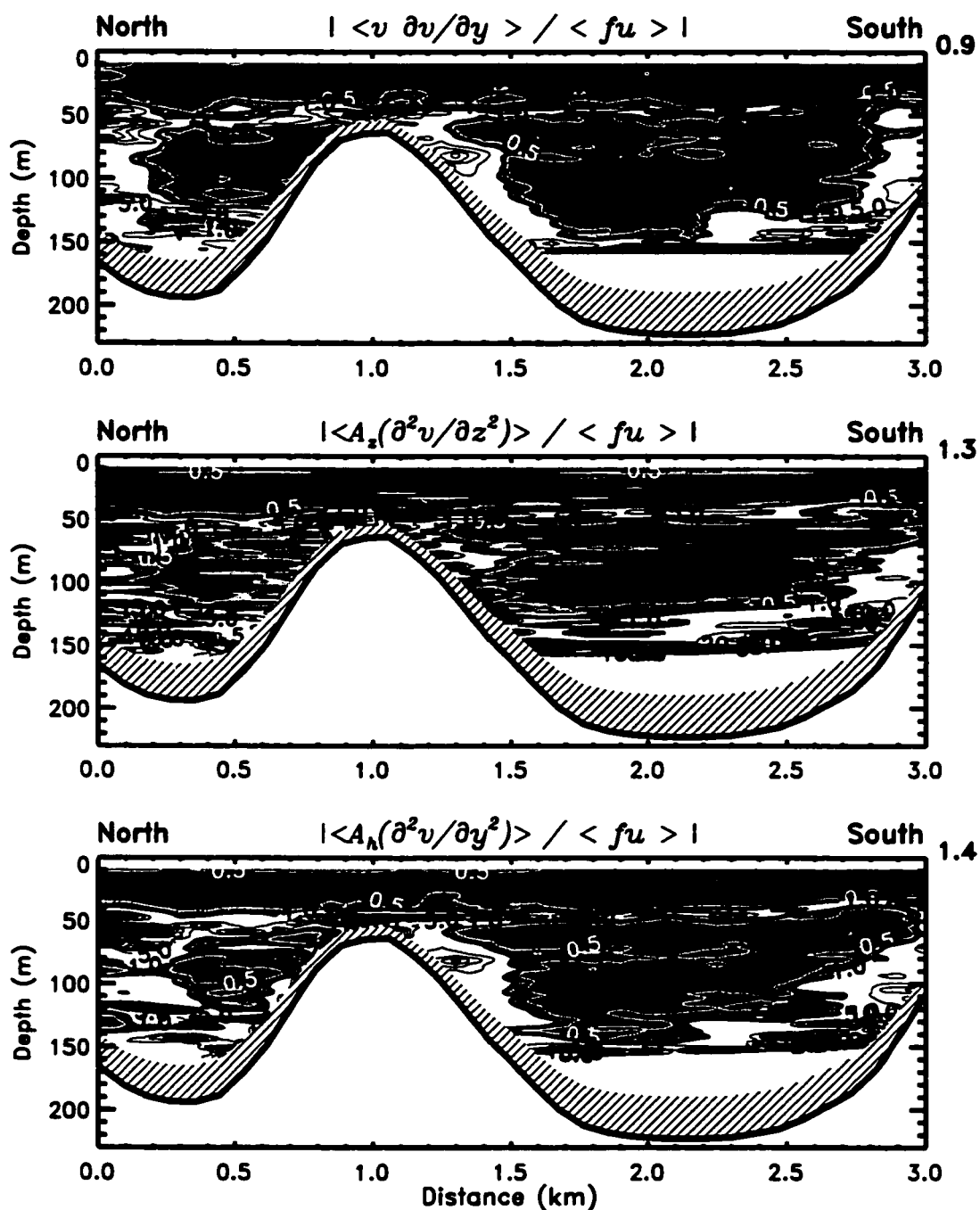
Figure 12. Ratios of absolute values of the tidally averaged advective term, vertical friction term and horizontal friction term to the tidally averaged Coriolis acceleration. Darker tones denote values below 1 and white denotes values over 1. The absolute value of the sectional mean is shown at the upper right corner of each panel. The advective, vertical friction and horizontal friction terms were comparable to Coriolis accelerations (contours shown: 0.5, 1, 5, 10, 15,..). Data in the shaded region near the bottom were not considered in the analysis due to side lobe effects. White region near the bottom was out of the profiling range of the ADCP.

Bernoulli-type flow, to a balance that also includes friction during wind events. The terms in the along-fjord momentum balance may be given by

$$<v(\partial u/\partial y)> - <fv> = - <1/\rho \, (\partial p/\partial x)> + <A_z(\partial^2 u/\partial z^2)> + <A_h(\partial^2 u/\partial y^2)> \qquad (2.2)$$

Again, with the exception of the pressure gradient term, these were the terms that could be reliably estimated from the measurements. The ratios of the advective term, vertical friction term and horizontal friction term to Coriolis term (not plotted here) showed absolute values of the sectional means of 1.4, 2.6, and 1.3, respectively. This revealed that, in the along-fjord momentum balance, vertical and horizontal friction were also as important as advection.

The contribution of advection to the momentum balance is supported by the distribution of the tidal current amplitudes. The greatest value was observed over the shallow areas as expected from a Bernoulli-type balance. In other systems, where bottom friction is influential, the transverse distribution of tidal current amplitudes follows the bathymetry with greatest values appearing in the region where the depths are greatest [*Li and Valle-Levinson*, 1999].

With respect to the frictional influences, further investigations are required to reveal the main frequencies of the wind stress in the region. If a strong diurnal (24 h) period is found, as observed by *Pickard and Rodgers* [1959], *Farmer* [1976] and *Farmer and Osborn* [1976] in fjords of British Columbia, the system could be affected by high-frequency (>1 cycle/day) fluctuations in the across-fjord momentum balance.

In summary, during the sampling period the mean flow showed a three layer structure that was consistent with up-fjord wind-induced exchange: a thin (< 8m) weak outflow close to the surface due to river discharge; a layer of inflow (down-wind) underneath attributed to the effect of wind-stress; and a deep compensatory outflow due to the barotropic pressure gradient set up by the wind. The bank had salient effects on the across-channel distribution of subtidal flow by shifting the location of strongest near-surface inflow and strongest mid-depth outflow to the channels, by masking the three layer vertical structure, by shifting the flow direction away from the bank, by inducing recirculation at its top, and by causing a bifurcation of the flow below the pycnocline. Evidences of wind-induced upwelling observed during the sampling period indicated that the across-fjord momentum balance likely switches from quasigeostrophic during calm winds to a balance that in the surface is influenced by non linear effects (from wind stress and advection) during wind episodes, and remains quasigeostrophic in the interior.

REGION OF CHACAO CHANNEL

3.1 Introduction

Extremely energetic tidal channels where currents exceed 3 m/s are rare. Maximum

currents of 8 m/s for Seymour Narrows in British Columbia, Canada, are frequently

quoted among the highest speeds measured [*Pond and Pickard*, 1998]. The common

feature observed in every case of an energetic tidal channel is a high tidal range. Some of

the highest tidal ranges have been reported for St. John River, Bay of Fundy, Canada

[*Redfield*, 1980], Minas channel, Bay of Fundy [*Tee*, 1976], South Korea [*Wells*, 1983],

and St.Malo, France [*Defant*, 1961, p.377], with records of 7 m, 15 m, 5-9 m, and 8-10 m,

respectively. Examples of strong tidal currents in relatively deep (>80 m) channels or

fjords are unusual. Some of them may be found in southern Chile, where a characteristic

fjord-like coastal morphology covering about 2000 km of the Chilean coastline shows a

variety of channels connecting the open ocean to the Inland Sea (Figure 13a). One of

those channels is Chacao Channel, located in the northernmost part of the region of fjords

in the Chilean Inland Sea. It represents one of the two direct openings between the ocean

and the Inland Sea, the other being Guafo Mouth. Chacao Channel connects the open

ocean with the Gulf of Ancud in the east-west direction and is approximately 40 km long

with an average width of 4 km (Figure 13b).

The channel exhibits tidal currents of 3 to 4.5 m/s and tidal ranges of 5.5 to 6.0 m

[*SHOA*,1993a; *SHOA*, 1995]. These currents are developed from the differences in tidal

range between the east and west ends of the channel. Tidal range enlarges as the tidal

wave propagates from west to east, with a remarkable increase from ~2 m in the west side
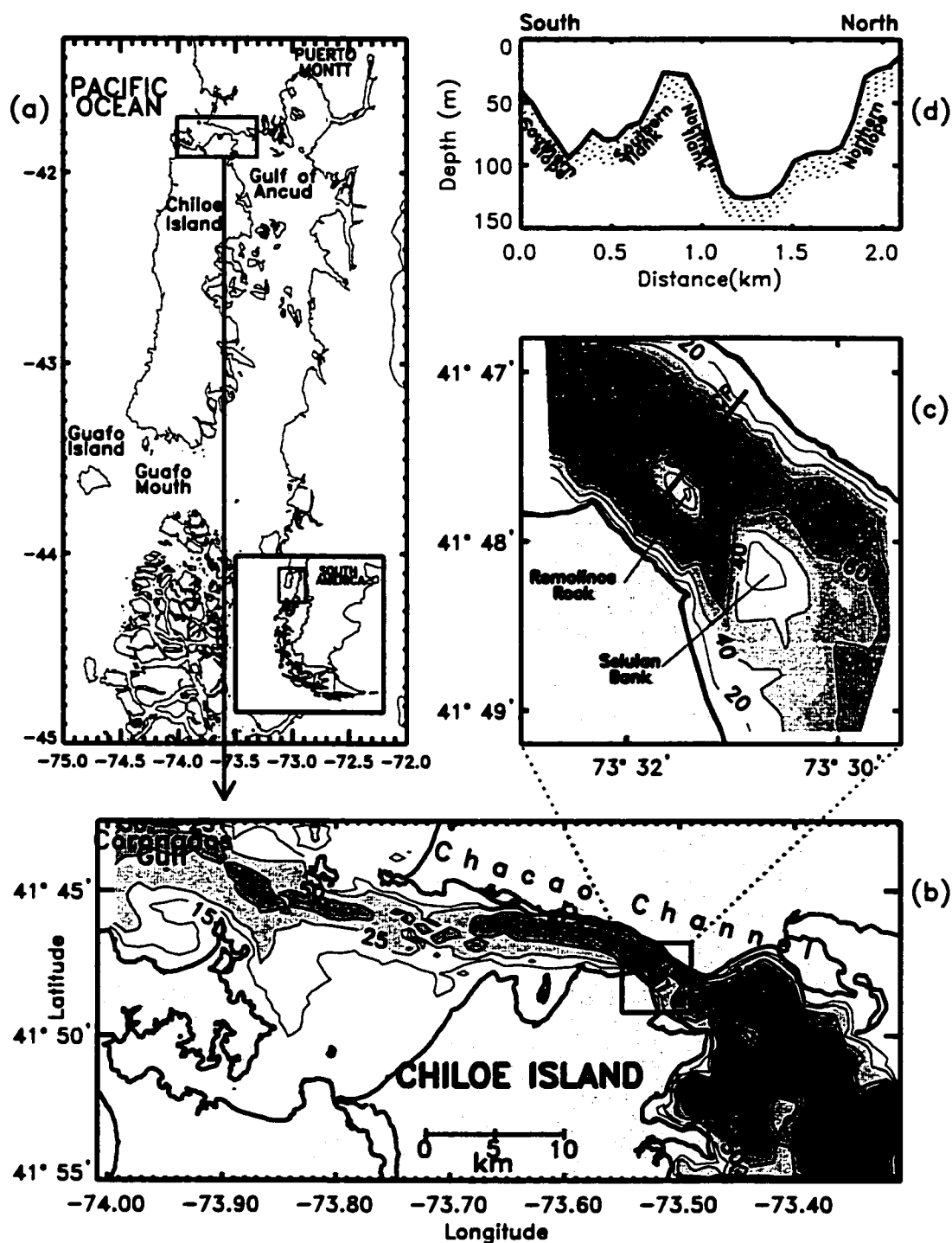
Figure 13. (a) General study area on the southern coast of Chile. (b) The measurements obtained during this experiment were made in the box shown at the narrowest part of Chacao. Channel. (c) The ADCP profiles were made in the transect (~2.2 km length) over Remolinos Rock. (d) Bottom profile associated with the ADCP transect (looking toward the ocean). Contours shown: 15, 25, 50, 75, 100, 200, 250 m.

(Coronados Gulf) to ~6 m in the east side (Gulf of Ancud). The reason for this amplification is still under investigation, but it may be partially explained by resonant effects of the tidal wave that enters through Guafo Mouth to the south and propagates northward, along the east side of Chiloe Island up to the Gulf of Ancud. This hypothesis is supported by tidal gauge records showing a continuous increase of tidal ranges in the transit from Guafo Mouth (~2 m) to Gulf of Ancud (~6 m). Slack waters in Chacao Channel are brief (<15 min) and some times they are undetectable to the casual observer. Northwesterly and southwesterly winds may enhance the tidal current entering the channel during flood and decelerate it during ebb, enhancing sea roughness.

Freshwater input to Gulf of Ancud comes from rivers draining westward from the Andes. The water circulation in Chacao Channel is weakly influenced by river flow with typical salinities during the spring season in Coronados Gulf and in the center of Gulf of Ancud in the range of 32.9 - 33.1 and 29.0 - 32.0, respectively (SHOA, pers.comm). The geomorphology of Chacao Channel reflects carving by past glaciation. Its bathymetry features an isolated pinnacle ca. 20 m depth located at ~0.7 km from the southern side (Chiloe Island) in the narrowest part of the channel (Figures 13c and 13d). This pinnacle separates two channels, a southern channel (~85 m depth), and a northern channel (120 m depth). During very low tides, the rocks at the summit of the pinnacle may be seen above water [*SHOA*, 1995]. These rocks are called Rocas Remolinos (from spanish "eddies rocks") in nautical charts [*SHOA*, 1993a]. The flanks of the pinnacle have slopes of ~16° in its northern side and ~14° in its southern side. At ~1.5 km to the southeast of

Remolinos Rocks, toward the Inland Sea, is Seluian Bank (Figure 13c): a shoal of ~20 m

depth skewed towards the southern side of the channel.

In terms of the transverse dynamics, the geostrophic approximation might be

appropriate for flow over low aspect ratio (vertical scale/horizontal scale) bathymetric

features, and relatively weak currents (<1 m/s). However, for features with high aspect

ratio, where the fractional height (feature relief / water column depth) is greater than 0.7

[following *Chapman and Haidvogel*, 1992], the fluid column may be stretched and

compressed, leading to relatively large velocities and particle excursions. In Chacao

Channel the interaction of strong tidal currents with a pinnacle at the narrowest region of

the channel suggests the generation of nonlinear tidal effects, such as overtides and

bathymetrically-induced flow accelerations. The stretching and contraction of streamlines

around the pinnacle would invalidate the geostrophic approximation and make the

frictional and advective accelerations relevant to the across-channel momentum balance.

In particular, enhanced mixing processes would dominate stratifying tendencies.

Overtides, which are harmonic motions with higher frequencies than the semidiurnal,

may be caused by nonlinear accelerations and frictional terms [*LeBlond*, 1991]. The

source terms for quarter-diurnal tides (e.g. M_4) usually arise from nonlinearities in the

continuity equation, advection, and the depth effect on bottom friction; while the sixth-

diurnal tides (e.g. M_6) are forced mainly by terms from bottom friction [*Parker*, 1991;

Walters and Werner, 1991]. In any case, overtides indicate predominance of non-linear

effects.

This study quantifies and describes the transverse variability produced by the interaction of strong tidal currents with a pinnacle in the middle of a channel. It presents estimates of key terms in the across-channel momentum balance to assess the validity of the geostrophic approximation.

3.2 Data collection and processing

A 307.2 kHz RD Instruments ADCP and a Trimble Global Positioning System (GPS) interfaced to a laptop computer were used to obtain velocity profiles in the sampling area during one complete semidiurnal tidal cycle on October 7, 1998, three days after secondary neap tides (the weakest neap tides of the month). The ADCP was mounted on a catamaran ~ 1.2 m long, which was towed from the starboard side of the diving boat "Virago" at approximately 2.5 m/s. A current profile was recorded every ~4 seconds (or ping rate= 4 s) with a 30 second averaging period. An across-channel transect (Figure 13c) was traversed 25 times during the 12.5 hours of data collection. The ADCP data were calibrated according to *Trump and Marmorino* [1997] and bad data removed following the procedure explained by *Valle-Levinson and Atkinson* [1999]. After the heading correction was applied, the data were rotated 13° clockwise to an along- (u flow) and across- (v flow) channel coordinate system. This was the direction of greatest variability of the tidal currents and of weakest across-channel tidal flows. CTD stations were made at the end of each transect and at a deeper (ca. 120 m) station in the channel. The present work was carried out during calm wind conditions.

The semidiurnal tide (represented by the M_2 constituent) and its harmonic overtides (represented by the M_4 and M_6 constituents) were separated from the subtidal signal of the

observed flow components using sinusoidal least squares regression analysis [e.g. *Lwiza et al.*, 1991]. The overtides were obtained for a preliminary assessment of non-linear influences to the momentum balance. The root-mean-squared (rms) errors of the least-square fits were between 0.2 and 0.5 m/s and the mean error was about 0.3 m/s. This was between 5 and 10 % of the currents observed.

After determining the relevance of nonlinear influences through overtides, the relative magnitude of the advective and frictional terms was compared to that of the Coriolis accelerations. To do this a right-hand coordinate system was adopted for which *y* (across-channel direction) was positive toward 13° true and *x* (along-channel direction) was positive to 103° true. It followed that the along-channel and across-channel components of the velocity were given by *u* and *v*, respectively. In the across-channel direction, the subtidal momentum balance can then be given by

$$<v(\partial v/\partial y)> + <fu> = - <1/\rho\ (\partial p/\partial y)> + <A_z(\partial^2 v/\partial z^2)> + <A_h(\partial^2 v/\partial y^2)> \qquad (3.1)$$

where $v(\partial v/\partial y)$ is representative of the advective term, fu is the Coriolis term ($f= 9.7\times10^{-5}$), $1/\rho(\partial p/\partial y)$ is the pressure gradient term ($\rho=$ seawater density), $A_z(\partial^2 v/\partial z^2)$ is the vertical frictional term, $A_h(\partial^2 v/\partial y^2)$ is the horizontal frictional term and brackets ($< >$) denote tidal averages. With exception of the pressure gradient term, these were the terms of the complete momentum balance that could be reliably approximated.

The magnitudes of each term were used to compare their relative contribution to the momentum balance in the across-estuary direction. A constant vertical eddy viscosity

A_z=0.01 m²/s was used following estimates of *Bowden and Hamilton* [1975], *Csanady*

[1975], *Ott and Garrett* [1998], and *Geyer et al.* [2000]. Also a constant horizontal eddy

viscosity A_h=90 m²/s was used following estimates of *Smith* [1996] and *Pingree and*

Maddock [1978]. Both A_z and A_h are probably underestimated relative to the strong tidal

currents observed here. Although A_z and A_h are expected to change in space and time,

constant values were used here for diagnostic purposes and to facilitate the calculations.

3.3 Results

This section presents the across-channel distribution of the subtidal and tidal flows

for the period of observation. It also describes the time evolution of vertical salinity

profiles made at the extremes of the ADCP transect and a vertical density profile made in

the middle of the northern channel to illustrate stratification conditions. Additionally, it

presents the magnitudes and across-channel distributions of the terms indicated in (3.1),

with exception of the pressure gradient term. A comparison among the magnitude of

various terms is shown at the end of this chapter.

Mean flow

The along-channel mean flow over the period of observations is shown in Figure 14.

The flow structure was significantly influenced by bathymetry. Net inflows were located

over the slopes (as denoted in Figure 13d) and over the top and southern flank of the

pinnacle. Net outflows were observed over the southern channel and over the northern

flank of the pinnacle. The pinnacle seemed to play a role in determining this distribution.

The residual flow might be attributed to the nonlinearities of the dynamics of tidal flow as

indicated by the theoretical results of *Li and O'Donnell* [1997]. They also found that the
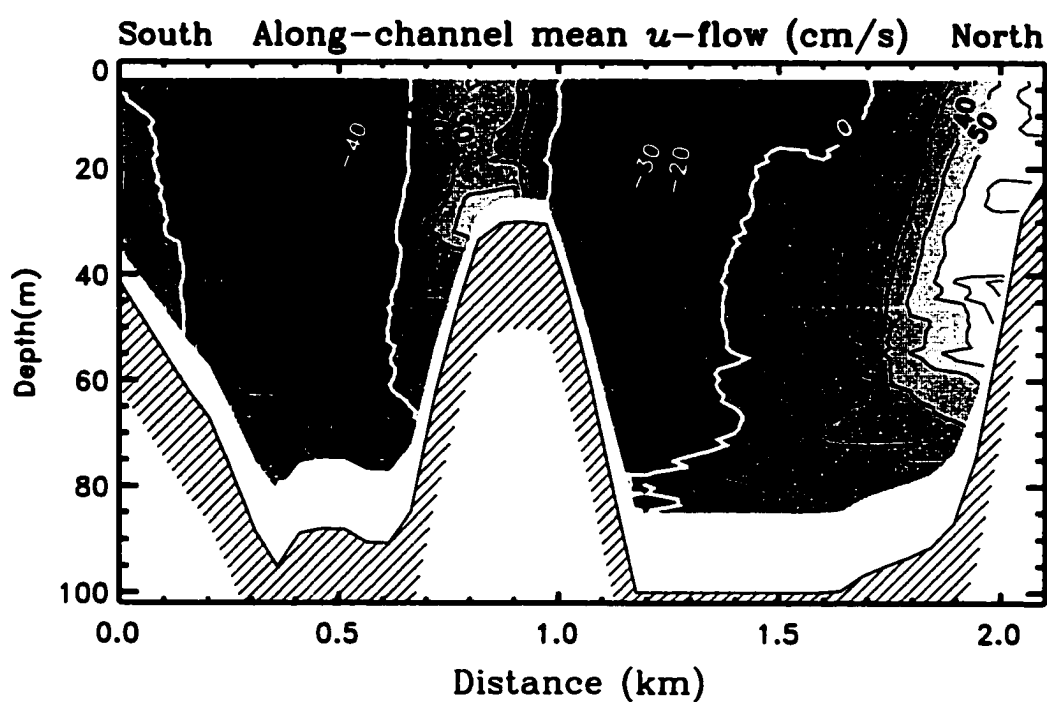
Figure 14. Across-channel distribution of the along-channel mean flow (looking toward the ocean). The mean flow showed a transverse structure where net inflows (lighter) were observed over the shallow regions and net outflows (darker) over the southern channel and northern flank of the Remolinos Rock. Data in the white region near the bottom were not considered in the analysis due to side lobe effects of the ADCP measurements.

exchange flow was correlated with the topography, as a net landward flow occurred over the shoals and a return flow in the channels. In the case of this work, the distribution exhibited weak vertical structure dominated by strong lateral shears ($\partial u/\partial y$). Over the sloping bathymetry the lateral shears were comparable to the vertical shears. Maximum velocities were about 60 cm/s in the northern slope, a comparable value to 76 cm/s observed in Minas Channel, a tidal channel with currents of 5.6 m/s [*Tee*,1976].

The mean v flow (Figure 15a) exhibited a mean absolute magnitude in the section of about ~9 cm/s, which was almost one half of the mean value (~22 cm/s) of the along-channel mean flow (Figure 14). It also showed five changes of direction near the surface from north (positives) to south (negatives) in just 2 km, thus determining regions of strong convergence and divergence dominating the upper 40 m. This was more clearly seen in the distribution of the transverse gradients $\partial v/\partial y$ (Figure 15b). Two strong changes in direction (negative values, darker tones) are observed on both flanks of the pinnacle, while sudden increases in v velocity (positive values, lighter tones) are represented by the gradients over the southern slope and over the pinnacle. The magnitude of these gradients is up to ~ 10^{-3}, i.e., they are one order of magnitude greater than those reported for example in the lower Chesapeake Bay [*Valle-Levinson and Atkinson*, 1999]. Magnitudes of the lateral variations of the v component were comparable in some regions of the section to those of the vertical variations $\partial v/\partial z$ (not plotted here).

Tidal current amplitudes

The distribution of the semidiurnal tidal current amplitude (Figure 16a) showed the
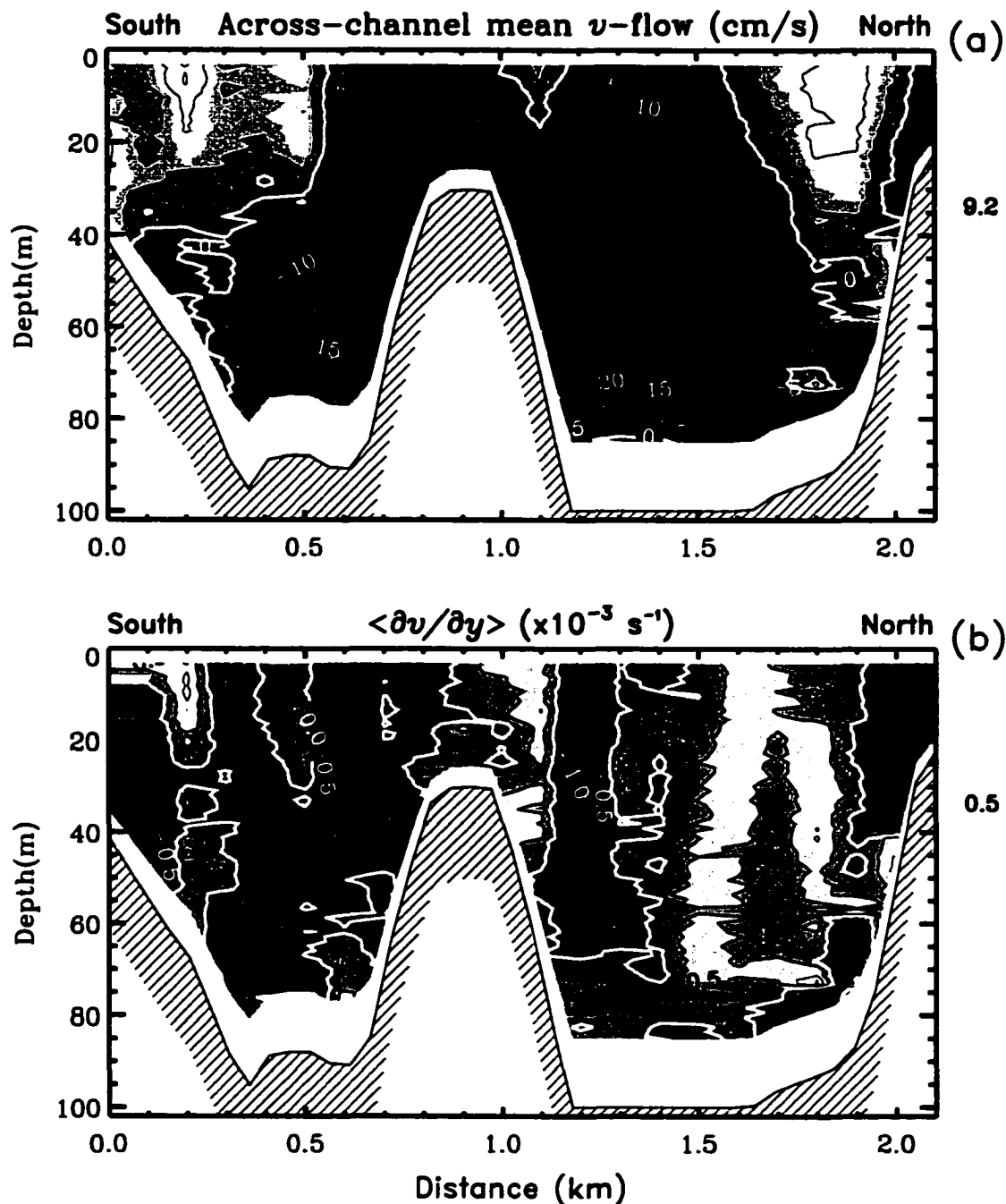
Figure 15. (a) Across-channel component of the mean flow. Negative values indicate currents toward the north. (b) Contours of the tidally averaged divergence of the across-channel flow. Positive values (darker tones) indicate convergence regions (looking toward the ocean). Data in the white region near the bottom were not considered in the analysis due to side lobe effects of the ADCP measurements.
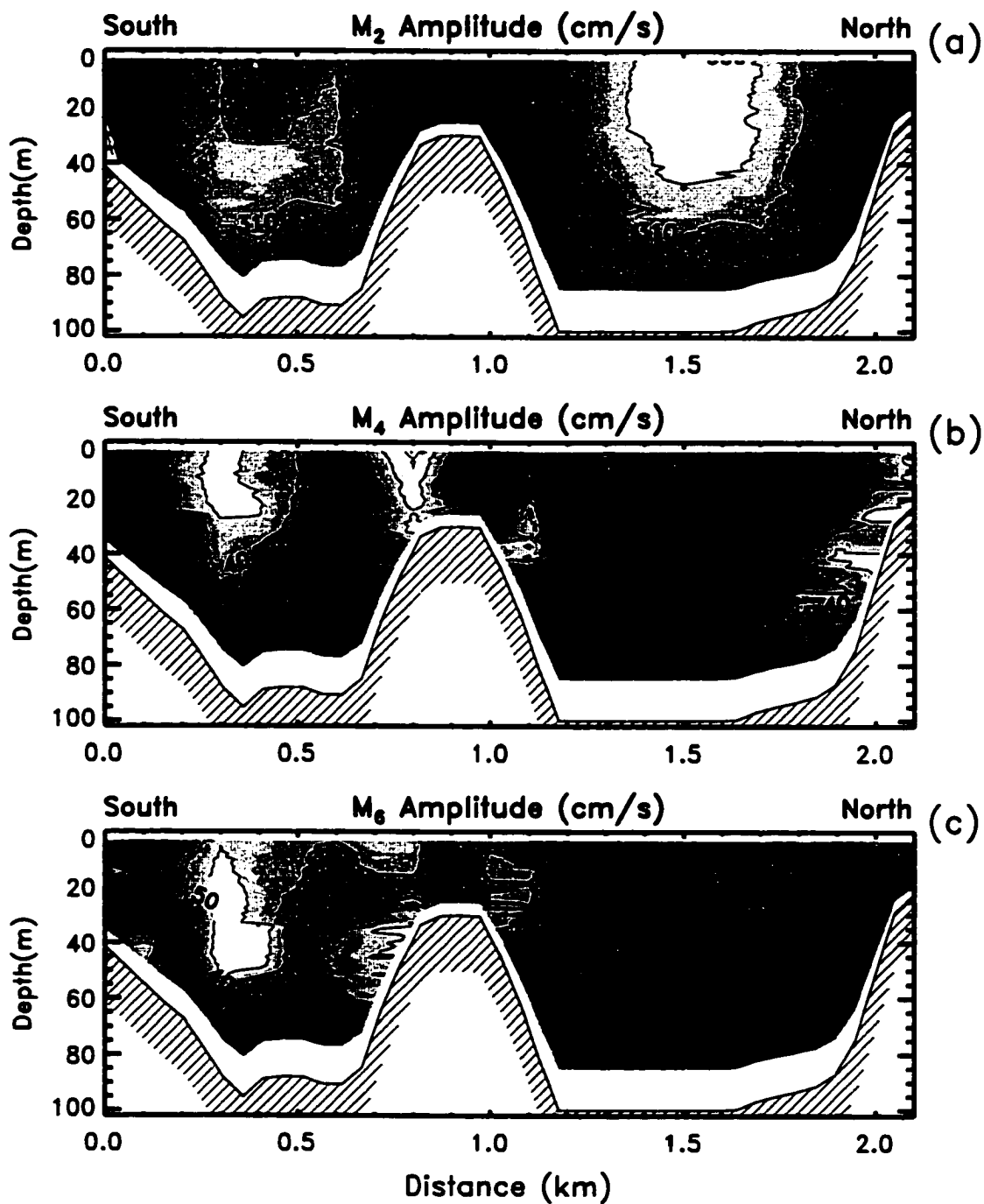
Figure 16. Across-channel tidal amplitude distributions for the (a) M_2 constituent, (b) M_4 and (c) M_6 obtained from the ADCP current measurements (looking toward the ocean). Data in the white region near the bottom were not considered in the analysis due to side lobe effects of the ADCP measurements.

highest velocities centered at mid-depth in the southern channel (~3.2 m/s) and near surface in the northern channel (~3.4 m/s). Effects of bottom friction were evident as velocities decreased near the bottom and over shallow areas. Similarly to the mean flow, the lateral variations were larger than the vertical variations. In general this was also the case for the distribution of the quarter-diurnal (Figure 16b) and sixth-diurnal (Figure 16c) tidal current amplitudes. Highest values of the quarter-diurnal current amplitudes were found at different locations: near surface in the southern channel, over the pinnacle, in the northern flank and in the northern slope. In the case of the sixth-diurnal tidal currents the highest values were located in the southern channel with a peak at mid-depth, in the southern flank, and around the summit of the pinnacle. It is noteworthy that the highest values of the quarter-diurnal and sixth-diurnal amplitudes overlap the surface region of the southern channel, and that semidiurnal highest values in this channel have been shifted to mid-depth. Thus, the strongest overtide amplitudes were located over the pinnacle, on the slopes and in the southern channel. The northern channel was mostly influenced by semidiurnal tidal currents. The southern channel is shallower and narrower than the northern and friction may play a role in determining the enhancement of overtides in the southern side. The large overtides in the southern channel may have been then caused by nonlinearities that arise from a) increased frictional effects because of its shallowness and b) spatial gradients in the flow at Seluian Bank to the southeast of the sampling transect.

The southern channel was also characterized by larger tidal velocities than the northern side (Figure 14), which could be explained by the effect of Bernoulli type

accelerations originated away from the pinnacle, possibly the Seluian Bank. In order to

further explore the strength of nonlinearities through tidal asymmetries [e.g. *Speer et al.*,

1991], the phase relationship (2 M_2-M_4) and a ratio of the amplitude of the quarter-diurnal

flow to the amplitude of the semidiurnal flow (M_4/M_2) were explored . Tidal distortion

was observed in the relative phase (2 M_2-M_4) shown in Figure 17. Values between $0°$ and

$180°$ indicated a longer falling than rising tide and hence a tendency toward flood-

dominance. Longer rising tide and ebb-dominant conditions were indicated by a (2 M_2-

M_4) relative phase between $180°$ and $360°$ [*Speer et al.*, 1991]. This indicated a tendency

for a flood-dominated regime over the shoals, in agreement with the net inflow observed

there. Figure 17 remarkably matches the regions of mean inflow and mean outflow in

Figure 14, exhibiting a tendency to flood and ebb-dominance, respectively. The ratio of

M_4 to M_2 amplitude (not plotted here) also showed the highest values over the pinnacle

and over the northern slope, consistent with the mean flow. It then follows that the main

characteristics of the mean flow were derived from strong tidal asymmetries as observed

in these tidal patterns.

Overtidal current amplitudes observed in other channel systems with tidal currents of

~1 m/s have shown that quarter-diurnal amplitudes were typically about three times larger

than the sixth-diurnal amplitudes in English Channel [*Le Provost and Forferino*, 1985].

The results reported here have shown that both components exhibit comparable values,

which has been rarely reported. This suggests that in the generation of the sixth-diurnal

overtide there is probably a source that is less relevant in other systems but important

here, such as horizontal friction, and since this is an initial indication of the importance of
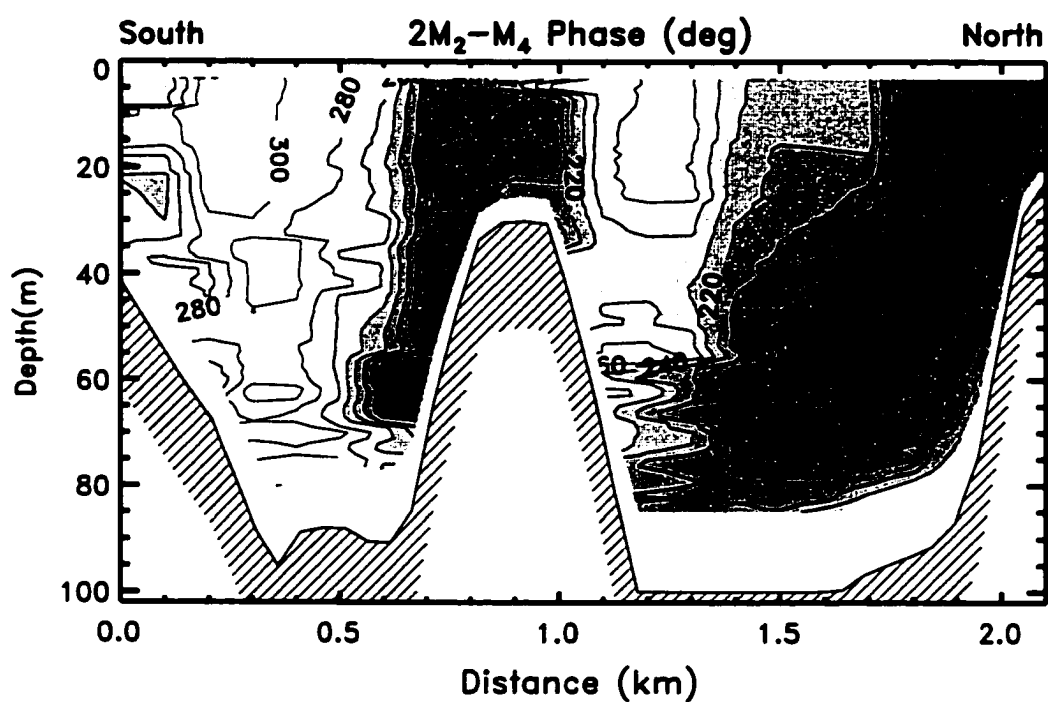
Figure 17. Across-channel distribution of the $2M_2$-M_4 phase relationship. Values below 180° suggest flood-dominance (looking toward the ocean). Data in the white region near bottom was not considered in the analysis due to side lobe effects of the ADCP measurements.

friction (both horizontal and vertical) to the momentum balance, it should be worthy of further investigation.

Salinity and temperature profiles

In general all the stations showed a nearly vertically homogeneous water column. Figure 18 corresponds to the vertical profile of temperature and salinity CTD data obtained from a station in the deepest part of the northern channel. Stratification was very weak in the deepest water column of the section, as temperature changed by 0.2 °C and salinity by 0.15 over a depth of 130 m. All profiles showed a strong correlation between temperature and salinity data (correlation coefficient =-0.92), indicative of near-conservative mixing. Figure 19 shows the evolution in time of the salinity field for the CTD stations in the northern and southern extremes of the transect. Current vectors are plotted on it to show the tidal phases. No vertical structure was observed and changes in salinity seemed to respond to changes in the velocity field. Highest and lowest salinity values approximately appeared at the times of slack waters. Differences in time for maximum values of salinity appearing in the northern side relative to the southern side, were consistent with flood-dominance (northern) and ebb-dominance (southern) asymmetry shown in the relationships between the quarter-diurnal and sixth-diurnal tidal constituents (Figure 17).

Across-channel dynamics

The across-channel distributions of the tidally averaged Coriolis term $< fu >$, the advective term $< v(\partial v/\partial y) >$ and the frictional terms $< A_z(\partial^2 v/\partial z^2) >$ and $< A_h(\partial^2 v/\partial y^2) >$ were used to establish their relative contribution to the across-channel momentum
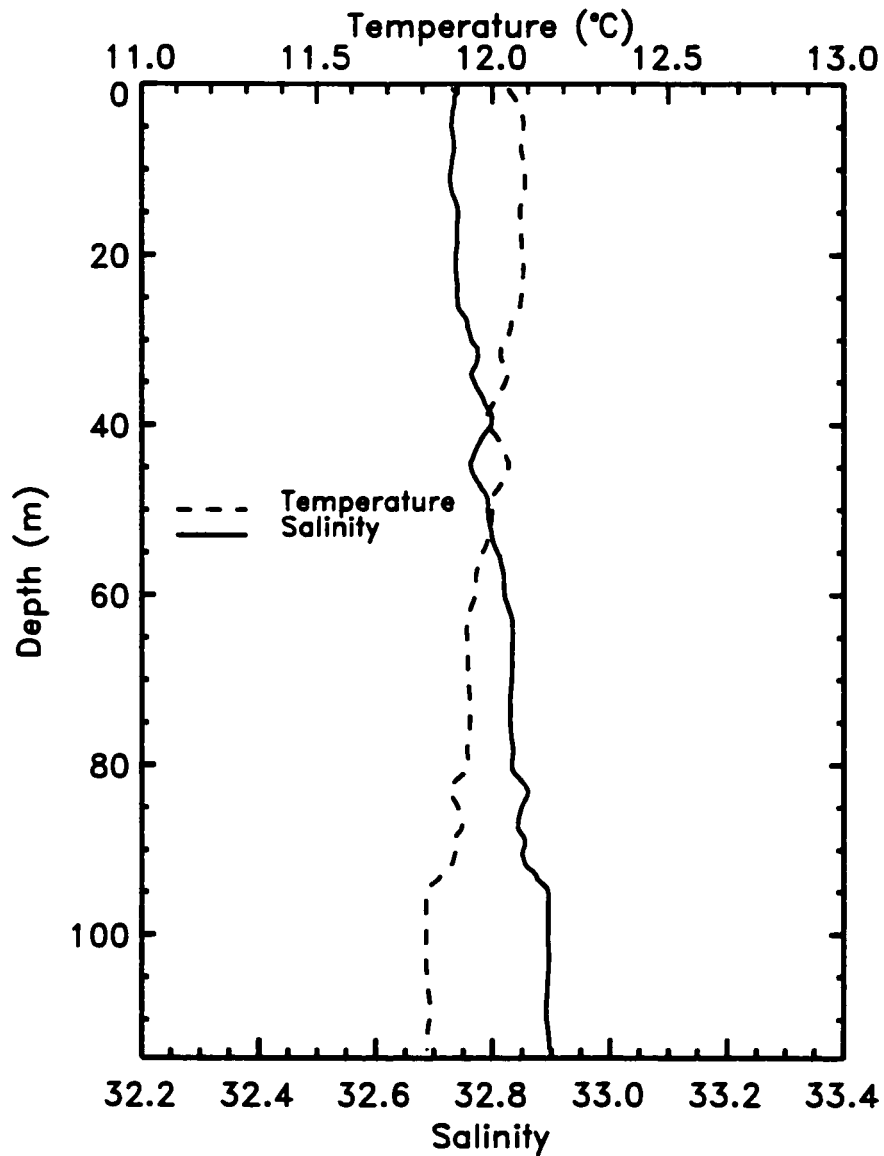
Figure 18. Salinity and temperature profiles in the deepest (~120 m) region of the northern channel. Vertical stratification is weak and an inverse correlation between temperature and salinity is observed.
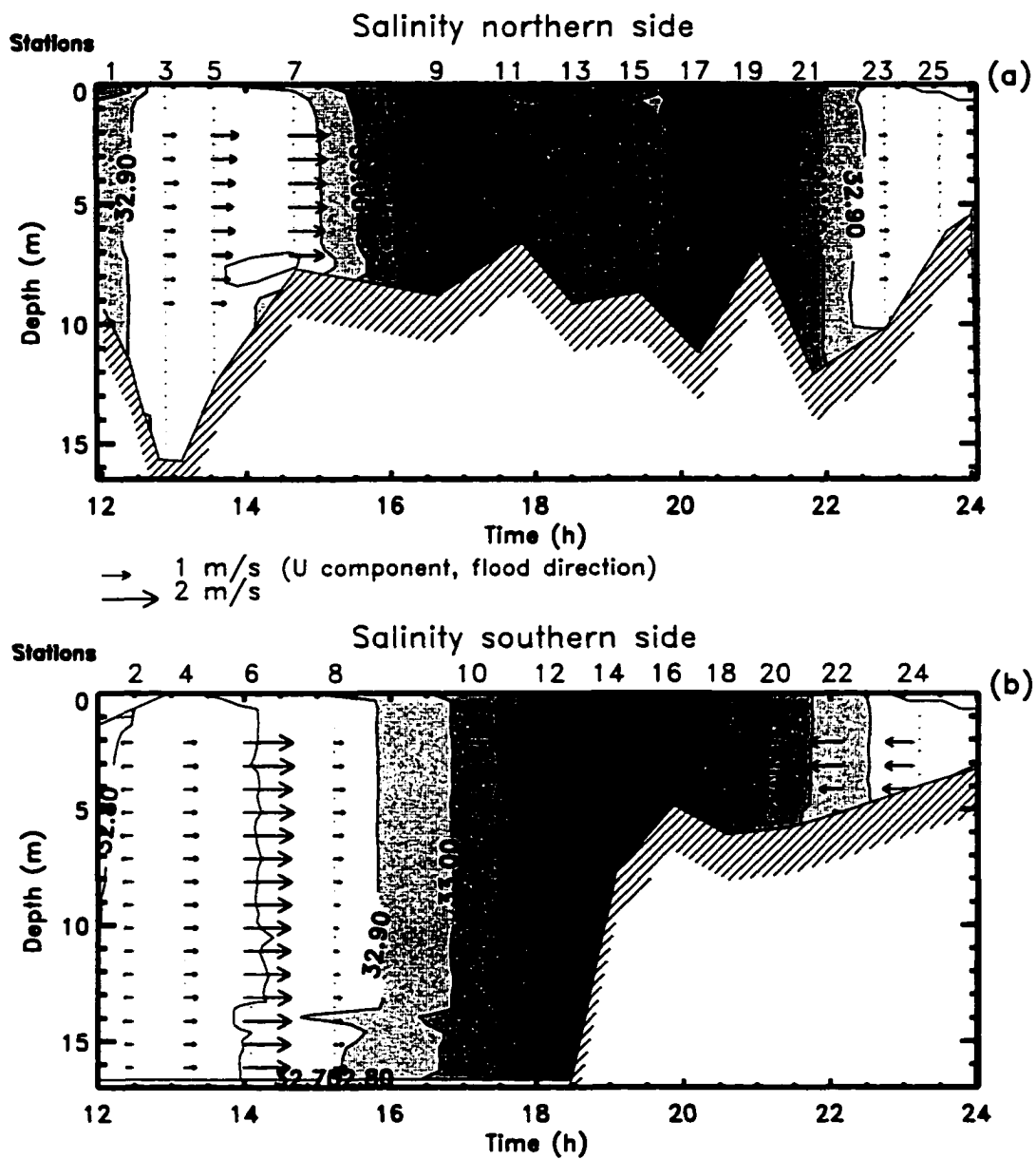
Figure 19. Time series of salinity profiles at the (a) northern and (b) southern sides. Contour interval is 0.1. Bottom changes are due to tidal variability but also to the inability to occupy the same location because of the current-induced drift of the idle boat.

balance. Figures 8 and 9 show the distribution of the Coriolis, advective and frictional

terms. As expected, the Coriolis term (Figure 20a) resembled the u mean flow

distribution (Figure 14), as it is directly proportional to it. The advective term (Figure

20b) distribution showed values of almost one order of magnitude greater than those of

the Coriolis term. They were highest over the northern flank of the pinnacle and over the

southern slope. The dominance of this term is derived from the extraordinarily high

absolute values of the lateral convergence $|(\partial v/\partial y)|$ previously mentioned, which were

typically 1.0 to 2.0 x10^{-3}, i.e, a change of 0.1 to 0.2 m/s in just 100 m in the cross-channel

direction. The vertical friction term $A_z[\partial^2 v/\partial z^2]$ (Figure 21a), which again is diagnostic

owing to the constant A_z, showed the highest values not only around the flanks but also

over the pinnacle and close to the bottom, as expected from bottom friction effects. This

term was typically five times greater than fu (Figure 20a). In turn, the horizontal friction

term $A_h[\partial^2 v/\partial y^2]$ (Figure 21b) was also strongly influenced by the changes of the v

velocity component in the cross-channel direction. The greatest values appeared on both

sides of the pinnacle and over the southern slope. Their magnitudes were about four times

greater than those observed for the advective term (Figure 20b) and they were at least one

order of magnitude greater than the Coriolis term (Figure 20a). This is a revealing result

as this term is customarily neglected from the momentum balance. Although the value of

A_h used here is nominal, the order of magnitude of the horizontal friction term suggests

that it is important to the dynamics. This becomes evident from the marked boils and

recirculations observed during the data collection, similar to those described in *Farmer et*

al. [1995].
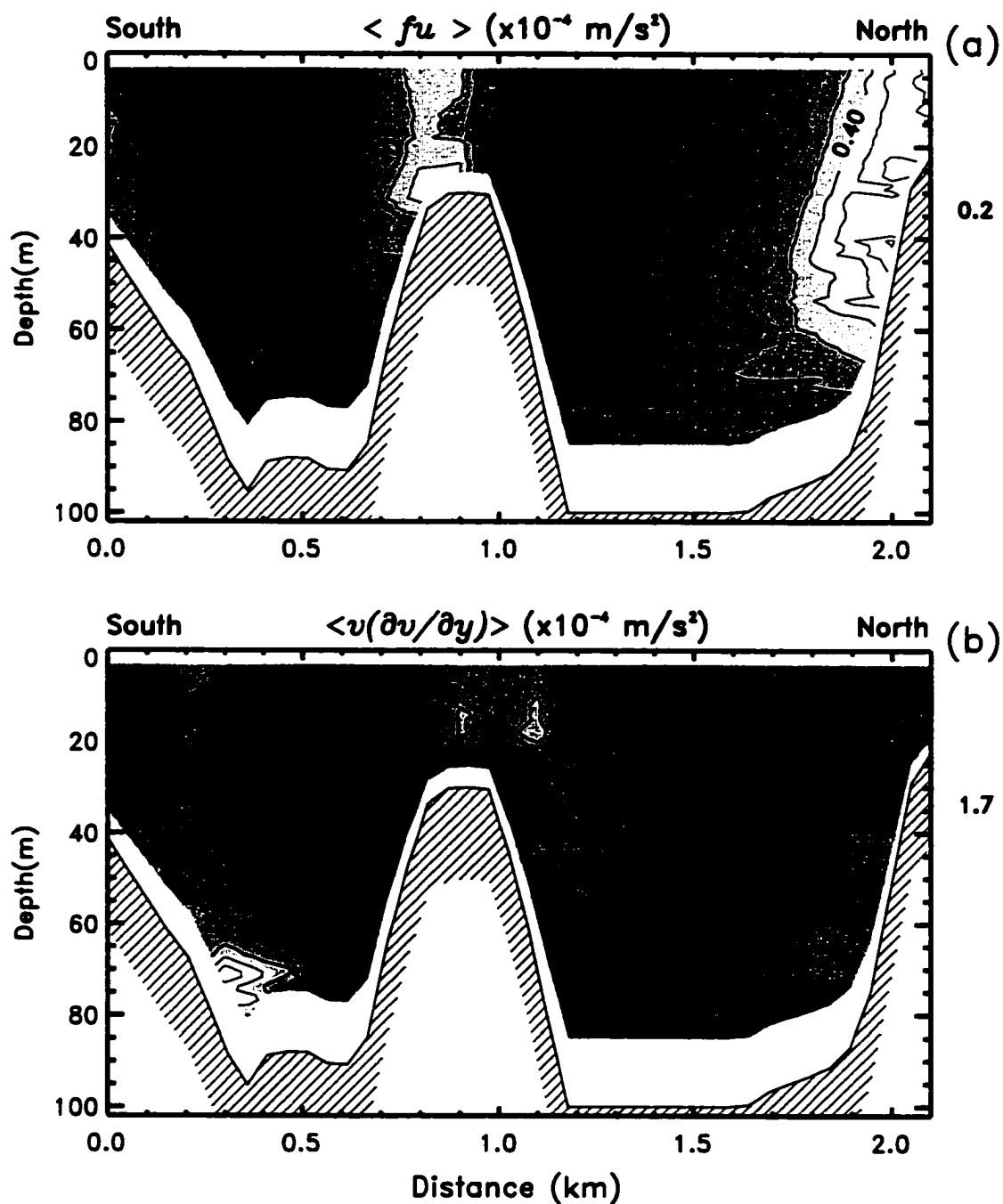
Figure 20. Contours of the tidally averaged (a) Coriolis term and (b) advective term. Looking toward the ocean. Data in the white region near the bottom were not considered in the analysis due to side lobe effects of the ADCP measurements.
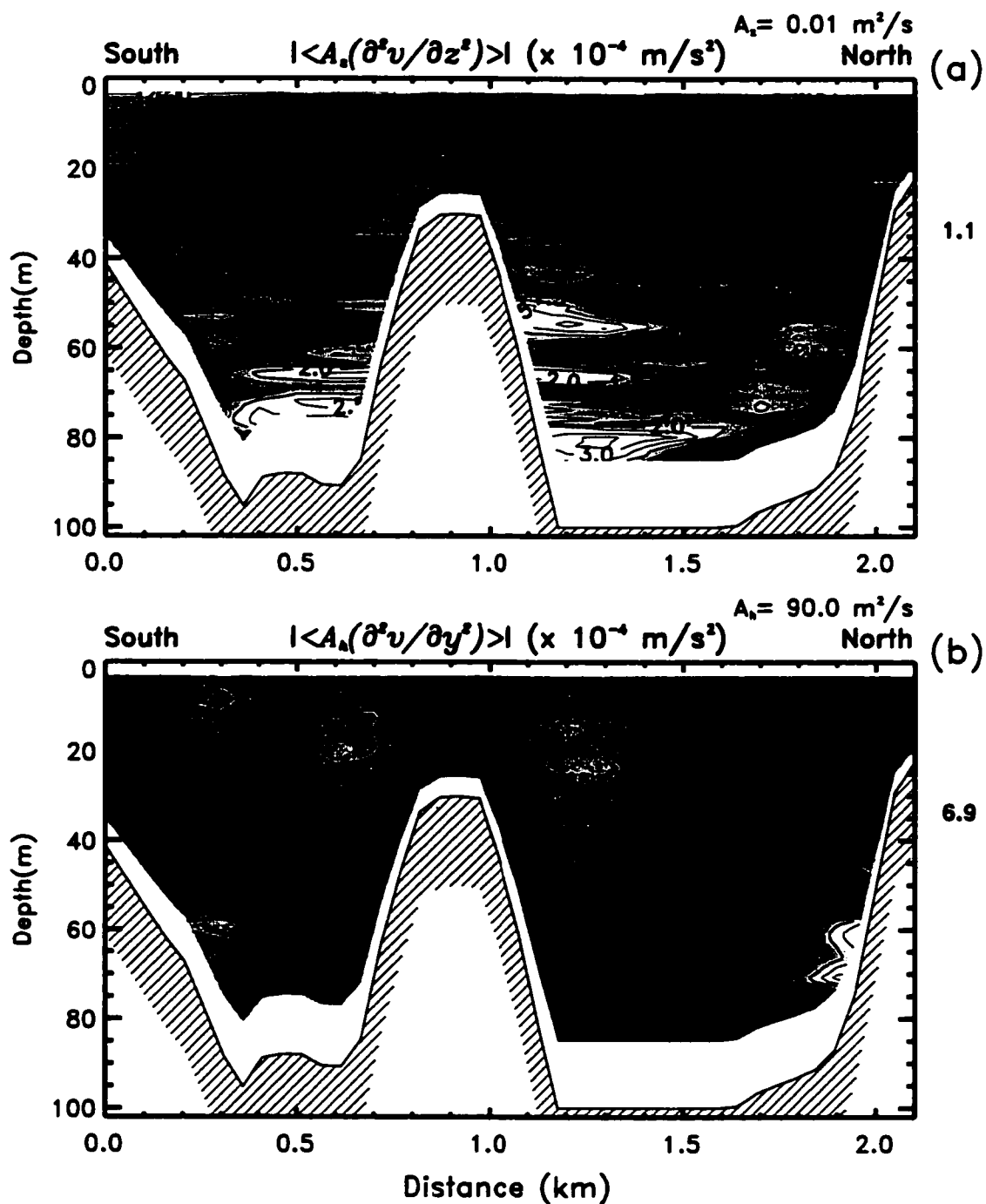
Figure 21. Contours of the tidally averaged (a) vertical frictional term and (b) horizontal frictional term. Looking toward the ocean. Data in the white region near the bottom were not considered in the analysis due to side lobe effects of the ADCP measurements.

Sectional means for the distributions of the absolute values of the Coriolis term, the

advective term, the vertical frictional term and the horizontal frictional term were 0.22

(Figure 20a), 1.7 (Figure 20b), 1.09 (Figure 21a) and 6.88 (Figure 21b), respectively.

Then the approximate relative magnitude of these terms in the y direction diagnostically

becomes:

$$ 1 \quad : \quad 8 \quad : \quad 5 \quad : \quad 31 \qquad (3.2) $$

Coriolis Term	Advective Term	Vertical Frictional Term	Horizontal Frictional Term

The dominance of the advective term and the horizontal friction term in this balance

is clearly due to the influence of the lateral divergence $\partial v/\partial y$, which was particularly high

around the pinnacle and on the southern slope. This is most likely induced by the effect of

the Remolinos Rocks in shaping the across-channel current distribution. Values in (3.2)

also suggested that the across-channel dynamic balance is mostly between advective

accelerations and friction. The baroclinic pressure gradient might not be relevant to this

balance as differences in salinity (Figure 18) between both sides of the channel were low.

However, the barotropic pressure gradient could be important if the transverse slopes in

sea level are of the order of 10^{-5} or 1 cm in 1 km, which may be possible in this area. A

spatial comparison between the Coriolis accelerations and the advective and frictional

terms is presented in Figure 22. As suggested by the mean values in (3.2), the

distributions show a clear dominance of frictional over Coriolis accelerations, because the

ratios are greater than 1 nearly everywhere, except for spotty regions. On the other hand,

highest values in the northern channel (Figures 22a and 22c) might be attributed to the
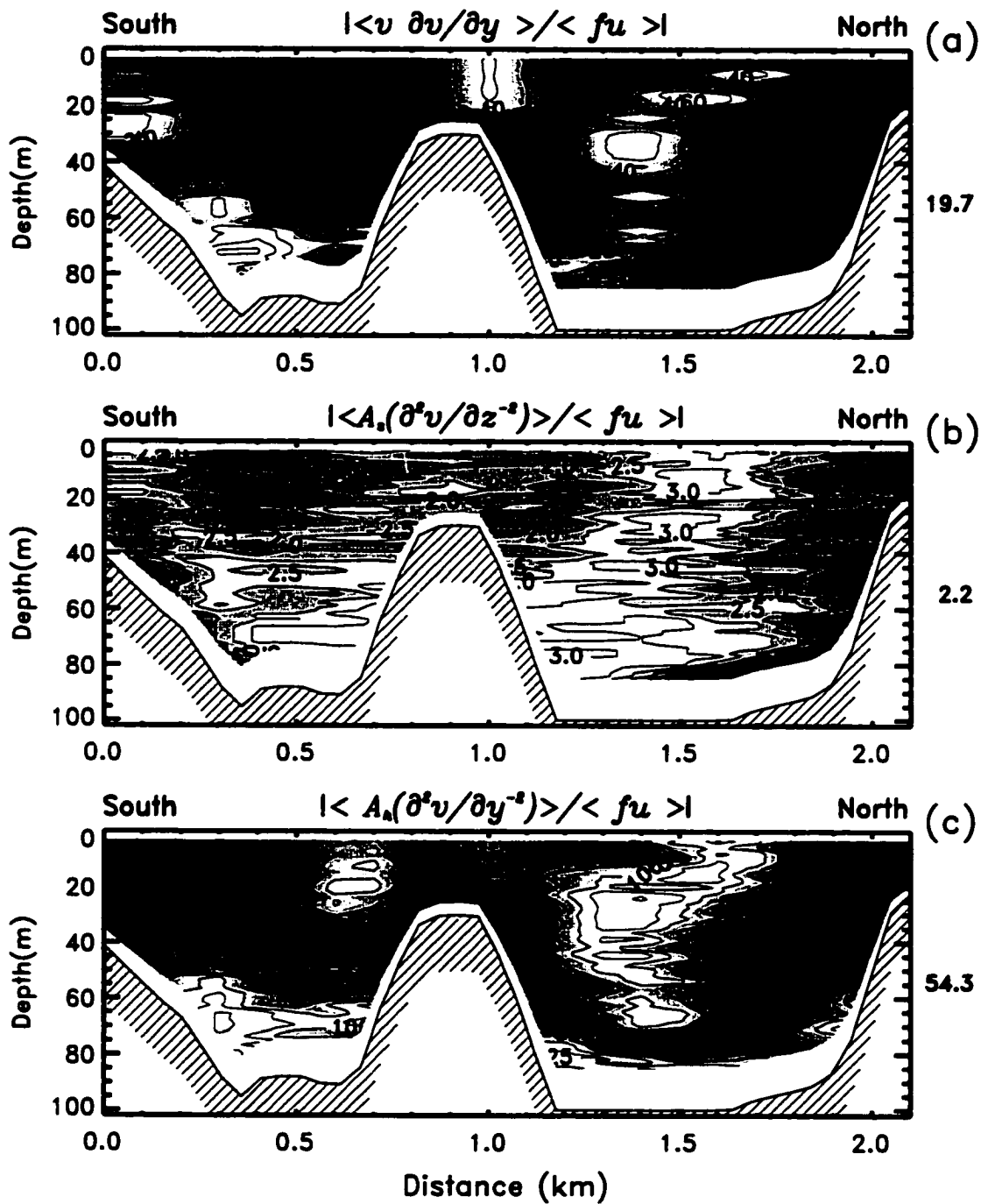
Figure 22. Ratios of the absolute values of (a) subtidal nonlinear term to Coriolis acceleration, (b) vertical frictional term to Coriolis acceleration, and (c) horizontal frictional term to Coriolis acceleration. Looking toward the ocean. Data in the white region near bottom was not considered in the analysis due to side lobe effects of the ADCP measurements.

lower values of u. The distributions of the ratios Advective / Coriolis (Figure 22a) and

Horizontal friction / Coriolis (Figure 22c) showed again the influence of the horizontal

gradient $\partial v/\partial y$. It follows from Figure 22 that advective accelerations and friction

(vertical and horizontal) should be important contributors to the lateral momentum

balance. It is noteworthy to highlight the potential role of horizontal friction in energetic

channels, as it is often neglected. Similar behavior related to horizontal friction has been

observed in North Inlet, South Carolina by Kjerfve (pers. comm.).

3.4 Discussion

In the results presented above, I have shown that horizontal friction is one of the

important terms in the across-channel momentum balance. Here I will further explore this

balance and I will make some comparisons with the along-channel momentum balance.

From (3.2) the relevant terms in the across-channel momentum balance become

$$<v(\partial v/\partial y)> \ = \ <A_h(\partial^2 v/\partial y^2)> + \ < A_z(\partial^2 v/\partial z^2) > \ - <1/\rho(\partial p/\partial y)> \qquad (3.3)$$

which is a balance weakly dependent in depth and strongly dependent on the variations of

v in the y direction $(\partial v/\partial y)$. Note that the pressure gradient term has been included

because it also may contribute to the momentum balance. Otherwise, this balance could

be regarded as one in which the advection of momentum is balanced by the diffusion of

momentum (i.e. advection-diffusion balance). It is also noteworthy that lateral stresses are

dominant over vertical stresses, although the latter are still more important than Coriolis

accelerations.

As indicated in the Data Collection and Processing Section, the coefficients used for the frictional terms A_h and A_z were held constant in the balance. This was done only in the interest of simplicity and represents an approximation. The coefficients used here (A_h=90 m²/s and A_z= 0.01 m²/s) are roughly the same used for the English Channel [*Pingree and Maddock*, 1978] and Juan de Fuca Strait [*Ott and Garrett*, 1998], which are both energetic (tidal currents > 1 m/s) and of similar depths to the Chacao Channel.

The sensitivity of these coefficients to our results was explored using the values indicated in Table 1.

Table 1.- Approximated relative magnitude of the across-channel momentum balance with different values of both vertical and horizontal eddy viscosity coefficients.

	Coriolis term	Advective term	Vertical Frictional term	Horizontal Frictional term
A_h=90 m²/s and A_z= 0.01 m²/s	1	8	5	31
A_h=180 m²/s and A_z= 0.01 m²/s	1	8	5	62
A_h=90 m²/s and A_z= 0.1 m²/s	1	8	11	31

When A_h is increased, the importance of the horizontal friction term increases linearly. When A_z increases one order of magnitude, the vertical frictional term becomes more important than advective accelerations in the momentum balance. Thus, both parameters have some effect in the solution but the contribution of both advective accelerations and horizontal friction remains relevant. In any case, the values used in this

work are considered conservative underestimates for the magnitude of the currents and the channel bathymetry in Chacao.

The strong divergences documented above are expected to be linked to large lateral shears $(\partial u/\partial y)$ [e.g. *Valle-Levinson et al.*, 2001b], which might translate into the importance of advective terms (e.g.. $v\partial u/\partial y$) to the along-channel momentum balance. To explore this we can see that the distributions of $(\partial v/\partial y)$ (Figure 20b) and $(\partial u/\partial y)$ (Figure 23) coincide with their corresponding regions of maximum and minimum, although the values of $(\partial u/\partial y)$ are typically three times those of $(\partial v/\partial y)$. In particular, the southern slope and both flanks of the pinnacle are regions where the strongest lateral shears and divergences are observed. Thus, analogously to the across-channel momentum balance, the relevance of lateral shears seem to be also important to the along-channel momentum balance. The along-channel pressure gradients should then be balanced by advection and friction because the terms reliably computed $<fv>$, $<v(\partial u/\partial y)>$, $<A_z[\partial^2 u/\partial z^2]>$ and $<A_h[\partial^2 u/\partial y^2]>$ show sectional means (not plotted here) of 0.1, 5.1, 1.2 and 14.7 (x 10^{-4}), respectively. The approximate relative magnitude of the terms in the along-channel dimension becomes:

1	:	50	:	10	:	150	(3.4)
Coriolis Term		Advective Term		Vertical Frictional Term		Horizontal Frictional Term	

Again, the magnitude and distribution of the lateral shears of velocity $\partial u/\partial y$ (Figure 23), are potentially playing a key role in this behavior. Another way to conceptualize this
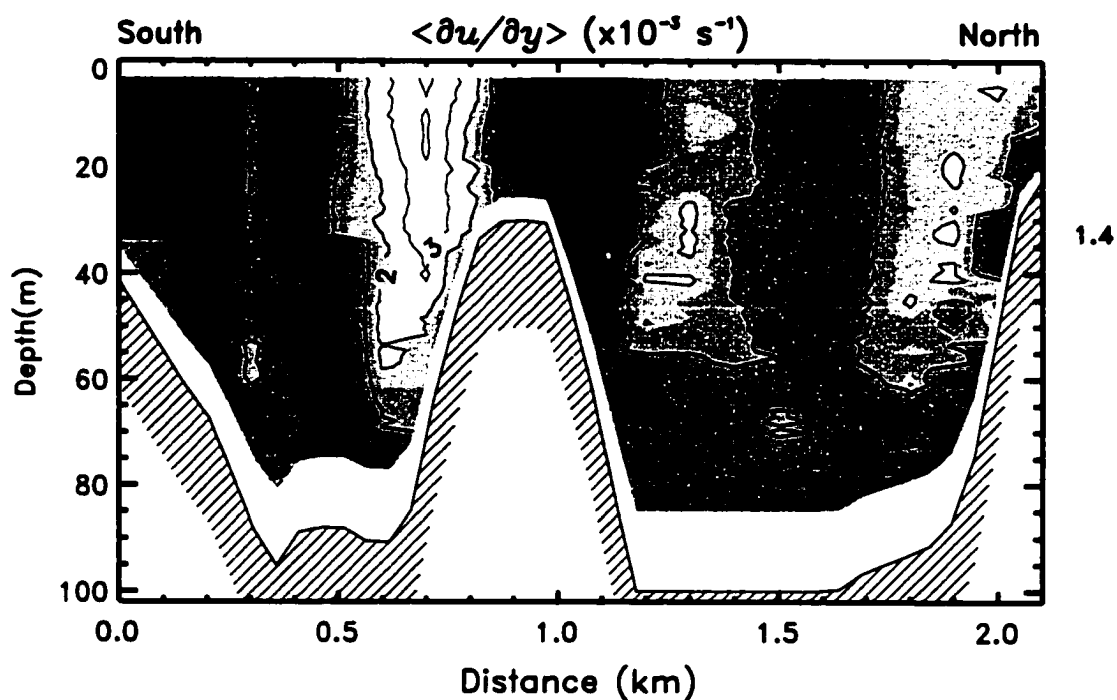
Figure 23. Contours of the tidally averaged lateral shear of the along-estuary flow. Lighter shades indicate positive shears (negative relative vorticity) and darker shades represent negative shears (positive relative vorticity). Looking toward the ocean. Data in the white region near the bottom were not considered in the analysis due to side lobe effects of the ADCP 5measurements.

is to consider that the advective acceleration $u(\partial u/\partial x)$ may be scaled as U^2/L_x where U=2

m/s and L_x= 5000 m. In this case, the advective term will be 8 x 10^{-4} and will balance the

mean of the lateral friction term $A_h[\partial^2 u/\partial y^2]$, estimated at ~11.4 x 10^{-4}. Then in the along-

channel momentum balance advective accelerations and friction (both lateral and vertical)

are important contributors to the dynamics.

Friedrichs and Madsen [1992] investigated the magnitudes of advective

accelerations relative to friction in 13 estuaries with different depths, tidal ranges and

typical tidal velocities. They found the greater values(>1) of these ratios in deeper

estuaries (40 m), as bottom friction becomes less important. In contrast, the ratios

advective/(bottom friction + horizontal friction) for the present work were 0.2 (across-

channel) and 0.3 (along-channel), obtained from (2) and (4), respectively, which once

more show the relevance of horizontal friction to the dynamic balance. These ratios

support the idea that in energetic and bathymetrically complex channels, such as Chacao

Channel, horizontal friction plays a key role in the momentum balance.

3.5 Conclusion

This study of flow over a pinnacle in an energetic tidal channel features a mean flow

pattern consisting of recirculation around the pinnacle and over the slopes of the channels

that resemble theoretical results [e.g. *Park*, 1990; *Li and O'Donnell*, 1997], as illustrated

by the schematic diagram presented in Figure 24. These recirculations reflect strong

divergences and lateral shears that translate into a relevant contribution of the nonlinear

terms (advection, horizontal and vertical friction) to the momentum balance. In particular,

this study highlights the prominence that horizontal friction may exert on the dynamics of
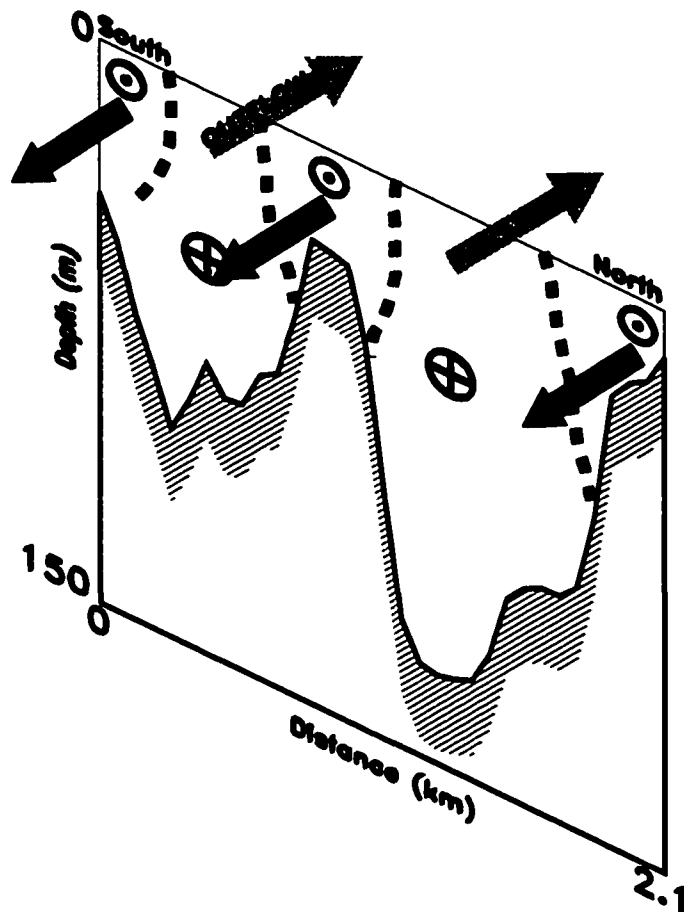
Figure 24. Schematic representation of the along-channel mean flow across the channel. Outflow (gray arrows) and inflow (black arrows) regions are separated by strong convergences or lateral shears, both denoted by the dashed lines.

an energetic tidal channel. This constitutes one of the few reported examples where horizontal friction may be relevant to the dynamics of a naturally occurring flow. Some of the results presented here might be also important in studies of dispersion of particulated material in the region.

In summary, the mean flow exhibited weak vertical structure because of strong vertical mixing. The predominant lateral structure consisted of mean outflow (toward the ocean) in the channels, and mean inflow (toward Gulf of Ancud) over the pinnacle and the sides of the channel. This lateral structure pattern was consistent with the mean flow pattern expected from tidal rectification, as robust overtides were generated throughout the transect. The contributions to flow divergence and vorticity by the lateral variations of the lateral flow ($\partial v/\partial y$) and by the lateral shears of the along-channel flow ($\partial u/\partial y$), respectively, were both of the order of 10^{-3} s^{-1}. This caused advective and frictional forces (both horizontal and vertical) to be dominant in the across-channel momentum balance, as they were more than twenty times the Coriolis acceleration. The present work, then represents one of the few examples reported where lateral friction (proportional to $\partial^2 v/\partial y^2$) appears relevant to the transverse momentum balance.

REGION OF VENTISQUERO SOUND

4.1 Introduction

As indicated previously, the transverse momentum balance in fjords might be modified by nonlinearities arising from different sources, such as friction, bottom profile, coastal morphology, and others. In regions of sills and coastline contractions, the geometric properties might be relevant in determining the across-channel momentum balance. The stretching and contraction of streamlines by the effect of sills and/or contractions would invalidate the geostrophic approximation and make advective accelerations relevant to the across-channel momentum balance.

In a previous paper [*Valle-Levinson et al.*, 2001a], a study was made of the intratidal variability of the flow over a sill/contraction combination in a Chilean fjord. That work was focused to describe the intratidal variability of the flows within Galvarino Pass (Figure 25), a pass connecting the northern and southern portions of Ventisquero Sound, and to assess the observed variability in the context of the existing theories. They found a two layer flow with falls and rises of the pycnocline, transitions from subcritical to critical flow, and enhanced vertical mixing within the pass.

Nevertheless, the full data set collected during that field work included not only the portion of the sill, but also the northern and southern sides of the pass, which were covered with transverse transects of Acoustic Doppler Current Profiler (ADCP) current measurements. These transects were intended to improve the understanding of the transverse variability of flow in both sides of the contraction. I seek 1) to study the transverse variability of the flow in both sides of the pass, describing the main
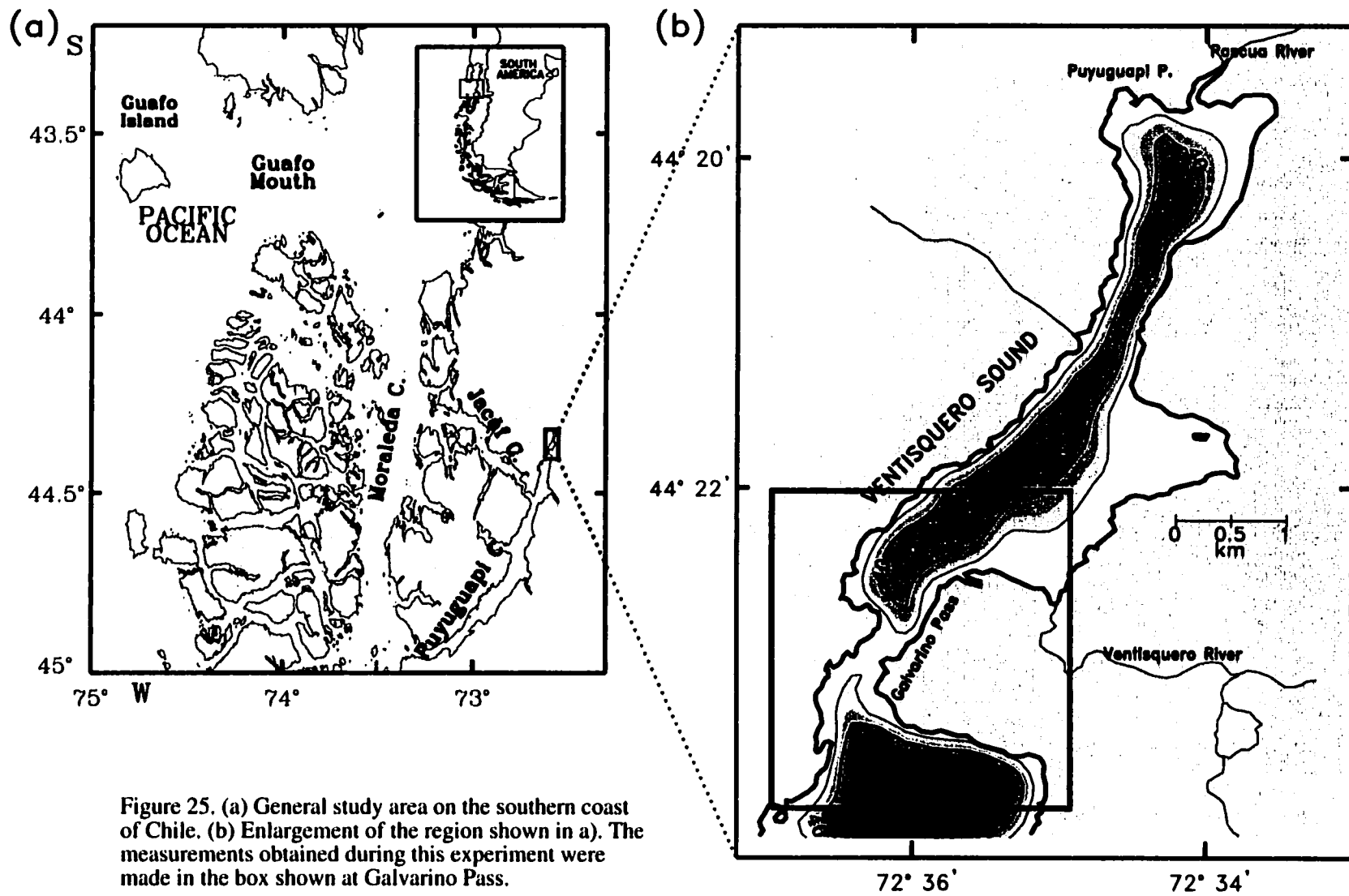
Figure 25. (a) General study area on the southern coast of Chile. (b) Enlargement of the region shown in a). The measurements obtained during this experiment were made in the box shown at Galvarino Pass.

73

characteristics of the residual (or mean) flow, and 2) to assess the main terms contributing

to the across-channel dynamic balance. The analysis of these data should provide insights

on the differences in the characteristics of flow, density, and dynamic balance at either

side of the morphological constriction. This study quantifies and describes the transverse

variability produced by the interaction of tidal currents with a sill in the contraction of a

channel. It also presents estimates of key terms in the across-channel momentum balance

to assess the validity of the geostrophic approximation. The objectives are pursued with

observations of a towed ADCP and of conductivity-temperature-depth (CTD) profiles

throughout one semidiurnal tidal cycle.

4.2 Study area

Ventisquero Sound is a fjord-like inlet located in the northern region of the Chilean

Inland Sea. It is part of the northernmost end of Puyuguapi Channel (Figure 25a). The

position of Ventisquero Sound suggests that it may be little affected by the shelf

processes occurring adjacent of the Chilean Inland Sea. The tidal wave propagates

eastward entering to the Inland Sea through Guafo Mouth and bifurcates to the north and

to the south through Moraleda Channel. Tidal ranges reported in the confluence of

Moraleda Channel and Jacaf Channel are 2.3 m [SHOA, 1994], which suggests a typical

semidiurnal tidal amplitude of about 1.1 m in the region of Ventisquero Sound. This

confirms the field observations of Valle-Levinson et al. [2001a] and their theoretical

approximation to this value based on Stigebrandt [1977].

Because of its orientation at nearly 11° true, and because of the steep land

topography surrounding this inlet, hydrodynamics in Ventisquero Sound are believed to

be weakly affected by seasonal northwesterly and southerly winds. Nevertheless, funneling of winds by Puyuguapi Channel (Figure 25a) could be probably a mechanism to induce currents by winds in this Sound. No field measurements are available to confirm this hypothesis.

Freshwater inputs to Ventisquero Sound are provided mainly by Ventisquero River and Pascua River (Figure 25b), two ungauged streams discharging in the northern side of the contraction. Rivers in the Puyuguapi Channel follow the annual regime of freshwater discharges in the region, with two annual peaks of discharges corresponding to the autumn increase in precipitation (April-June) and the summer melting of snow. Sampling for this study was carried out in January, not far from the snow melting peak in November. The mean total annual precipitation (1968-1999) for stations around the study area fluctuates between 1100 and 2100 mm (SMA, pers. comm.). By the effect of these inputs there is a well defined pycnocline shallower than 10 m depth in the northern region of Puyuguapi Channel [*Silva et al.*, 1995, *Silva et al.*, 1997].

As indicated by *Valle-Levinson et al.* [2001a], the geomorphology in Galvarino Pass represents a coastline constriction of about 90%, decreasing from 2000 m to 200 m in just 1500 m in the along-channel direction. Depth varies from 40 m on the landward side of the pass to 10 m at the shallowest portion of the sill to 80 m south of the pass.

4.3 Data collection and processing

A 614.4 kHz RD Instruments Broadband ADCP and a Trimble Global Positioning System (GPS) interfaced to a laptop computer were used to obtain velocity profiles in the sampling area during one complete semidiurnal tidal cycle on January 12, 1998, during

spring tides. The ADCP was mounted on a catamaran ~1.2 m long, that was towed from the starboard side of the R/V *Arturo Prat* (of the Technical Fisheries Institute in Puerto Cisnes, Chile.), at speeds between 2 and 2.5 m/s. Velocity profiles with a vertical resolution (bin size) of 0.5 m and ping rates of ~1 Hz were averaged every 15 s, yielding a spatial resolution of ~30-40 m. Four across-channel transects (numbers 1 to 4) and one along-channel transect (number 5), covering the circuit indicated in Figure 26 were traversed 8 times during the 12 hours of data collection. The ADCP data were calibrated according to *Trump and Marmorino* [1997]. Bad data were removed following the procedure explained by *Valle-Levinson and Atkinson* [1999]. After the heading correction was applied, the data were rotated counter clockwise $10°$ (transect 1), $-5°$ (transect 2), $30°$ (transect 3), $50°$ (transect 4) and $-10°$ (transect 5) to an along- (v-flow) and across- (u-flow) channel coordinate system. These angles were oriented to the direction of greatest variability of the tidal currents and of weakest across-channel tidal flows. The present work was carried out during calm wind conditions.

Density profiles were measured with a Hydrolab Datasonde 4 CTD multiprobe in the stations A to D indicated in Figure 26. The accuracy of the salinity and temperature measurements was ±0.2 and ±0.1 °C, respectively, and the resolution of these measurements was 0.01 for salinity and 0.01 °C for temperature. Problems with the pressure sensor during the CTD casts invalidated the values below of ~15 m. Density values were obtained from temperature, salinity, and pressure with the international equation of sea state of seawater [*e.g. Gill*, 1982]. The sampling rate of the CTD was 0.2 Hz, thus making each CTD cast a time-consuming task (~10 min).
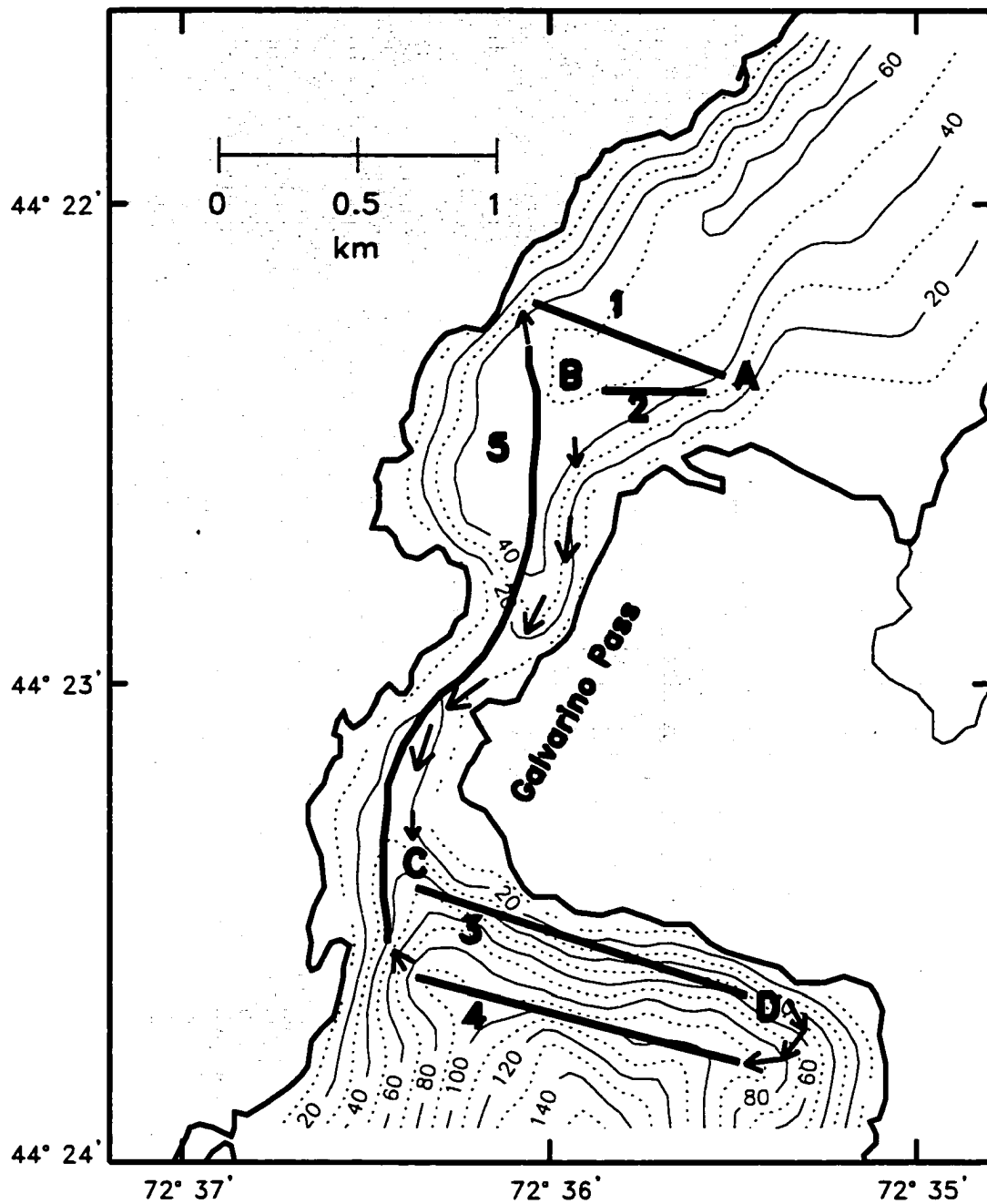
Figure 26. The ADCP profiles were made in the circuit shown in the figure, following the arrow directions. The approximate position of the ADCP transects is shown (numbers 1 to 5). CTD profiles were made in positions A to D.

The semidiurnal tide (represented by the M_2 constituent) was separated from the subtidal signal of the observed flow components using sinusoidal least squares regression analysis [*e.g.* Lwiza *et al.*, 1991]. After determining the mean subtidal flow, the relative magnitude of the advective and frictional terms was compared to that of the Coriolis accelerations. To do this, a right-handed coordinate system was adopted for which y (along-channel direction) was positive toward nearly 10° (transect 1), 355° (transect 2), 30° (transect 3), 50° (transect 4) and 350° (transect 5); while the x (across-channel direction) was positive to nearly 100° (transect 1), 85° (transect 2), 120° (transect 3), 140° (transect 4) and 80° (transect 5). It followed that the along-channel and across-channel components of the velocity were given by v and u, respectively. In the across-channel direction, the subtidal momentum balance for transects 1 to 4 may be then given by

$$<u(\partial u/\partial x)> - <fv> = - <1/\rho(\partial p/\partial x)> + <A_z(\partial^2 u/\partial z^2)> + <A_h(\partial^2 u/\partial x^2)> \qquad (4.1)$$

and for transect 5

$$<v(\partial u/\partial y)> - <fv> = - <1/\rho(\partial p/\partial x)> + <A_z(\partial^2 u/\partial z^2)> + <A_h(\partial^2 u/\partial y^2)> \qquad (4.2)$$

where $u(\partial u/\partial x)$ and $v(\partial u/\partial y)$ are the advective terms, fv is the Coriolis term ($f=1.01 \times 10^{-4}$), $1/\rho(\partial p/\partial x)$ is the pressure gradient term, $A_z(\partial^2 u/\partial z^2)$ is the vertical frictional term, $A_h(\partial^2 u/\partial x^2)$ and $A_h(\partial^2 u/\partial y^2)$ are the horizontal frictional terms, and brackets (< >) denote tidal averages. The coefficients A_z and A_h denote the vertical and horizontal eddy viscosities. These were the terms of the complete momentum balance that could be reliably approximated, with exception of the pressure gradient term. The magnitudes of

each term were used to compare their relative contribution to the momentum balance in the across-estuary direction.

For the vertical eddy viscosity, A_z, I used the empirical form $A_z = 1.5 \times 10^{-5} u^2_{rms}/f$ of Bowden and Hamilton [1975] to obtain a first estimate for the magnitude of this coefficient, where u_{rms} is the rms tidal velocity. For the magnitudes of the currents and depths observed in this experiment, the applicability of this solution seemed to be acceptable, following the procedure of Ianniello [1977]. The relationship proposed by Csanady [1975], $A_z = u_*^2 / 200 f$ for estuaries of large depth, where u_* is the frictional velocity $(\tau/\rho)^{1/2}$, also leads to similar results. The values obtained from both solutions for our data set are in the range of $A_z = 0.0001$ to $A_z = 0.0014$ m²/s. I use a constant eddy viscosity coefficient of 0.0005 m²/s for transects 1 to 4 and 0.001 m²/s for transect 5. Similar empirically derived forms for the magnitude of the horizontal eddy viscosity in tidal channels are less widely used. Tee [1976] used a value of $A_h = 100$ m²/s for an energetic tidal channel (currents of ~5 m/s), Ianniello [1979] used estimates ranging from 1 to 10 m²/s for tidal channels, and Jones and Elliot [1996] used estimates of 0.5 to 10 m²/s in the parametrization of friction in rivers. Ianniello [1979] also proposed a way to estimate the width of the channel that makes horizontal friction comparable to the vertical friction. According to this, the widths in Ventisquero Sound are within the ranges where horizontal friction is important. Then I will use a conservative estimate of $A_h = 0.5$ m²/s for transects 1 to 4 and $A_h = 1$ m²/s for transect 5, according to the velocities observed in this system.

4.4 Results

This section presents the across-channel distribution of the subtidal (or mean) and

tidal flows for the period of observation in the five transects. It also describes mean vertical density profiles made at the four stations(A-D, Fig. 26). It also presents the magnitudes and across-channel distributions of the terms indicated in (1), with exception of the pressure gradient term. A comparison among the magnitude of various terms is shown at the end.

Mean flow

The along-channel mean flow over the period of observations for transects 1 and 2 is shown in Figure 27. The northern transect 1 showed inflows over the channel and outflows over the slopes, which was more evident in the east side. Theoretical results have shown that this last pattern may be attributed to the effect of the cross sectional bathymetry [*Wong*, 1994]. This pattern is partially suggested in the east side of transect 2, as this transect did not covered the full width of the channel. The along-channel mean flow for transects 3 and 4 (Figure 27) showed the greater magnitudes (~10 cm/s) in the west side, consistent with the presence of the channel on the left (west) and the constriction on the right (east). In the channel, outflow occurred in the upper 15 m and inflow between 15 and 30 m. It is interesting to note that partition between inflows and outflows also appears in the horizontal plane and that waters below 25 m are nearly quiescent. As expected, in transect 5 the along-channel flow showed maximum net velocities of about 12 cm/s over the sill.

In the case of the across-channel mean u-flow (Figure 28), it remarkably showed mean sectional values comparable to those of the along-channel mean flow. Means of transects 1 and 2 were greater than their equivalent in the along-channel mean flow. This pattern might be attributed to the marked effect of the coastal geometry in the region of
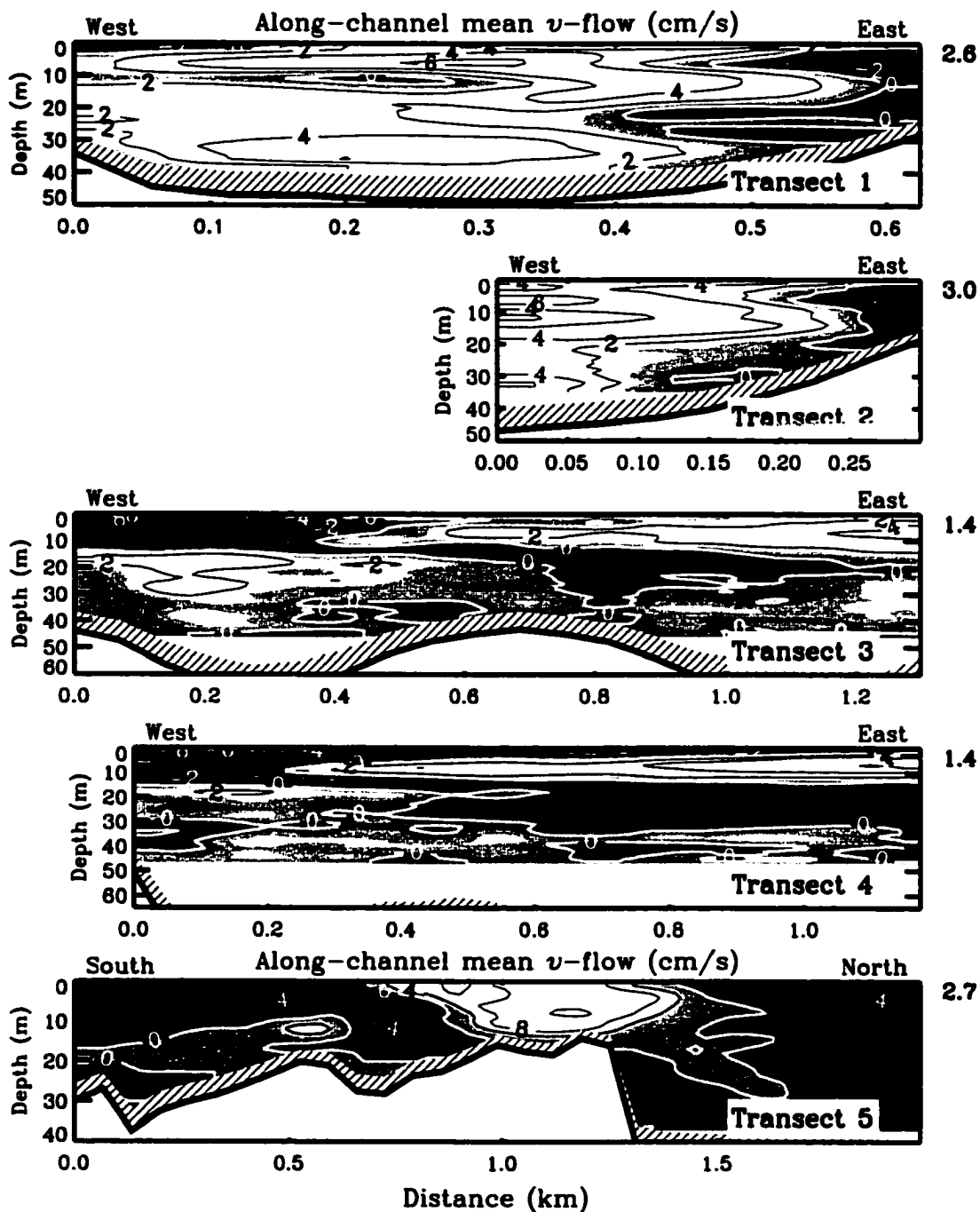
Figure 27.- Across-channel distribution of the along-channel mean flow. Net inflows are lighter and net outflows are darker. Transects 1 and 2 show evidence of inflows in the center and outflows on the sides. Transects 3 and 4 show the strongest outflows in the west side in the first 15 m. Inflows dominate below 15 m and in the east side near surface. Transect 5 shows along-channel (not across) distribution. The strongest inflows are observed over the sill. Near the upper right corner of each panel there are the absolute values of the sectional means. Contour interval is 2 cm/s, except in transect 5 where it is 4 cm/s. Horizontal scales are comparable between transects 1 and 2, and between transects 3 and 4. Data in the shaded region near the bottom was not considered in the analysis due to side lobe effects. White region near the bottom was out of the profiling range of the ADCP.
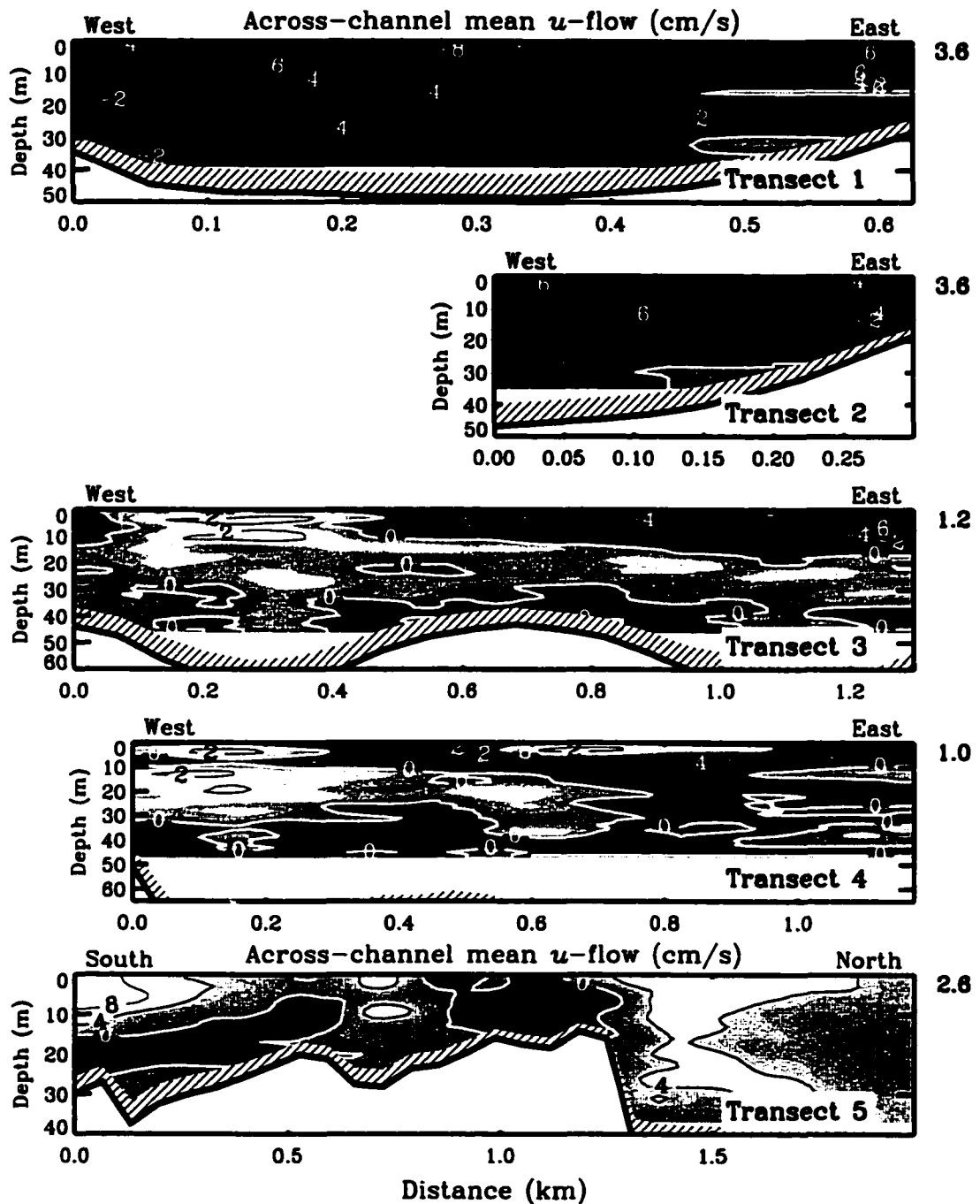
Figure 28.- Across-channel component of the mean flow. Flows toward the east are lighter and flows toward the west are darker. Transects 1 and 2 show dominance of flow toward the west. Westward flow in transects 3 and 4 dominates near surface in the east side, while eastward flow is important near surface in the west side. Below 15 m lateral flows are less important (< 2 cm/s). Transect 5 shows the strongest west flows (out of the paper) in the north and near surface in the south. Near the upper right corner of each panel there are the absolute values of the sectional means. Contour interval is 2 cm/s, except in transect 5 where it is 4 cm/s. Horizontal scales are comparable between transects 1 and 2, and between transects 3 and 4. Data in the shaded region near the bottom was not considered in the analysis due to side lobe effects. White region near the bottom was out of the profiling range of the ADCP.

the contraction, which accelerates the flows in the transverse direction. Transects 1 and 2 in the northern side showed dominance of negative values (flow to the west) in the sections. This produced a tendency of the flow to rotate anticlockwise throughout the water column to the north of the sill, which is evidenced at all depths. On the other hand, to the south of the pass the flow exhibited a convergence in the first 20 m at about 400 m from the western side. This pattern might be attributed to the coastal geometry, which deviated to the east the flow coming from the south, converging to the channel outflow. The across-channel mean flows of transect 5 also confirmed the tendency for recirculations at the north end of the transect, as flow was directed to the east (positive values) in this region. In the southern side of this transect, positive values were also consistent with the south-east direction of the outflow.

Vectors at selected depths plotted for the mean flow described above are presented in Figure 29. Circulation patterns suggested by the contours presented above, were confirmed in these figures. In the northern side there was a tendency of the flow to rotate anticlockwise at all depths. It was noticeable how in the deep region (depth of 34 m, Figure 29), residual flows were still about 5 cm/s in the northern region, which suggests that the presence of the sill favors retention of waters in the northern basin. South of the pass, there was a two-layer structure on the west with surface outflow (at 2 and 6 m)and inflow at depth (20 m), which is supported by density profiles that will be shown later.

Strongest outflows and inflows appearing to the south of the pass were concentrated over the west side. Convergence of the flow was more clearly observed at 6 m in Figure 29 in the west side of transects 3 and 4. This feature was observed in the field in at least
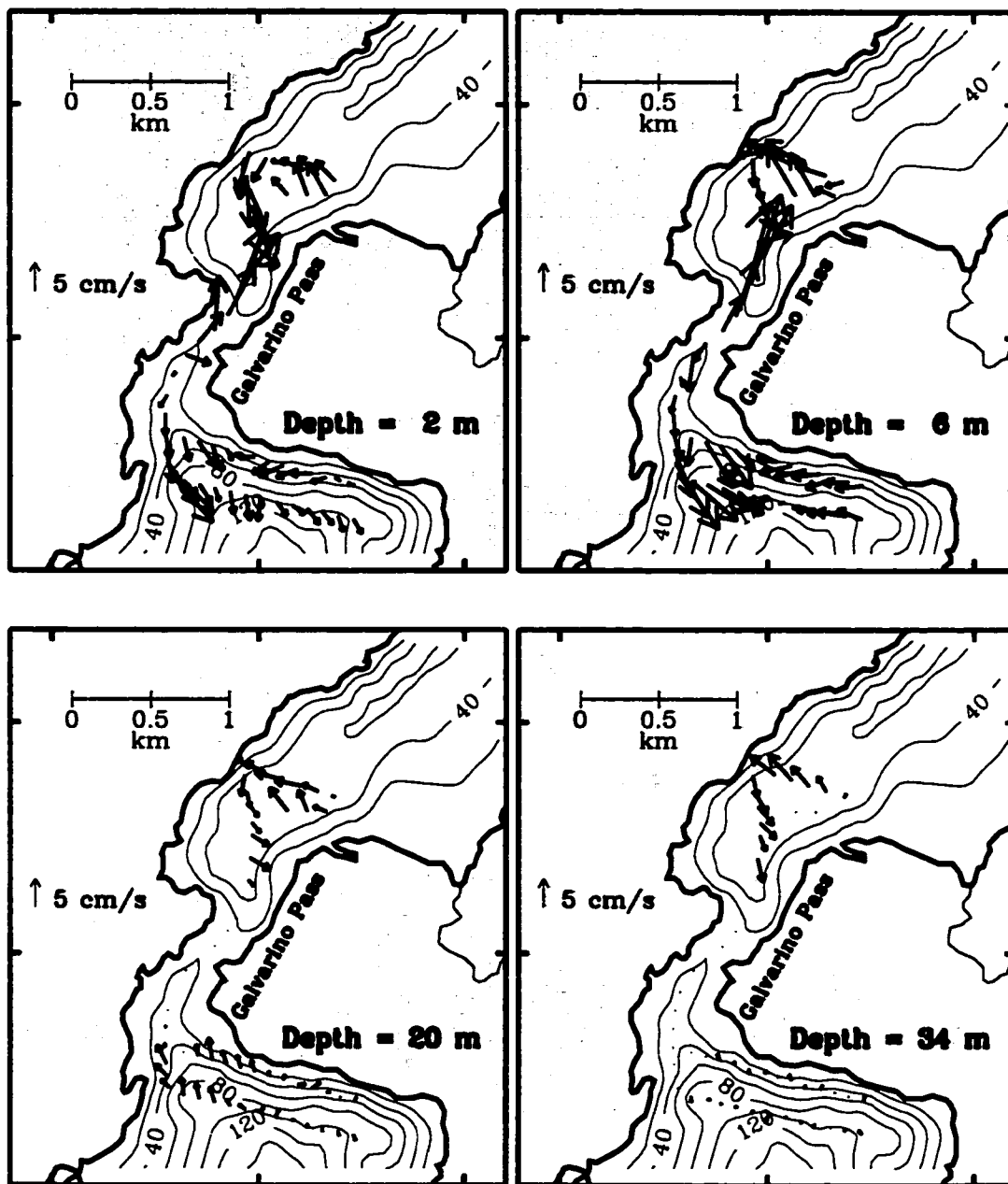
Figure 29. Arrows of the mean flow distribution at four selected depths (2, 6, 20 and 34 m).

four of the eight ADCP repetitions. The mean flow within the pass showed that the

boundary for outflows and inflows appears in the narrowest region. The strongest inflows

(~12 cm/s) were observed in the sill region and the strongest outflows (~8 cm/s) to the

south of the pass.

Tidal current amplitudes

The across-channel distribution of the semidiurnal tidal current amplitudes are

presented in Figure 30. To the north of the pass, maximum amplitudes of about 15-20

cm/s occurred preferentially at mid-depth and near surface. To the south of the pass, the

greatest amplitudes of about 22 cm/s (transect 3) and 15 cm/s (transect 4) were located

over the channel on the western side, near surface, with amplitudes tending to zero below

20 m depth. Transect 5 showed the greatest amplitudes of about 65 cm/s over the sill.

There is a pattern showing maximum amplitudes increasing northward, with the greatest

values over the sill, and decreasing northward to almost one half of those to the south of

the pass. This pattern seems to follow continuity constraints and reflect a Bernoulli-type

of dynamics.

Density profiles

Mean density profiles for stations A, B, C and D (Figure 26) are presented in Figure

31. Vertical stratification was stronger in the southern (C, D) side than in the northern

(A, B) side of the sill, as a result of greater supply of saline water to the southern side.

The evolution of the density in time for stations B and C, presented by *Valle-Levinson et*

al. [2001a], also revealed that the northern side experiences weak perturbations from tidal

forcing, as deduced by the position of the 15 σ_t isopycnal during one tidal cycle.
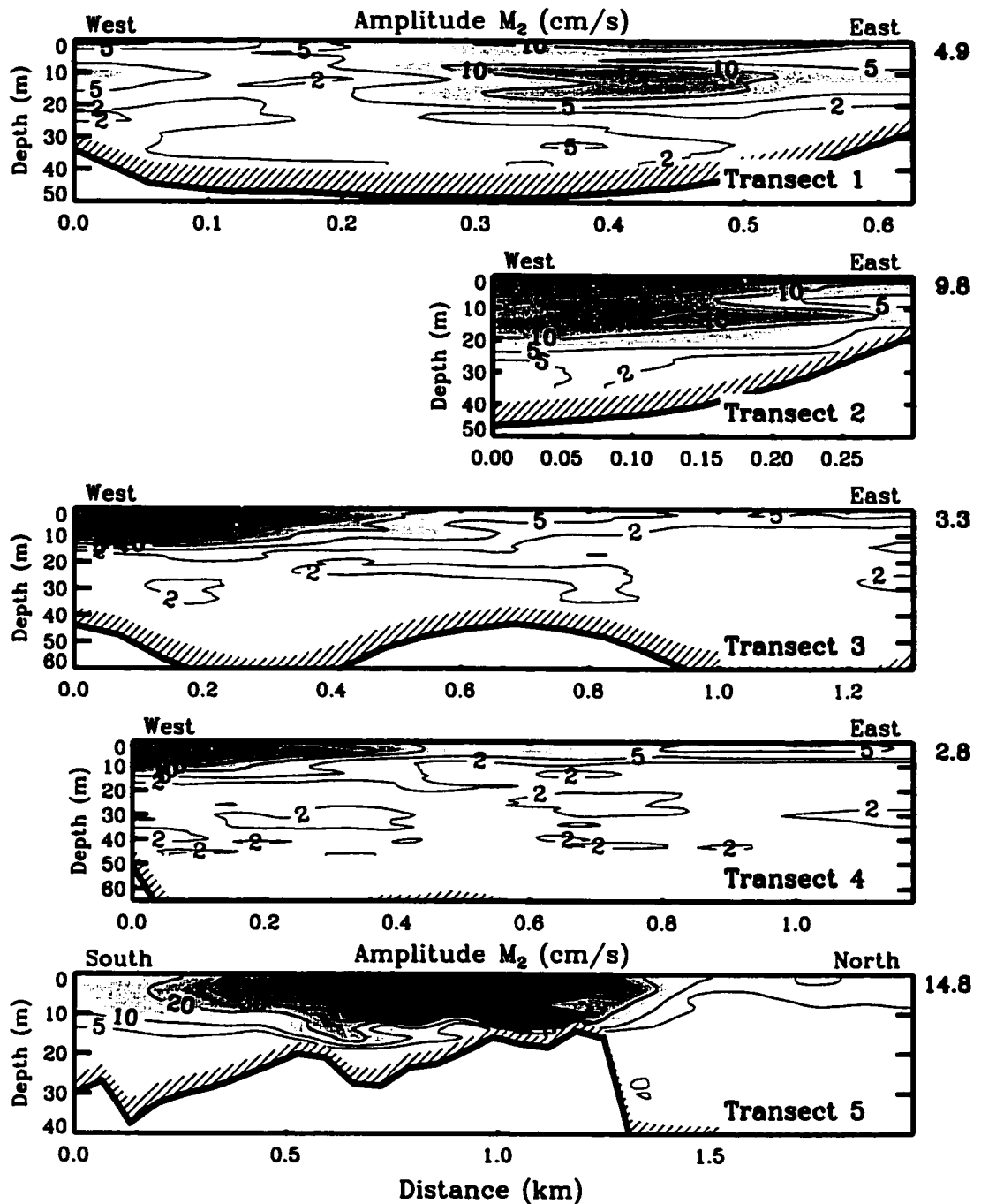
Figure 30. Across-channel distribution of the along-channel tidal amplitude for the semidiurnal component, obtained from the ADCP current measurements. Transects 1 to 4 looking up-estuary, transect 5 looking toward the west. Near the upper right corner of each panel there are the absolute values of the sectional means. Contours are 2, 5, 10, 15, ... cm/s, except in transect 5 where they are 5, 10, 20, 30, ... cm/s. Horizontal scales are comparable between transects 1 and 2, and between transects 3 and 4. Data in the shaded region near the bottom was not considered in the analysis due to side lobe effects. White region near the bottom was out of the profiling range of the ADCP.
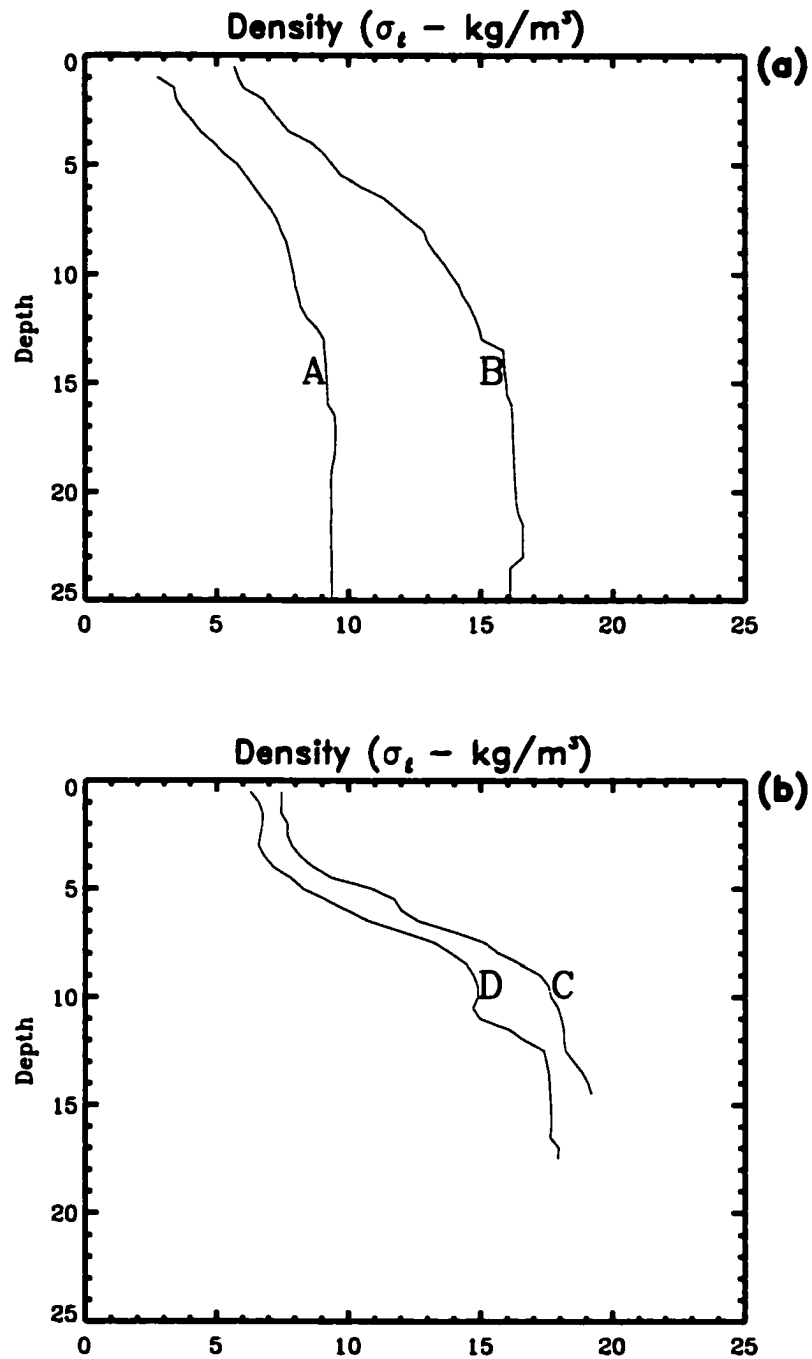
Figure 31.- Density profiles in the positions A to D indicated in figure 2. a) north of the sill and b) south of the sill. Vertical stratification is greater in the southern side of the pass. Stations close to the coast (A and D) are less saline than those near the center.

Water is less dense at coastal stations (A and C) than in the stations in the center of the channel. In the northern side, lower salinities at station A are probably due to the effect of a nearby river discharge and the effects of the earth's rotation. Differences in density between stations A and B might be also related to the along-channel mean flow (Figure 27). Net outflow, near the eastern coast, might be associated with lighter water (A), and net inflow, in the center, with heavier water (B).

Across-channel dynamics

The across-channel distributions of the tidally averaged Coriolis term $< fv >$, the advective term $< u(\partial u/\partial x) >$ and the frictional terms $< A_z(\partial^2 u/\partial z^2) >$ and $< A_h(\partial^2 u/\partial x^2) >$ were used to establish their relative contribution to the across-channel momentum balance. Figures 32, 33, 34 and 35 show the distribution of the Coriolis, advective, vertical frictional and horizontal frictional terms, respectively, with magnitudes expressed in units of acceleration m/s^2 x 10^{-6}.

In all of these figures transects 1 to 4 are looking up-estuary, and transect 5 is looking toward the west. Scales of distance and depth are comparable between transects 1 and 2, and between transects 3 and 4. Scales in transect 5 are not comparable with other transects.

As expected, the Coriolis term (Figure 32) resembled the mean v-flow distribution (Figure 28), as it is directly proportional to it. The advective term (Figure 33) showed greater sectional means to the north of the pass than south of the pass, as expected from the recirculation of the mean flow observed in figure 29. In the case of transect 5, the across-channel advective term was greater over the sill than in deeper regions, and its
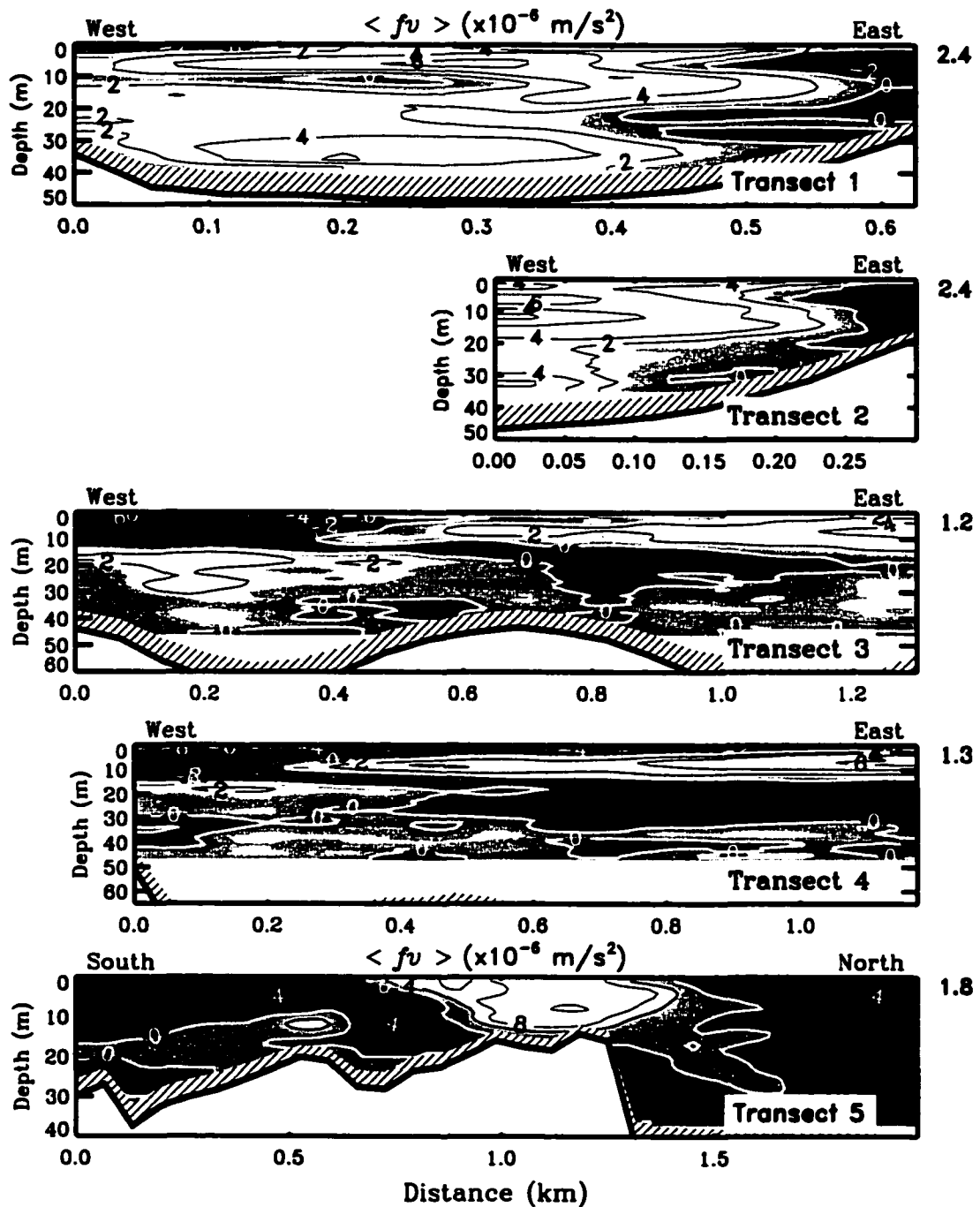
Figure 32.-. Contours of the tidally averaged Coriolis term in the five transects. Near the upper right corner of each panel there are the absolute values of the sectional means. Title of transect 1 is valid for transects 1 to 4. Contour interval is 2 ($\times 10^4$) m/s^2 except in transect 5 where it is 4 ($\times 10^4$) m/s^2. Horizontal scales are comparable between transects 1 and 2, and between transects 3 and 4. Data in the shaded region near the bottom was not considered in the analysis due to side lobe effects. White region near the bottom was out of the profiling range of the ADCP.
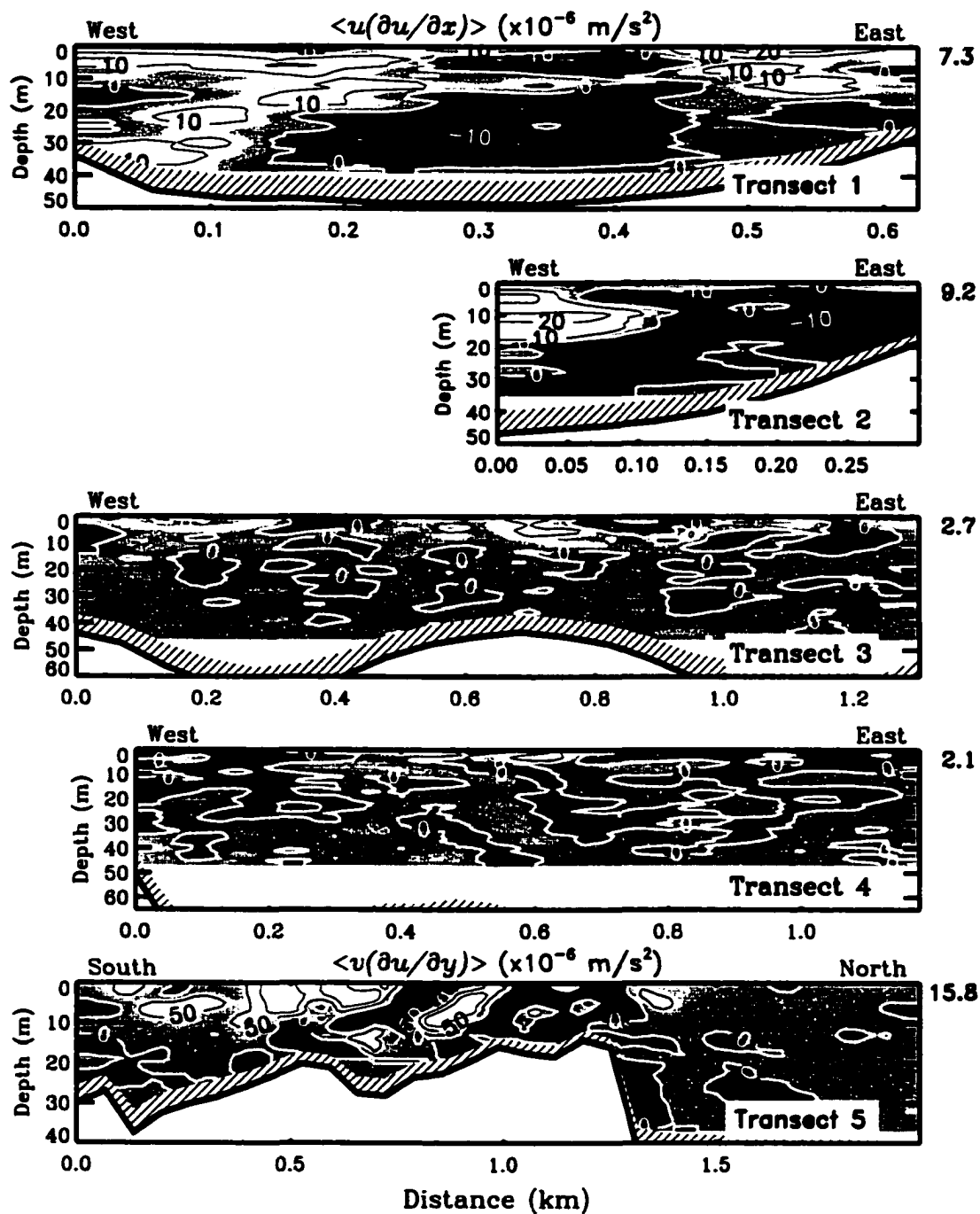
Figure 33.-. Contours of the tidally averaged advective term in the five transects. Near the upper right corner of each panel there are the absolute values of the sectional means. Title of transect 1 is valid for transects 1 to 4. Contour interval is 2 (x10⁴) m/s² except in transect 5 where it is 4 (x10⁴) m/s². Horizontal scales are comparable between transects 1 and 2, and between transects 3 and 4. Data in the shaded region near the bottom was not considered in the analysis due to side lobe effects. White region near the bottom was out of the profiling range of the ADCP.

sectional mean was the highest of the five transects. The sectional distribution of the

vertical friction term is presented in Figure 34. As expected, transect 5 showed the

highest values over the shallowest region and near the bottom. To the north of the pass, in

transects 1 and 2, the frictional terms exhibited a layered pattern, while to the south of the

pass, in transects 3 and 4, the pattern was spotty. This might be related to the depths of

both regions, as northern transects were shallower than southern transects. The horizontal

frictional term in Figure 35 showed similar sectional means in the five transects. The

layered and spotted patterns to the north of the pass and to the south of the pass,

respectively, were also observed.

4.5 Discussion

In the results presented above, the system under study seems to have different

residual circulation patterns on both sides and within the pass. To the north, there is a

tendency of the flow to rotate anticlockwise, with strong lateral flows and low

stratification. To the south, the system exhibits stratification, a two-layer vertical structure

and flow convergence in the westernmost third of the sections. Over the sill, there is an

enhancement of tidal current velocities by continuity effects. A schematic diagram

representing the main characteristics of the mean flow is presented in Figure 36. In

agreement with these different patterns, the across-channel dynamic balance also exhibits

some differences among the regions. The approximate relative magnitude of the terms in

the across-channel direction (Figures 32 to 35) is presented in Figure 37. They are the

absolute values of the sectional means from Figures 32 to 35. In general, they show that

the four terms are important to the across-channel momentum balance, with comparable
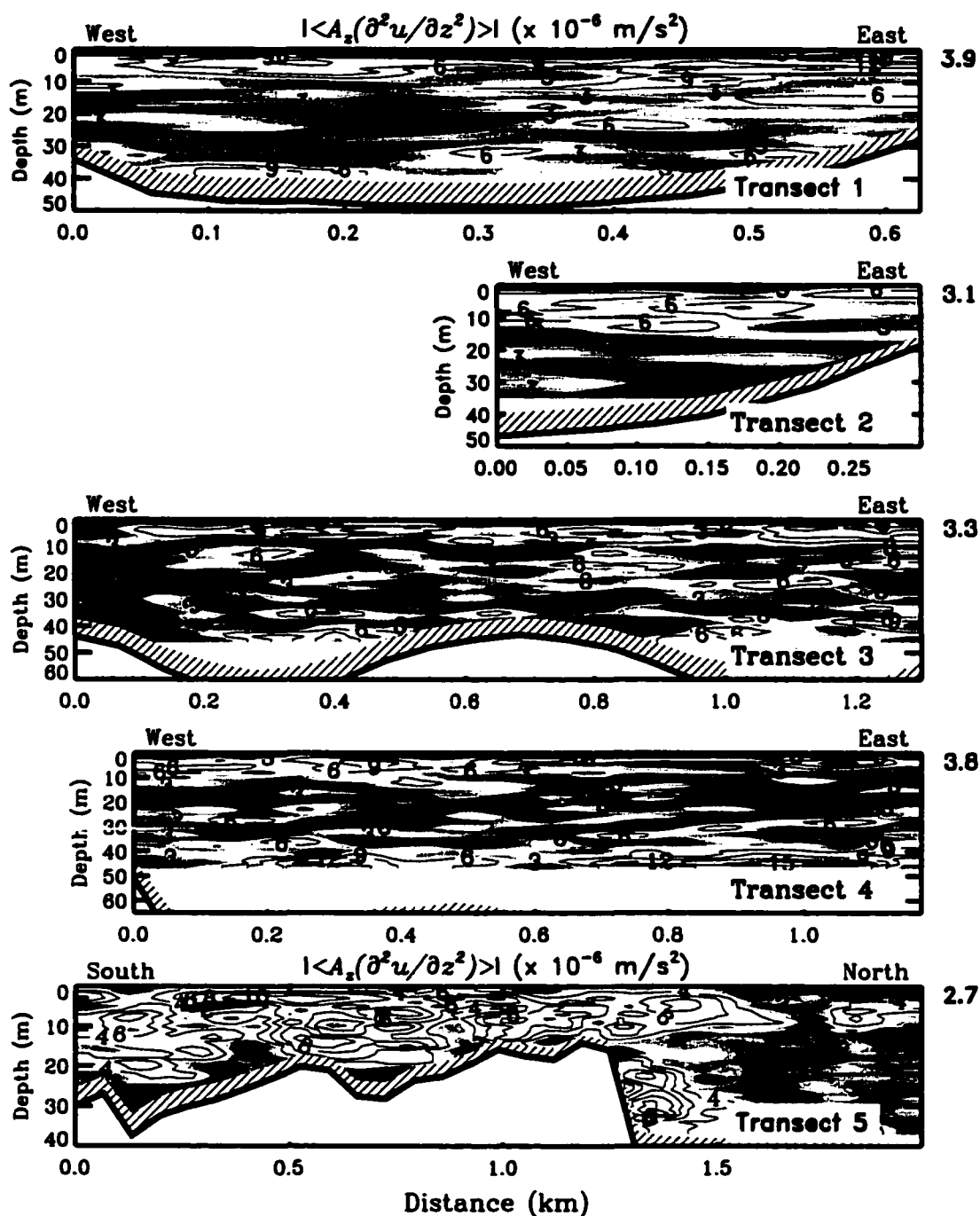
Figure 34.-. Contours of the tidally averaged vertical friction term in the five transects. Near the upper right corner of each panel there are the absolute values of the sectional means. Title of transect 1 is valid for transects 1 to 4. Contour interval is 2 (x10⁴) m/s² except in transect 5 where it is 4 (x10⁴) m/s². Horizontal scales are comparable between transects 1 and 2, and between transects 3 and 4. Data in the shaded region near the bottom was not considered in the analysis due to side lobe effects. White region near the bottom was out of the profiling range of the ADCP.
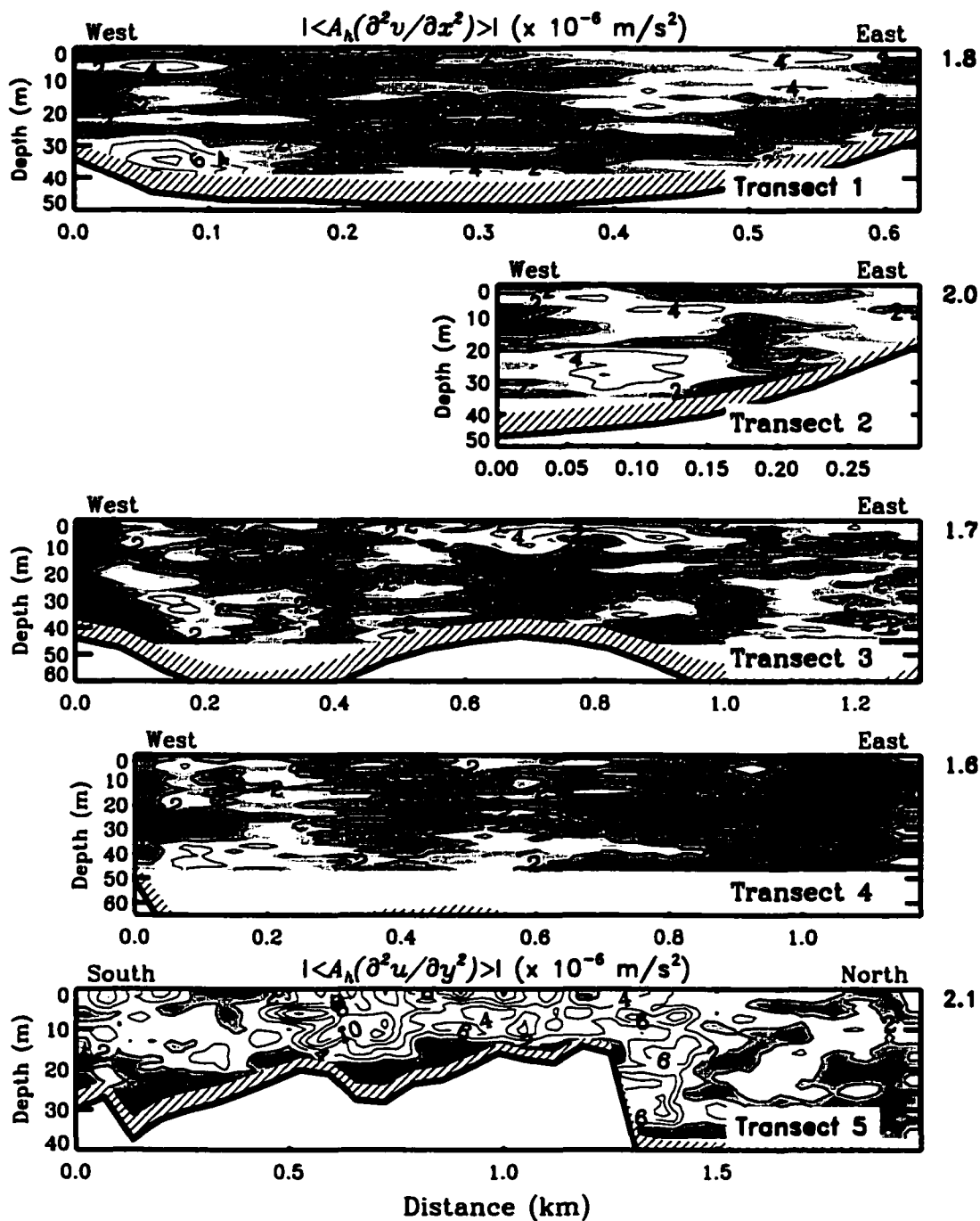
Figure 35.-. Contours of the tidally averaged horizontal friction term in the five transects. Near the upper right corner of each panel there are the absolute values of the sectional means. Title of transect 1 is valid for transects 1 to 4. Contour interval is 2 ($\times 10^4$) m/s^2 except in transect 5 where it is 4 ($\times 10^4$) m/s^2. Horizontal scales are comparable between transects 1 and 2, and between transects 3 and 4. Data in the shaded region near the bottom was not considered in the analysis due to side lobe effects. White region near the bottom was out of the profiling range of the ADCP.
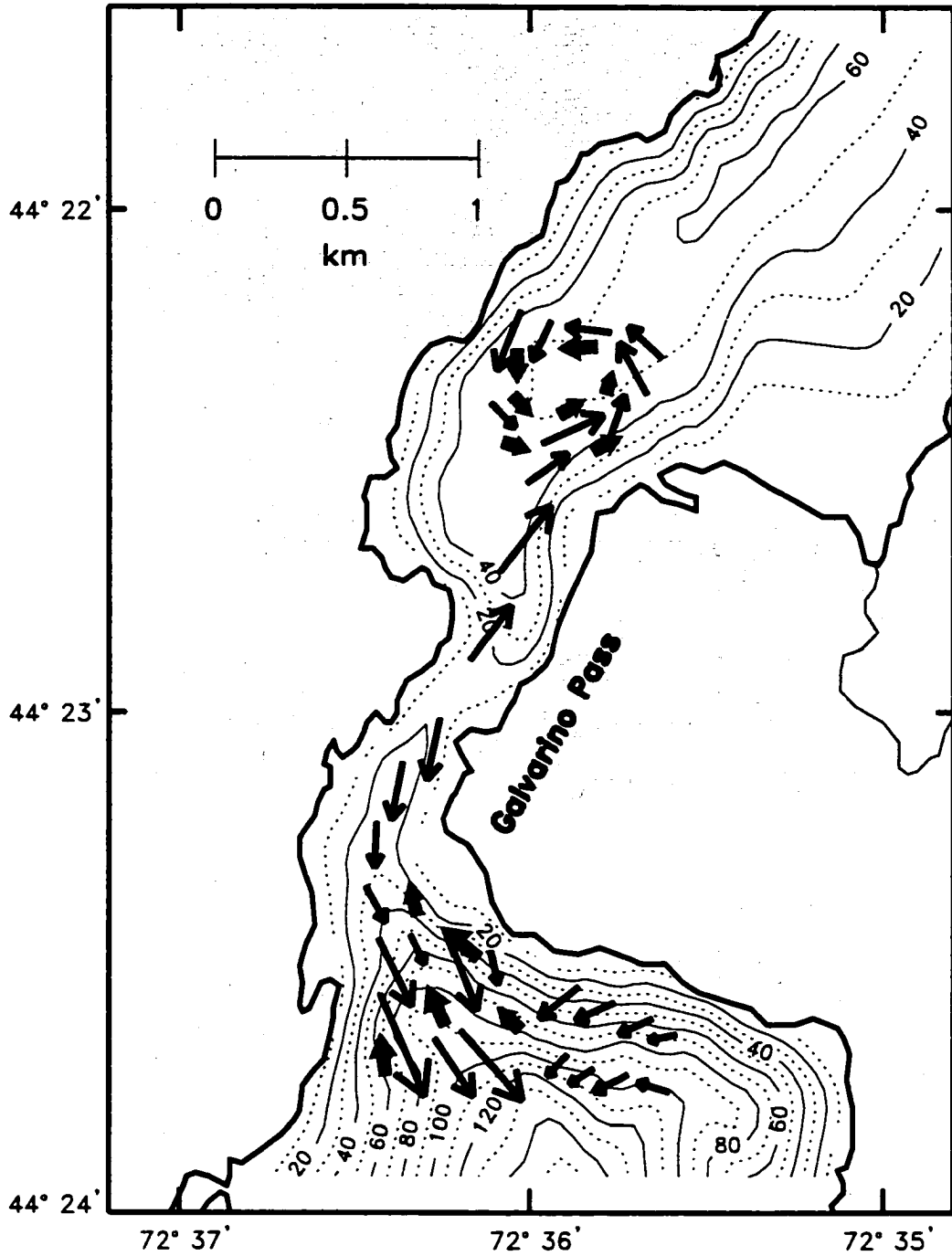
Figure 36.- Schematic representation of the mean flow at surface (black arrows) and at ~20 m depth (solid gray arrows) in the study region.
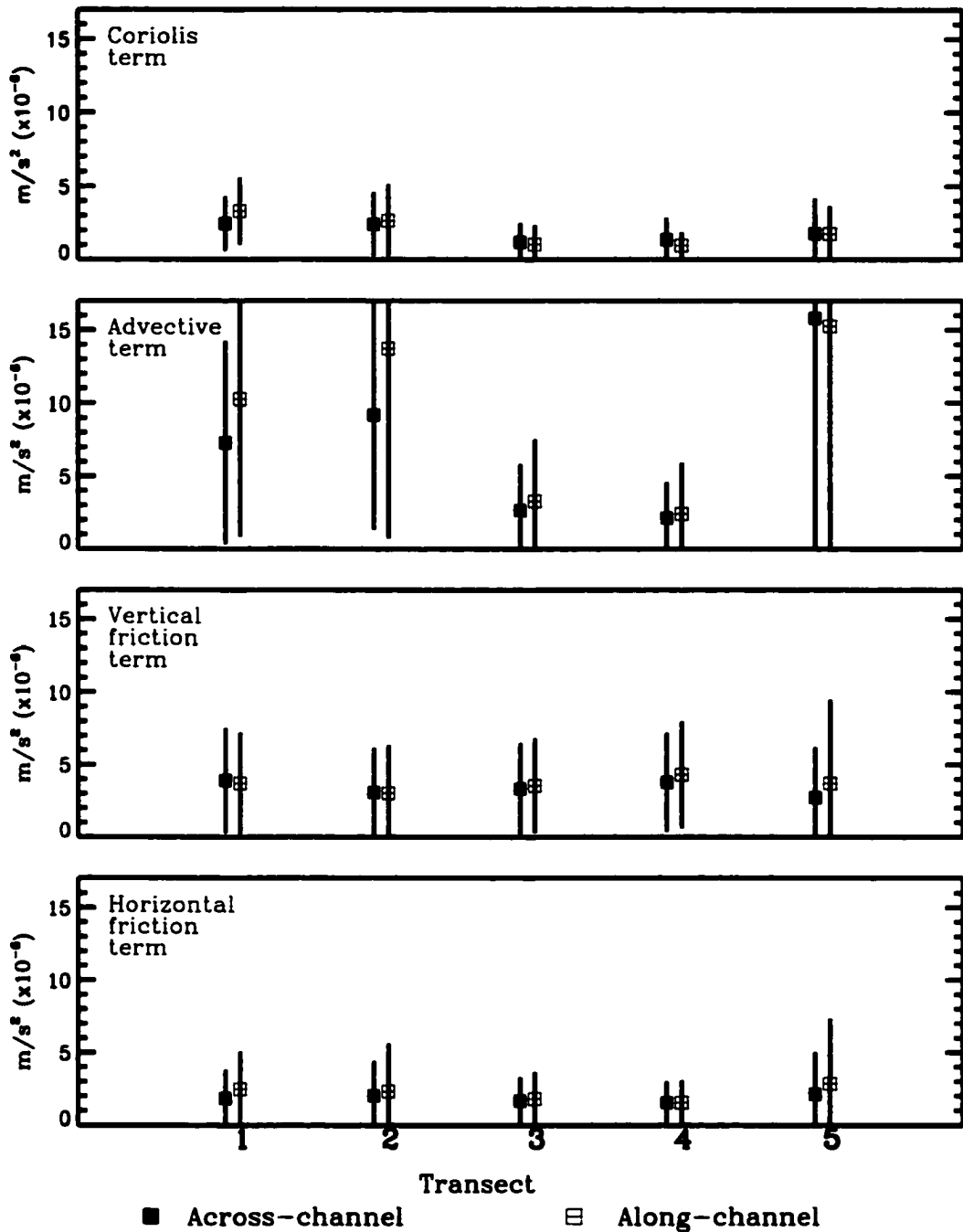
Figure 37.- Absolute values of the sectional means (squares) of the across and along-channel terms. Advective terms were more important than the rest of the terms in the northern side and within the pass. Across-channel values were comparable to along-channel values. Bars denote one standard deviation. See equations 1, 2, 3, and 4 for specifications of the terms.

values among them. The exception to this is the advective term, which seems to be about

four times greater to the north of the pass than to the south of the pass, and about six

times greater in transect 5 than to the south of the pass. This is probably a result of the

recirculation produced in the northern basin and nonlinearities induced by bathymetry and

coastline geometry in the sill, respectively. The baroclinic pressure gradient might also be

relevant to this balance as differences in density (Figure 31) between both sides of the sill

are noticeable and also there is marked stratification to the south of the pass. The

barotropic pressure gradient would be less important here as the transverse slopes in sea

level are probably less than $\sim 10^{-5}$ or 1 cm in 1 km, which might not be possible in this

area. It follows from Figure 37 that most of the terms in (4.1) and (4.2) should be

important contributors to the lateral momentum balance. Nevertheless, as mentioned

before in the analysis of figures of the along-channel and across-channel mean flow

(Figures 27 and 28, respectively), the magnitudes of the mean flow in both dimensions

seemed to be comparable between them. In order to further explore the effect of this

similarity in the dynamic balance, we will make some comparisons with the along-

channel momentum balance.

In the along-channel direction, the subtidal momentum balance for transects 1 to 4 is

given by

$$<u(\partial v/\partial x)> + <fu> = - <1/\rho(\partial p/\partial y)> + <A_z(\partial^2 v/\partial z^2)> + <A_h(\partial^2 v/\partial x^2)> \tag{4.3}$$

and for transect 5

$$<v(\partial v/\partial y)> + <fu> = - <1/\rho(\partial p/\partial y)> + <A_z(\partial^2 v/\partial z^2)> + <A_h(\partial^2 v/\partial y^2)> \tag{4.4}$$

which contain the terms that, with the exception of the pressure gradient term, may be reliably computed with the sampling design. As shown in Figure 37, sectional means obtained for these terms on each transect (contours not plotted here) are remarkably similar to the magnitudes of the means in the across-channel direction. The importance of the advective term in both directions in transects 1, 2 and 5 is also observed in the along-channel terms. This behavior might be attributed to the similar magnitudes of the u velocities and v velocities in the transects of the northern side and over the sill (Figures 27 and 28), which make the terms $u(\partial u/\partial x)$ and $v(\partial v/\partial y)$ also the largest in the transects. It is noteworthy to highlight the resemblance of the magnitudes between the terms in the across-channel and along-channel direction, as the across-channel dimension is customarily neglected in estuarine systems. Convergence of the coastline in the region of the contraction might be responsible for the enhancing of lateral accelerations of flow in these regions, making lateral flow comparable to the along-channel flow. River discharge in the northern side could also be a factor influencing the tendency of the flow to rotate, enhancing the lateral flow to the west exhibited in transect 1 at all depths. The effects of river discharge in the formation of tidal eddies in the northern side is a matter that requires more attention.

It is also notable that recirculation in the northern region might constitute a mechanism of retention of water, making residence times of the water in the northern basin much longer than in the south. This finding should be a matter of further investigations in the region as the mechanisms of dispersion of pollutants and particulate material are strongly restricted by the presence of the sill in Galvarino Pass. This issue

might become particularly sensitive as the main population area (Puyuguapi Port, Figure 25) is located in the northernmost region of Ventisquero Sound.

In summary, the mean flow in the northern side of the pass showed a tendency of the flow to rotate anticlockwise throughout the water column . This feature should result in a sluggish flushing of the northern side. South of the pass, mean surface outflow and mean bottom inflow (at 20 m) developed near the western side of the fjord. Within the pass, the shallowest and narrowest section represented a boundary between inflows and outflows. The strongest net inflows (~15 cm/s) were observed in the sill region and the strongest outflows (~10 cm/s) were seen to the south of the pass. The magnitude of the tidal flows increased toward the north, reaching a maximum over the sill, and then decreased northward owing to continuity conservation of mass. In the across-channel momentum balance the advective terms seemed to be greater than the rest of the terms to the northern of the pass and over the sill. Magnitudes of the terms in the along-channel momentum balance were comparable to those in the across-channel direction, highlighting the importance of the transverse dimension under strong geometric constraints.

DYNAMIC SIMILARITY AND NONDIMENSIONAL ANALYSIS

5.1 Introduction

The basis for the concept of dynamic similarity, a principle at the heart of experimental fluid mechanics, is that two flows having different length scales, flow speeds, or fluid properties can be apparently different, but still "dynamically similar"[Kundu, 1990]. The concept of similarity is intimately associated with the idea of dimensionless products, in which there is an intensive use of unified data presented in terms of nondimensional parameters. For example, flows having similar values of Reynolds number may be dynamically similar. Very useful relationship between models in the laboratory and natural systems may be established on the basis of sound physical considerations, coupled with a dimensional analysis. The similarity principles are widely used in presenting experimental (laboratory) data, where the use of dimensionless products of the variables under study is especially useful. In establishing the magnitudes of the main dimensionless groups, there is also an essential benefit in scaling terms in the momentum balance, which allows determination of the relative importance of different physical forces to the dynamics.

The idea of similarity is also the basis of model testing, in which laboratory data of one flow can be applied to other flows. Thus, prototypes designed in laboratory, based in principles of dynamic similarity, may help in describing the behavior of other similar systems outside the laboratory. Nevertheless, in applying the similitude of laboratory to estuarine stratified flows, there is not always complete dynamic similarity, as the interfacial layer in the experiment may be in a quasi-laminar state, while the prototype

may be completely turbulent, leading to different rates of mixing [*Grubert*, 1989]. This would not be the case when comparing natural systems, as the flows are always turbulent.

But in studying dynamic similarity, the geometry of the systems also plays an important role, then geometric similarity is also desirable as a precondition to dynamic similarity. Nevertheless, this is difficult to attain in natural systems, and the geometric characteristics, usually described by a series of lengths and angles, can be used as a complement to the dynamic similarity analysis. In the case of across-channel sections, the characteristics of interest are customary referred to as the width (W), total depth (H), the ratio (H/W), the cross sectional area (A), and the hydraulic radius (A/w), where w is the wetted perimeter, i.e. the perimeter of the cross-section in contact with the fluid. For those bottom profiles where a topographic feature is present, there are also two parameters of interest, the aspect ratio $\Delta=H/L$, where L is the horizontal length of the feature, and the fractional height of the feature $\delta=h_m/H$, where h_m is the maximum height of the feature above the bottom.

In the preceding chapters, the relative importance of the inertial, Coriolis, and frictional effects in the across-channel variability has been investigated. Now it is necessary to determine if the scaling of the terms observed in the cross-sections are consistent with the size of the nondimensional flow groupings. The purpose of this study is to compare the flow characteristics in the three systems under study, in order to establish dynamic similarities among the cross-sections. To do this, a nondimensional analysis is performed, making use of four dimensionless numbers customarily used in oceanography: the Rossby number, the Ekman number, the Reynolds number and the

Richardson number. Tidal range to depth ratio, a parameter widely used in estuarine studies, is also used in comparing the three natural systems. A description of these numbers is shown in the following paragraphs.

5.2 Nondimensional numbers

Rossby number

An important measure of the significance of the earth's rotation for a particular phenomenon is the Rossby number.

$$R_o = \frac{Advection}{Coriolis} = \frac{U}{Lf} \tag{5.1}$$

The Rossby number (R_o) compares advection (or inertia) to Coriolis force, which considers the time (L/U) it takes for a fluid element moving with speed U to traverse the distance L. If this time is much less than the period of rotation of the earth, the fluid will have a weak sense of the earth's rotation over the time scale of the motion. For rotation to be important, then U/Lf, where f is the Coriolis parameter, has to be much less than 1. This number is currently used to define large-scale motions, which are significantly influenced by the earth's rotation [*Pedlosky*, 1987], as well as in modelling the vorticity generation on the shelf [*Janowitz and Pietrafesa*, 1982], and in the diagnosis of flow curvature [*Shearman et al*, 2000].

Ekman number

Another parameter where the significance of the earth's rotation is important is the Ekman number. The Ekman number (Ek) compares friction (vertical or horizontal) to

Coriolis force.

$$Ek_z = \frac{Vertical\ friction}{Coriolis} = \frac{A_z}{fH^2} \qquad (5.2)$$

$$Ek_z = \frac{Horizontal\ friction}{Coriolis} = \frac{A_h}{fL^2} \qquad (5.3)$$

Where A_z and A_h are the vertical eddy viscosity and the horizontal eddy viscosity, respectively, L is a typical horizontal scale and H is a typical depth. Small Rossby and Ekman numbers ($<<1$) indicate no departures from a quasi-geostrophic balance.

Reynolds number

The Reynolds number is one of the dimensionless numbers that can represent certain characteristics of the flow of homogeneous and stratified fluids in channels [*Dyer*, 1997]. The Reynolds number compare the relative importance of inertia and viscous forces in determining the resistance to flow.

$$Re = \frac{Inertia\ force}{Viscous\ force} = \frac{UL}{v} \qquad (5.4)$$

where U is a velocity, L is a distance and v is the kinematic viscosity, the ratio of molecular viscosity to density (μ/ρ). Equality of Re is a requirement for the dynamic similarity of flows in which viscous forces are important. (Kundu, 1990, p 260).

Reynolds numbers based on molecular friction have been used in studying and modelling of the benthic boundary layer [i.e *Sternberg*, 1968; *Green*, 1992], and also reported for studies of shear instabilities after passing through a lateral constriction [*Seim and Gregg*,

1994]. But in unstratified conditions in rivers and estuaries the flow is always transitional

to fully turbulent. While the Reynolds number based on molecular friction is out of the

scope of this study, the ratio of the non-linear terms and the friction terms, measured by

the Reynolds number based on eddy viscosities, remains an important parameter. Use of

eddy viscosities is based on the fact that in the ocean, where the motion is generally

turbulent, the effective value of kinematic viscosity is the eddy viscosity [*Tennekes and*

Lumley, 1972; *Pedlosky*, 1987; *Cushman-Roisin*, 1994; *Pond and Pickard*, 1995]. The

apparent friction effects in the ocean, as quantified by the eddy viscosities, are much

larger than molecular ones. As an example, horizontal eddy viscosities values are 10^7 to

10^{11} times molecular values while the vertical values are 10 to 10^5 times molecular values

[*Pond and Pickard*, 1995]. That is why eddy viscosity must replace molecular viscosity in

the momentum equations [*Cushman-Roisin*, 1994]. Applications of the Reynolds number

with eddy viscosity are found in studies of the flow in the lee of island wakes [*White*,

1973; *Pingree and Maddock*, 1980; *Wolanski et al.* 1984; *Pattiaratchi et al.* 1986], in

recirculating flows [*Dennis and Middleton*, 1994], in determining instabilities in the

western boundary layer [*Ierley and Young*, 1991], and in the instabilities associated to

internal gravity waves [*Skyllingstad and Denbo*, 1994], among others. It is also customary

to compare inertial and frictional forces by defining a Reynolds number, that involves the

nondimensional numbers discussed above $Re_z = Ro/Ek_z$ and $Re_h = Ro/Ek_h$ [*Cushman-*

Roisin, 1994].

We can, in fact, ignore molecular friction in the ocean, as it only becomes important

very close to solid boundaries, where low values of Re will occur at low values of U

and/or of *L*. An example using molecular friction in estimating *Re* in tidal channel beds is

provided by *Sternberg* [1968].

Richardson number

The competition between the stabilizing forces and the flow vertical shears is

customarily expressed as the Richardson number

$$Ri = \frac{Bouyancy}{Inertia} = \frac{N^2}{[\frac{\partial u}{\partial z}]^2 + [\frac{\partial v}{\partial z}]^2} \tag{5.5}$$

where N^2 is the Brunt-Väisälä frequency. This is also a measure of the relative importance

of mechanical and density effects. If *Ri* is less than zero, density variations enhance the

turbulence; if *Ri* is greater than zero they tend to reduce it. It has been postulated that the

neccesary but not sufficient condition for instability to occur in stratified flows is when *Ri*

is less than 0.25. [*Miles*, 1961]. This is a nondimensional number widely used in

estuarine systems [*Dyer*, 1997].

Tidal range to depth ratio

The first approximation to the understanding of flow similarities might be provided

by using the tidal range to depth ratio. This ratio may be used as an indicator of the

strength of the nonlinearities with respect to tidal forcing [*Giese and Jay*, 1989], as a

scaling of the continuity equation in convergent channels [*Friedrichs and Aubrey*, 1994],

as a tidal asymmetry factor [*Friedrichs and Aubrey*, 1994], and as a measurement of the

degree of damping or amplification in an estuary [*Savenije*, 1998]. It has been also used

as a restriction in the application of a numerical model of non-linear tidal interactions in a

tidal estuary [*Scott*, 1994], and as restriction to minimize error when computing net

discharge in estuaries with a large (> 0.3) tidal range to mean water depth [*Kjerfve*, 1975].

Typical values of this ratio in fjords are less than 0.1, but in many coastal plains and bar-

built estuaries they may reach 0.3 to 0.7 [*Kjerfve*, 1975].

5.3 Methods

Six cross-sections from the three systems under study were chosen to study their

dynamic similarity. They are Aysen Fjord, Chacao Channel, and Ventisquero Sound

transects 1 to 4. Transect 5 at Ventisquero Sound was not considered in this analysis as it

was a longitudinal transect. Their corresponding bottom profiles are presented in Figure

38. Notice the differences in lateral and vertical scales. Some geometric characteristics of

these cross-sections are presented in table 2.

Table 2. Main geometric parameters and other values of interest

	Aysen F.	Chacao C.	V1	V2	V3	V4
Tidal currents (m/s) [u_o]	0.2	3.5	0.35	0.35	0.25	0.25
Tidal range (m) [h_o]	2.2	6.5	2.2	2.2	2.2	2.2
Sectional area (m^2) x10^4 [A]	49.8	15.4	2.7.	1.1	7.3.	9.8
Hydraulic radius (m) [R]	163.7	72.2	43.9	37.1	56.0	83.6
Wetted perimeter (m) [w]	3047	2143	627	301	1302	1183
Mean depth /width [H/W]	0.05	0.03	0.07	0.12	0.04	0.07
Aspect ratio [Δ]	0.13	0.17	-	-	0.04	0.03
Fractional height [δ]	0.74	0.83	-	-	0.33	0.22
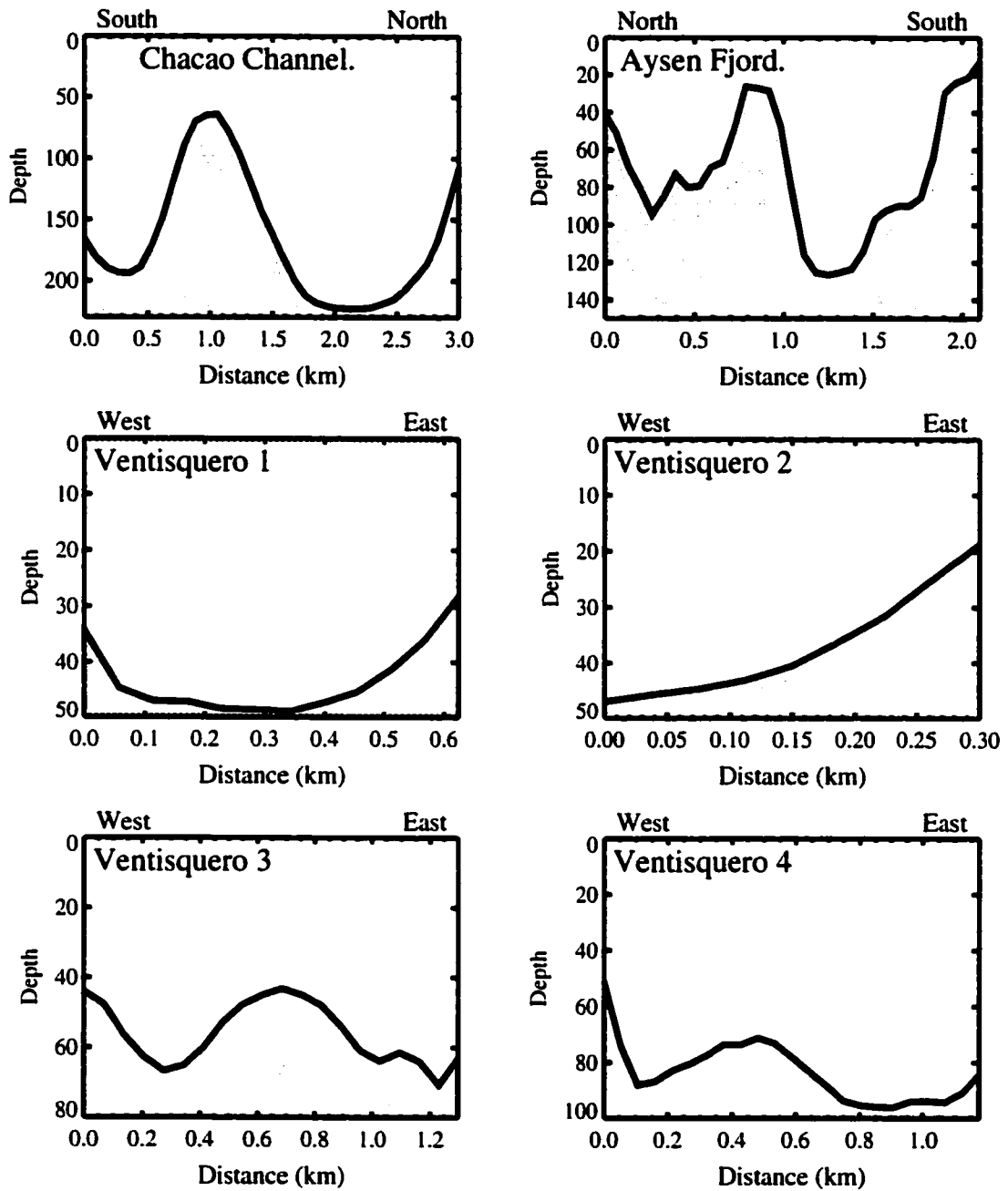
Figure 38. Bottom profiles in the six sections under study. Depth and wide scales are different in the sections.

For the lateral momentum balance, the dimensionless numbers may be given by

Rossby number

$$R_o = \frac{Advection\ term}{Coriolis\ term} = \frac{v(\partial v/\partial y)}{fu}$$

for the cross-sections in Aysen Fjord and Chacao Channel, or

$$R_o = \frac{u(\partial u/\partial x)}{fv}$$

or the cross-sections in Ventisquero Sound. These numbers will constitute a proxy of the

typical dimensionless number $R_o = U/fL$, where U is a typical velocity occurring in a

distance L.

Ekman number (vertical)

$$Ek_z = \frac{Vertical\ friction\ term}{Coriolis\ term} = \frac{A_z[\partial^2 v/\partial z^2]}{fu}$$

for the cross-sections in Aysen Fjord and Chacao Channel, or

$$Ek_z = \frac{A_z[\partial^2 u/\partial z^2]}{fv}$$

for the cross-sections in Ventisquero Sound.

Ekman number (horizontal)

$$Ek_h = \frac{Horizontal\ friction\ term}{Coriolis\ term} = \frac{A_h[\partial^2 v/\partial y^2]}{fu}$$

for the cross-sections in Aysen Fjord and Chacao Channel, or

$$Ek_h = \frac{A_h[\partial^2 u/\partial x^2]}{fv}$$

for the cross-sections in Ventisquero Sound. These numbers will constitute a proxy of the

typical dimensionless number $Ek_z=A_z/fH^2$ and $Ek_h=A_h/fL^2$.

Reynolds number (vertical)

$$Re_z = \frac{Advection\ term}{Vertical\ friction\ term} = \frac{v(\partial v/\partial y)}{A_z[\partial^2 v/\partial z^2]}$$

for the cross-sections in Aysen Fjord and Chacao Channel, or

$$Re_z = \frac{u(\partial u/\partial x)}{A_z[\partial^2 u/\partial z^2]}$$

for the cross-sections in Ventisquero Sound.

Reynolds number (horizontal)

$$Re_h = \frac{Advection\ term}{Horizontal\ friction\ term} = \frac{v(\partial v/\partial y)}{A_h[\partial^2 v/\partial y^2]}$$

for the cross-sections in Aysen Fjord and Chacao Channel, or

$$Re_h = \frac{u(\partial u/\partial x)}{A_h[\partial^2 u/\partial x^2]}$$

for the cross-sections in Ventisquero Sound.

The Richardson number was computed making use of the density profiles taken during the sampling in the three systems. Velocity measurements obtained in the near vicinity of the corresponding CTD cast were used together with density profiles to obtain

$$Ri = \frac{-\frac{g}{\rho}\frac{\partial \rho}{\partial z}}{[\frac{\partial u}{\partial z}]^2 + [\frac{\partial v}{\partial z}]^2}$$

Once the corresponding dimensionless groups were obtained in the way indicated above, outliers were removed from each series according to the following procedure. Unrealistic values over 1000 were removed from the series. Even for large Reynolds number obtained in laboratory experiments [Van Dyke, 1982], this number seemed to be large. For the remaining data sets, differences of the means were standardized by the standard deviation. Values over three standard deviations were removed from the series. The mean and range of the new series without outliers were plotted for each dimensionless number in order to establish similarities and differences among the systems. A comparison between means and variances of each dimensionless group was performed using the t-student and F-test, respectively. The analysis of similarity was based in matrices of resemblance of the means and variances of each dimensionless number for the 6 systems.

A similar procedure was applied with the data set of tidal range to depth ratio obtained for the six sections. Values of maximum tidal ranges during spring tides for the six places, reported in nautical charts of the three regions, divided by the depths in the

bottom profile for each section were considered. These ratios were calculated in order to assess the contribution of the nonlinearities to the dynamics in these systems.

5.4 Results

This section describes the results of the nondimensional analysis for the six cross-sections under study. The results are presented following the nondimensional groups. Figure 39 shows the distribution of the tidal range to depth ratio in the six sections. With exception of Chacao Channel, the sections had ratios less than 0.1, which were typical values of fjords. The large variability in the Chacao Channel data might be attributed to the large variations of the depths in the cross-section, owing to the pinnacle in the center. In this channel the largest tidal range (6.5 m) contributed to its highest mean value in the six distributions, and it was also an indication of the importance of nonlinearities in this section. Aysen had the smallest ratio suggesting smallest nonlinearities.

The results for the Rossby number are presented in Figure 40. Just the transects located in the south side of the Galvarino Pass (Ventisquero 3 and 4, hereafter "the pass") seemed to be similar, as their means were similar, while the rest of the transects exhibited differences among them. Hence, Aysen Fjord seemed to be the only section where Coriolis effects were important in the lateral momentum balance. On the other hand, in Chacao channel Coriolis effects seemed to have the lowest relative contribution in the six sections. This pattern suggested that, with exception of Aysen Fjord, advective processes were dominant over rotational effects on the flows in the sections.

The importance of the Coriolis effect was also observed in the results of the vertical Ekman number (Figure 41) and Horizontal Ekman number (Figure 42). Again, a similar
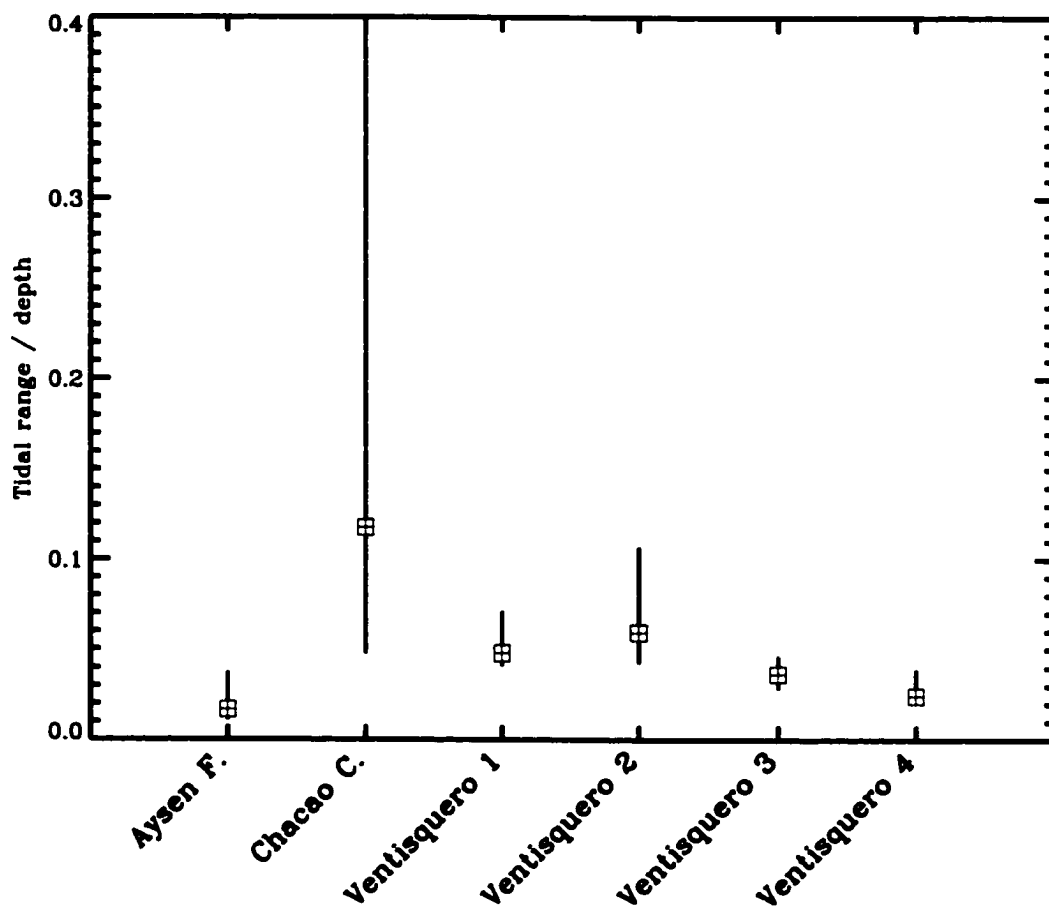
Figure 39. Tidal range to depth ratio. Values below 0.1 are typical values in fjords. Larger values denote effect of nonlinearities.

Figure 40. Rossby number values distribution. White box denotes mean, and the thin line is the range. With the exception of Aysen, advection dominates over Coriolis in these systems.

Figure 41. Vertical Ekman number values distribution. White box denotes mean, and the thin line is the range. With the exception of Aysen, vertical friction dominates over Coriolis in these systems.
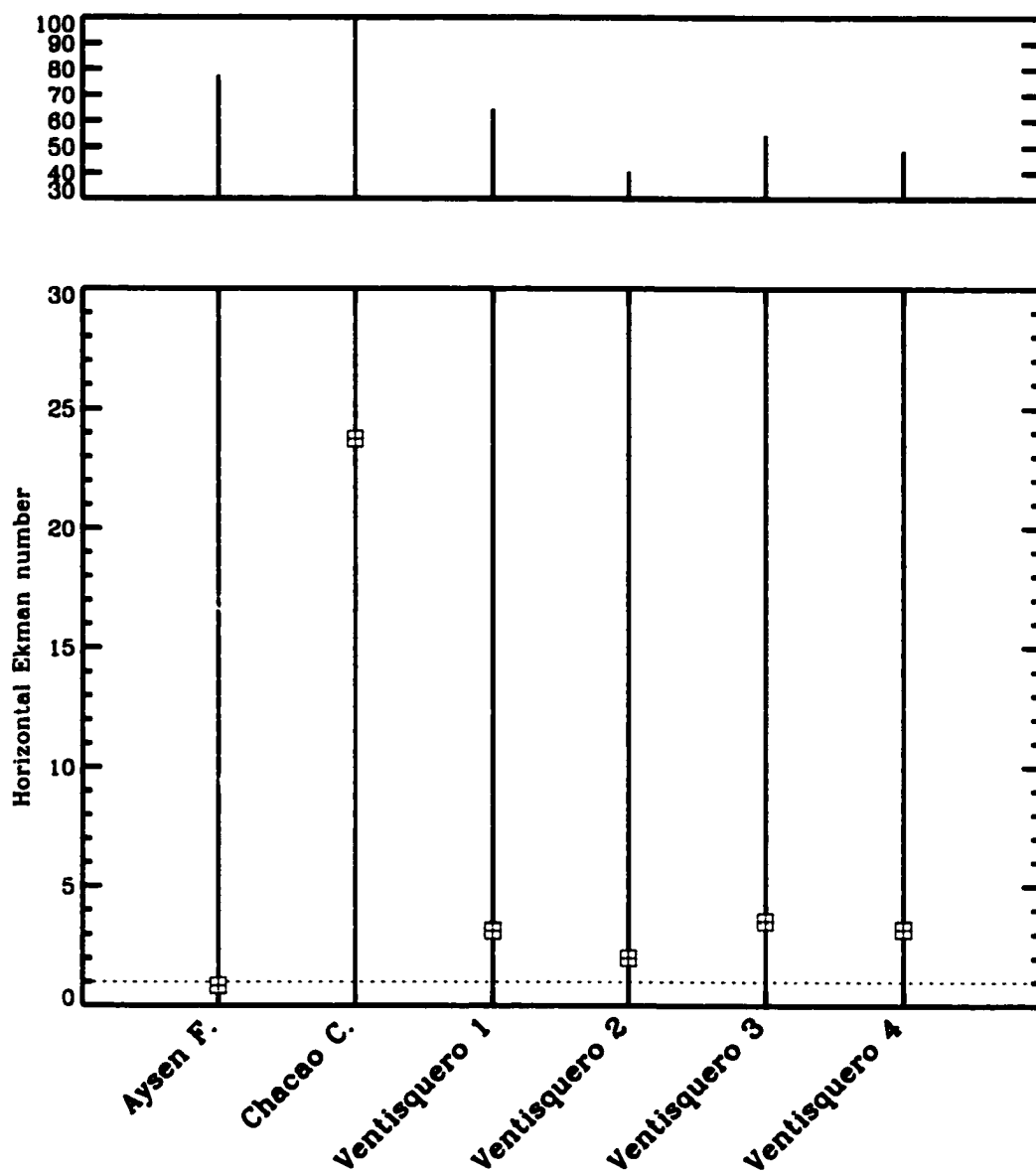
Figure 42. Horizontal Ekman number values distribution. White box denotes mean, and the thin line is the range. Horizontal friction dominates over Coriolis in Chacao Channel.

pattern to that observed for the Rossby number was seen. Aysen Fjord seemed to be the most influenced by the Coriolis effect, Chacao Channel had the highest mean and variability, and the sections Ventisquero 3 and Ventisquero 4 looked similar in their means. This pattern suggests that, with the exception of Aysen Fjord, vertical friction was more important in the sections than the Coriolis term.

From the Horizontal Ekman number (Figure 42), Aysen Fjord also exhibited a distribution about unity, similarly to the previous two figures, which indicated that Coriolis effects are important and comparable to horizontal friction. In this figure, there is also a decrease in the importance of the horizontal friction in the sections of Ventisquero Sound, when compared with vertical friction (Figure 41), as their means are much closer to one than in the vertical Ekman number. Variability and means are also comparable between both sides of the pass in Ventisquero Sound in this figure. Very large values were identified in the Chacao Channel section, owing to the effect of the large horizontal friction found there.

The pattern emerging from the three previous figures is that the only section where Coriolis term seemed to be important to the dynamics was in Aysen Fjord. This confirmed that the momentum balance in the across-fjord dimension is quasigeostrophic with weak effects of friction (vertical and horizontal) and advection.

The vertical Reynolds number was plotted in Figure 43. The means were comparable between Asyen Fjord and Chacao Channel, between Ventisquero 1 and Ventisquero 2, and between Ventisquero 3 and Ventisquero 4. In all the cases advection was more important than vertical friction. Something peculiar is observed here. Aysen Fjord and
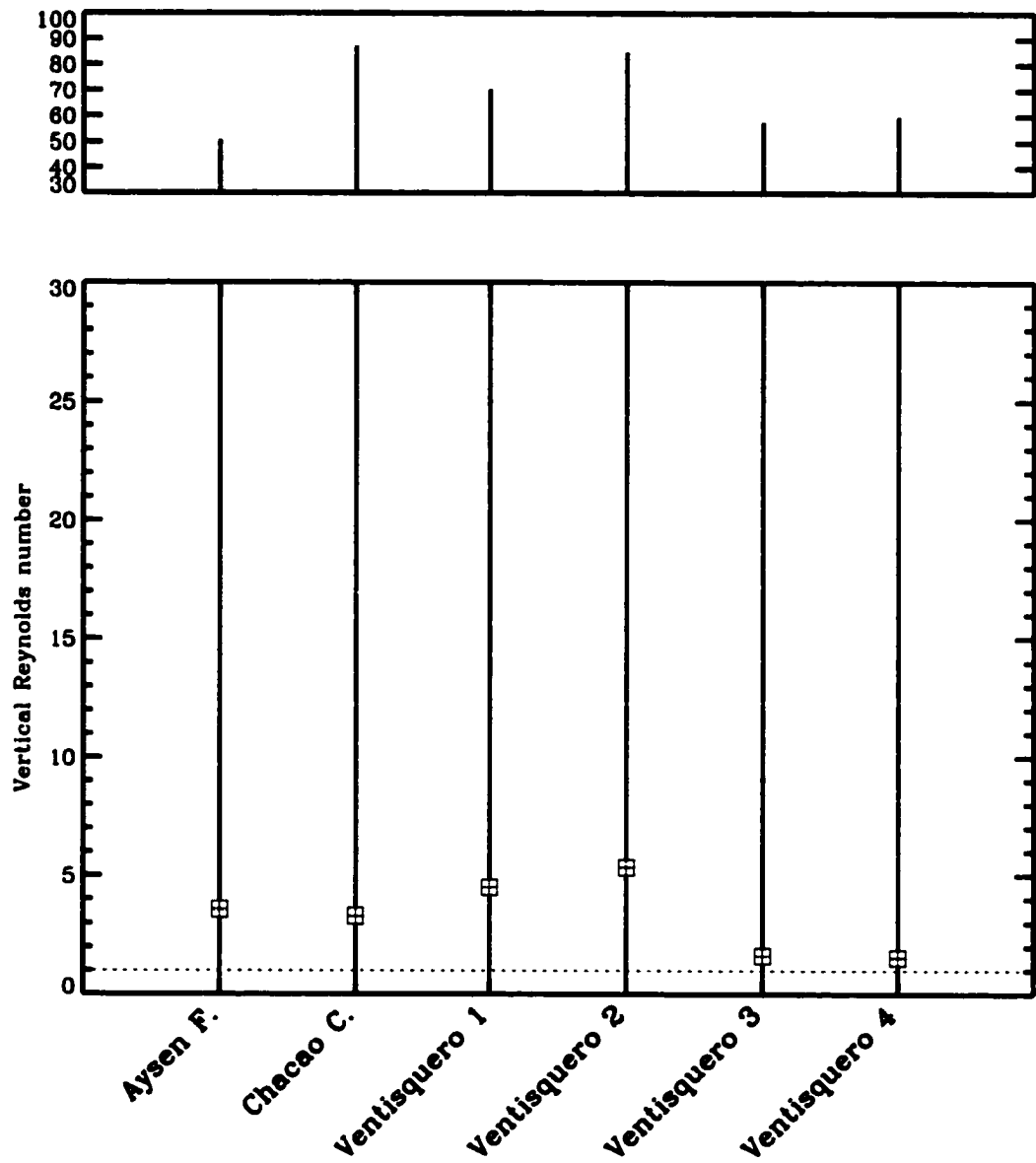
Figure 43. Vertical Reynolds number values distribution. White box denotes mean, and the thin line is the range. Advection dominates over vertical friction in these systems.

Chacao Channel, separated by about 400 km, were more similar in terms of their ratio of

advective to vertical friction effects, than the transects from the north (Ventisquero 1 and

2) to the south of the pass (Ventisquero 3 and 4), geographically separated by no more

than 3 km. The latter was also the only case where Chacao Channel seemed to be similar

to another system, which is surprising considering the peculiar characteristics of this

strong tidal current channel.

In the case of the horizontal Reynolds number (Figure 44), with the exception of

Chacao Channel, advection was also more important than horizontal friction in the

sections. A mean below one for Chacao Channel was derived from the extraordinarily

high values of the horizontal friction term (A_h =90 m^2/s) already presented for this

system. In this figure, the means observed for Ventisquero 3 and 4 were comparable

between them, and also with Aysen Fjord. This figure also suggests an advection-

diffusion type of momentum balance in the case of Chacao Channel because in the

previous nondimensional groupings, friction and advection terms were much larger than

the Coriolis term.

The Richardson number is presented in Figure 45. The effects of the different degrees

of stratification in the systems was suggested from the figure. Chacao had the lowest

values as buoyancy was less important in this channel and tendency to instabilities were

higher, as expected. The four transects of Ventisquero Sound showed higher means than

the critical Richardson number (=0.25) and greater variability than Chacao, suggesting

that contribution of buoyancy is important here. Aysen fjord had the largest values of the

six transects, which was probably attributed to the strong vertical gradients of salinity
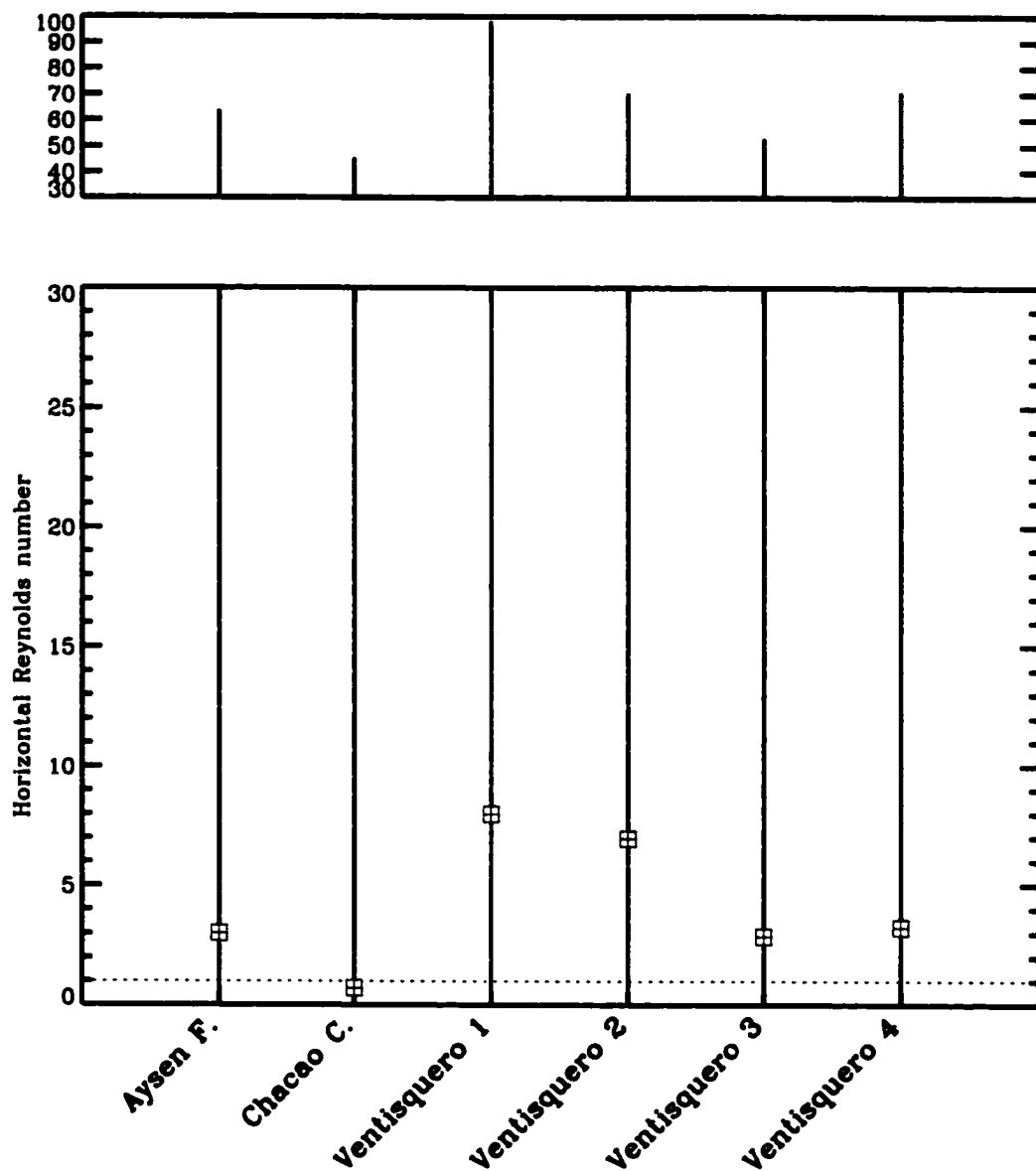
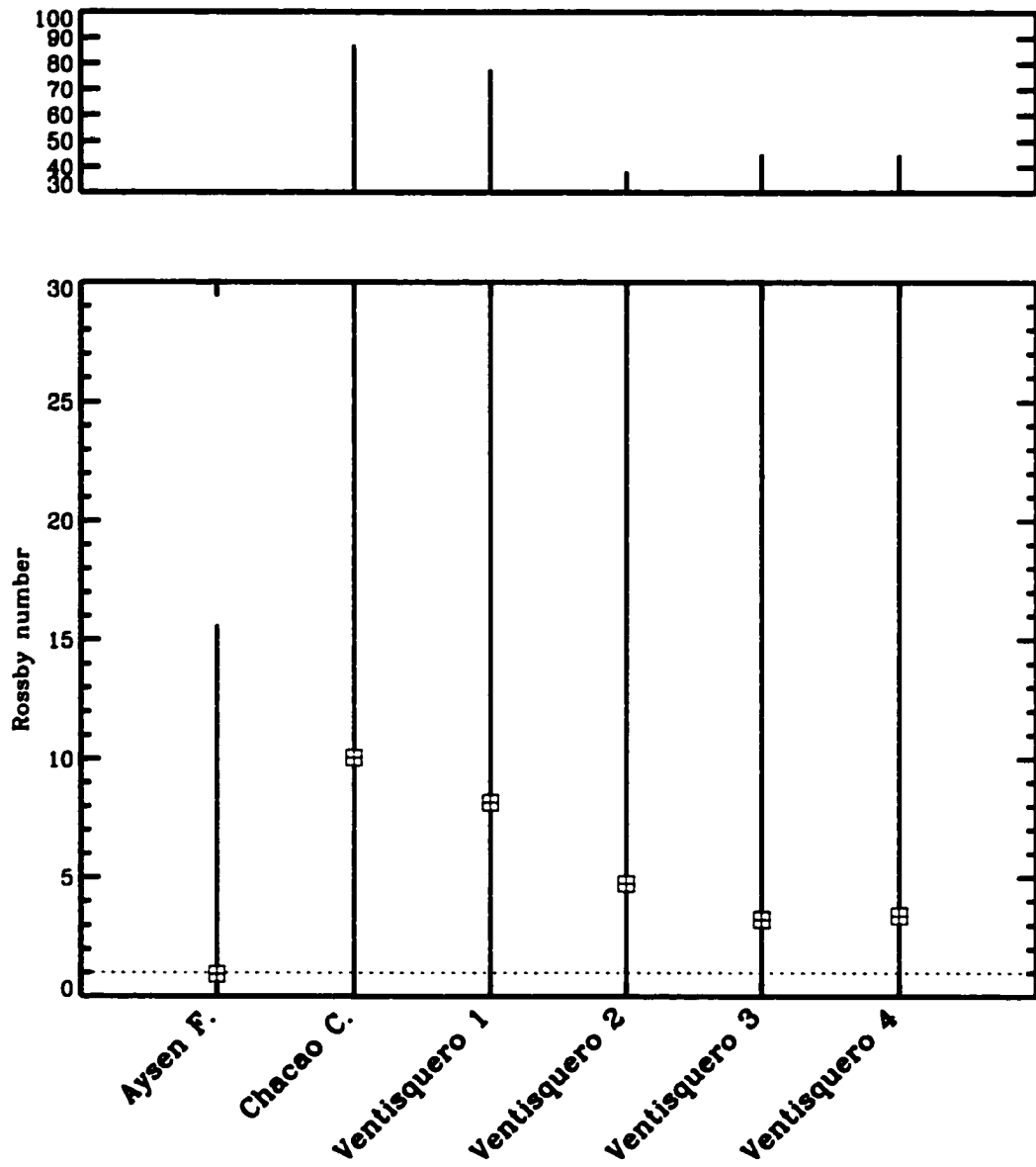Figure 44. Horizontal Reynolds number values distribution. White box denotes mean, and the thin line is the range. With the exception of Chacao Channel, advection dominates over horizontal friction in these systems.
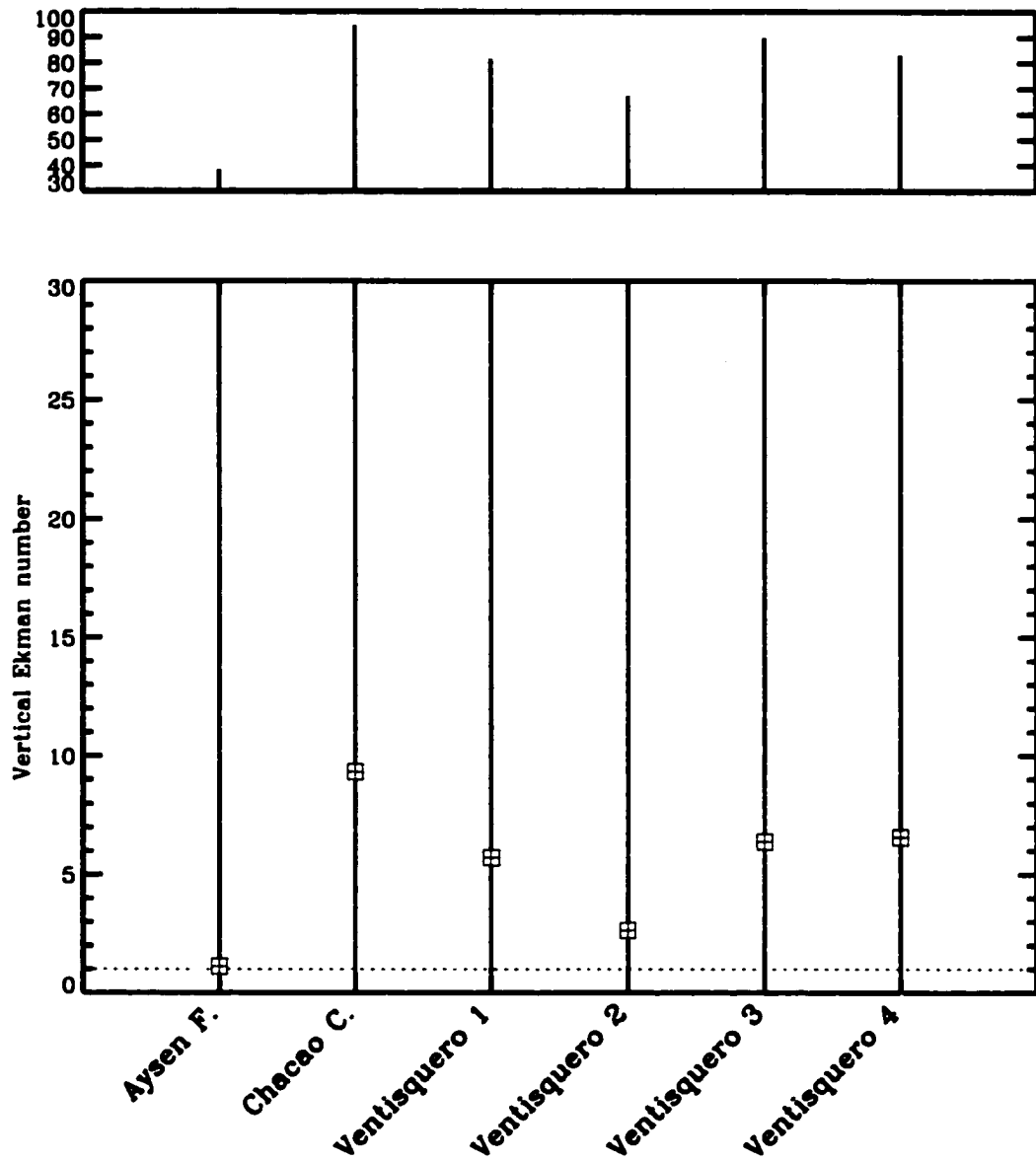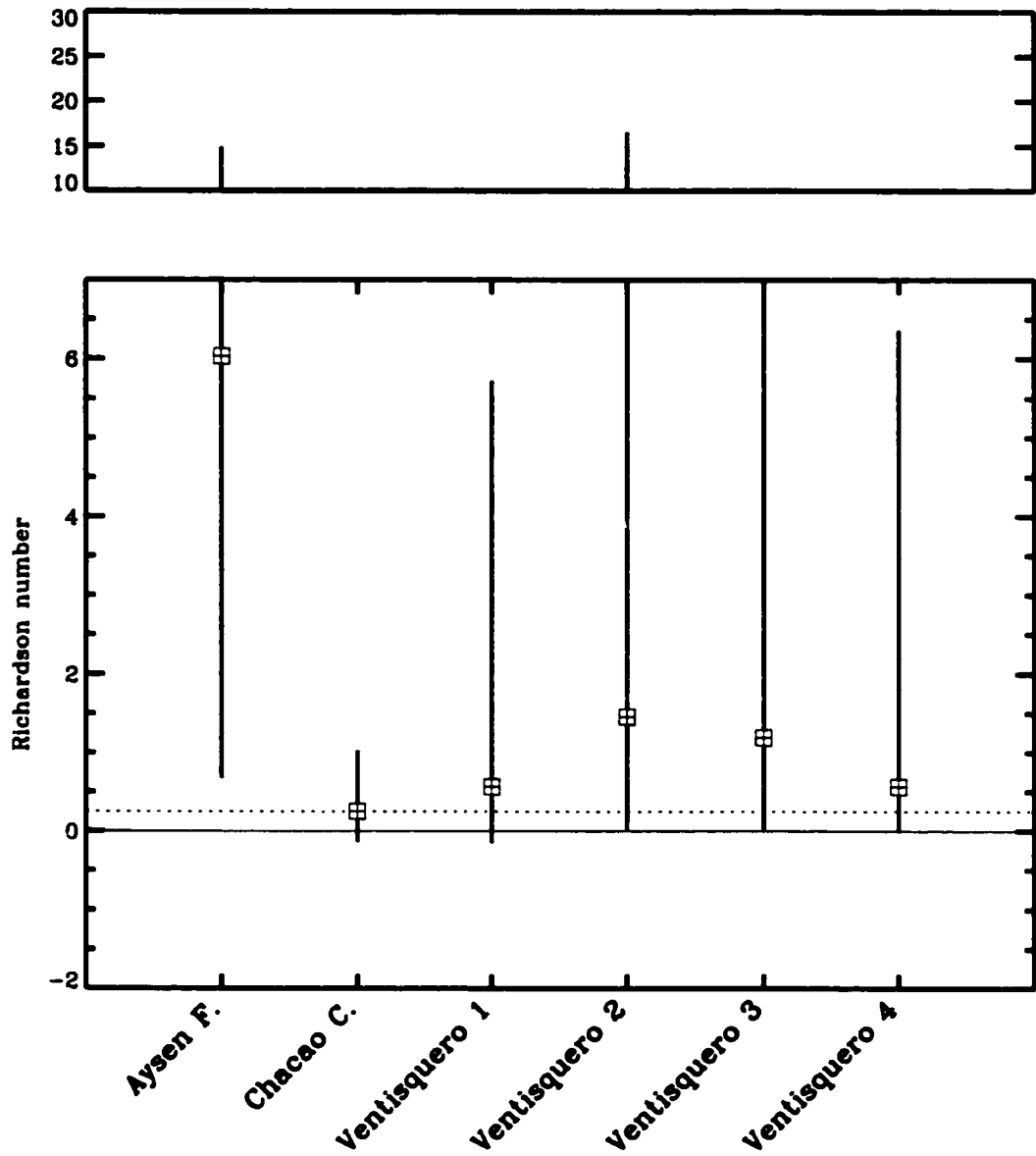
Figure 45. Richardson number values distribution. White box denotes mean, and the thin line is the range. Effects of the stratification in the first 15 m are evident in the case of Aysen.

observed during the experiment in the three stations. Nevertheless, this is probably not representative of the whole water column, as the maximum depth of the CTD casts was 50 m, a fourth part of the total depth.

Similarity matrices of means are presented in Figure 46. The different degrees of similarities were expressed as indicated in the legend. A value of zero indicated that the two distributions were significantly different. For each nondimensional number (or matrix) there was between one to three findings of similarities between the different systems. Ventisquero 3 and 4, at the southern side of the pass, showed similarities (in different degrees) in the six nondimensional numbers, which is not surprisingly as these parallel transects were placed close to each other, with similar bottom profiles. In the case of sections at Ventisquero 1 and 2, at the northern side of the pass, which were also located close to each other, moderate similarities were found just for the Reynolds (vertical and horizontal) and Richardson numbers. The fact that these two sections did not show more similarities might be attributed to the different bottom profiles. Ventisquero 1 covered almost the whole width of the fjord (about 600 m), while Ventisquero 2 just covered the eastern portion for about 300 m. In addition, they were not parallel and they had different mean depths, thus making the behavior of the advection and frictional terms significantly different between them.

When the northern and the southern sides of the pass were compared (Ventisquero 1-Ventisquero 2 with Ventisquero 3-Ventisquero 4), similarities were found among Ventisquero 1 with Ventisquero 3-Ventisquero 4 in the Ekman numbers (vertical and horizontal) and Richardson number, which was an indication of similar frictional and

Similarity of Means

R_o

	AYS	CHA	V1	V2	V3	V4
AYS		0.00	0.00	0.00	0.00	0.00
CHA			0.00	0.00	0.00	0.00
V1				0.00	0.00	0.00
V2					0.00	0.00
V3						0.36
V4						

Ek_z

	AYS	CHA	V1	V2	V3	V4
AYS		0.00	0.00	0.00	0.00	0.00
CHA			0.00	0.00	0.00	0.00
V1				0.00	0.13	0.05
V2					0.00	0.00
V3						0.58
V4						

Ek_h

	AYS	CHA	V1	V2	V3	V4
AYS		0.00	0.00	0.00	0.00	0.00
CHA			0.00	0.00	0.00	0.00
V1				0.00	0.16	0.82
V2					0.00	0.00
V3						0.08
V4						

Re_z

	AYS	CHA	V1	V2	V3	V4
AYS		0.23	0.00	0.00	0.00	0.00
CHA			0.00	0.00	0.00	0.00
V1				0.15	0.00	0.00
V2					0.00	0.00
V3						0.58
V4						

Re_h

	AYS	CHA	V1	V2	V3	V4
AYS		0.00	0.00	0.00	0.42	0.18
CHA			0.00	0.00	0.00	0.00
V1				0.19	0.00	0.00
V2					0.00	0.00
V3						0.06
V4						

Ri

	AYS	CHA	V1	V2	V3	V4
AYS		0.00	0.00	0.00	0.00	0.00
CHA			0.32	0.15	0.11	0.23
V1				0.31	0.34	1.00
V2					0.79	0.30
V3						0.32
V4						

0.01 - 0.1   Sligthly similar   0.5 - 0.75   Very similar

0.1 - 0.5   Moderately similar   0.75 - 1.0   Strongly similar

Figure 46. Matrices of similarity of means using t-student test in the five nondimensional numbers. Values correspond to the probability that means be equals in the range 0 to 1, 1 indicating equal means.

buoyancy characteristics between the northern and southern sides of the pass. In addition, the strongest similarity (0.82) was observed in the horizontal Ekman number between Ventisquero 1 and Ventisquero 4.

Examples of similarities among distant sections were found in three cases. Aysen Fjord was in the range of "moderately similar" with Ventisquero 3 and 4 (40 km apart) for the horizontal Reynolds number. The resemblance between these two systems was provided by the fact that both systems had comparable eddy viscosities (1 and 0.5 m^2/s, for Aysen and Ventisquero 3 and 4, respectively) and similar means of the corresponding advective terms. Nevertheless, the origin of the advective contribution is probably different, as in Aysen they were attributed to the effect of the seamount in the center of the bottom profile, while in Ventisquero 3 and 4 they were provided by the contraction of the coastline. The second case was the resemblance between Aysen Fjord and Chacao Channel (400 km apart), which showed moderate similarity in the vertical Reynolds number. In this case, the ratio of large advection over large vertical friction in Chacao, was comparable with relatively small advection over small vertical friction in Aysen, making their dynamics similar. There were also similarities between Chacao and the four transects of Ventisquero Sound for the Richardson number, which indicated similitude in the stabilizing forces. The Richardson number exhibited most similarities from transect to transect.

Similarity of variances between the systems was also explored (Figure 47). It was an expression of the resemblance in the variations of the data into every system. These similarities had a more complete meaning when associated with the similarities of the

Similarity of Variances

R_o

	AYS	CHA	V1	V2	V3	V4
AYS		0.00	0.00	0.00	0.00	0.00
CHA			0.00	0.00	0.00	0.00
V1				0.00	0.00	0.00
V2					0.58	0.02
V3				▨		0.00
V4				░		

Ek_z

	AYS	CHA	V1	V2	V3	V4
AYS		0.00	0.00	0.00	0.00	0.00
CHA			0.00	0.00	0.00	0.00
V1				0.00	0.00	0.49
V2					0.00	0.00
V3						0.00
V4				▨		

Ek_h

	AYS	CHA	V1	V2	V3	V4
AYS		0.00	0.00	0.00	0.00	0.00
CHA			0.00	0.00	0.00	0.00
V1				0.00	0.00	0.00
V2					0.00	0.00
V3						0.00
V4						

Re_z

	AYS	CHA	V1	V2	V3	V4
AYS		0.00	0.00	0.00	0.00	0.00
CHA			0.86	0.00	0.00	0.00
V1		▩		0.00	0.00	0.00
V2					0.00	0.00
V3						0.00
V4						

Re_h

	AYS	CHA	V1	V2	V3	V4
AYS		0.00	0.00	0.00	0.03	0.00
CHA			0.00	0.00	0.00	0.00
V1				0.16	0.00	0.00
V2			▨		0.00	0.00
V3	░					0.00
V4						

Ri

	AYS	CHA	V1	V2	V3	V4
AYS		0.00	0.00	0.90	0.04	0.00
CHA			0.00	0.00	0.00	0.00
V1				0.00	0.08	0.71
V2	▩				0.06	0.00
V3	░		░	░		0.03
V4			▨		░	

▨ 0.01 – 0.1 Sligthly similar ▧ 0.5 – 0.75 Very similar
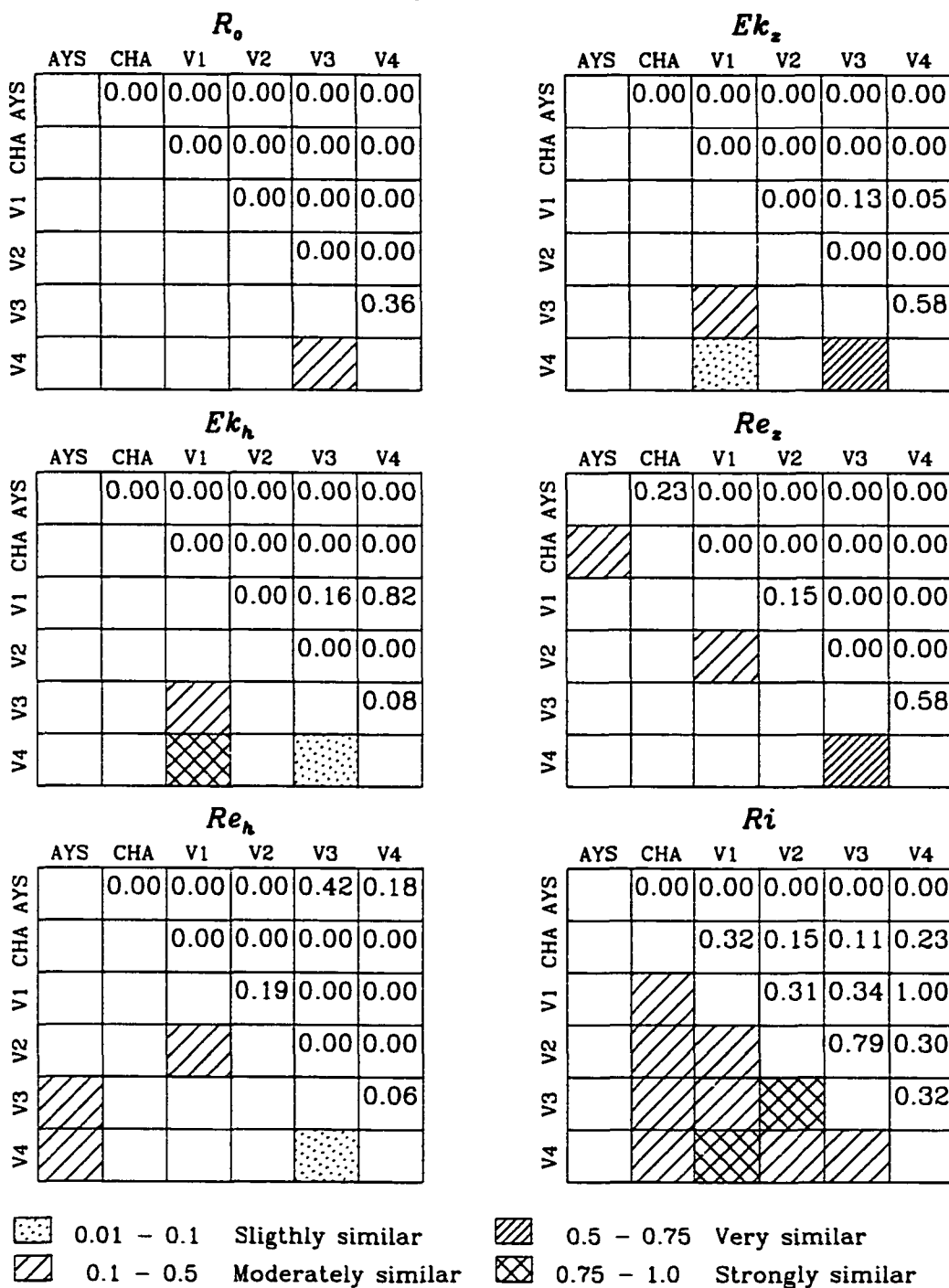▥ 0.1 – 0.5 Moderately similar ▩ 0.75 – 1.0 Strongly similar
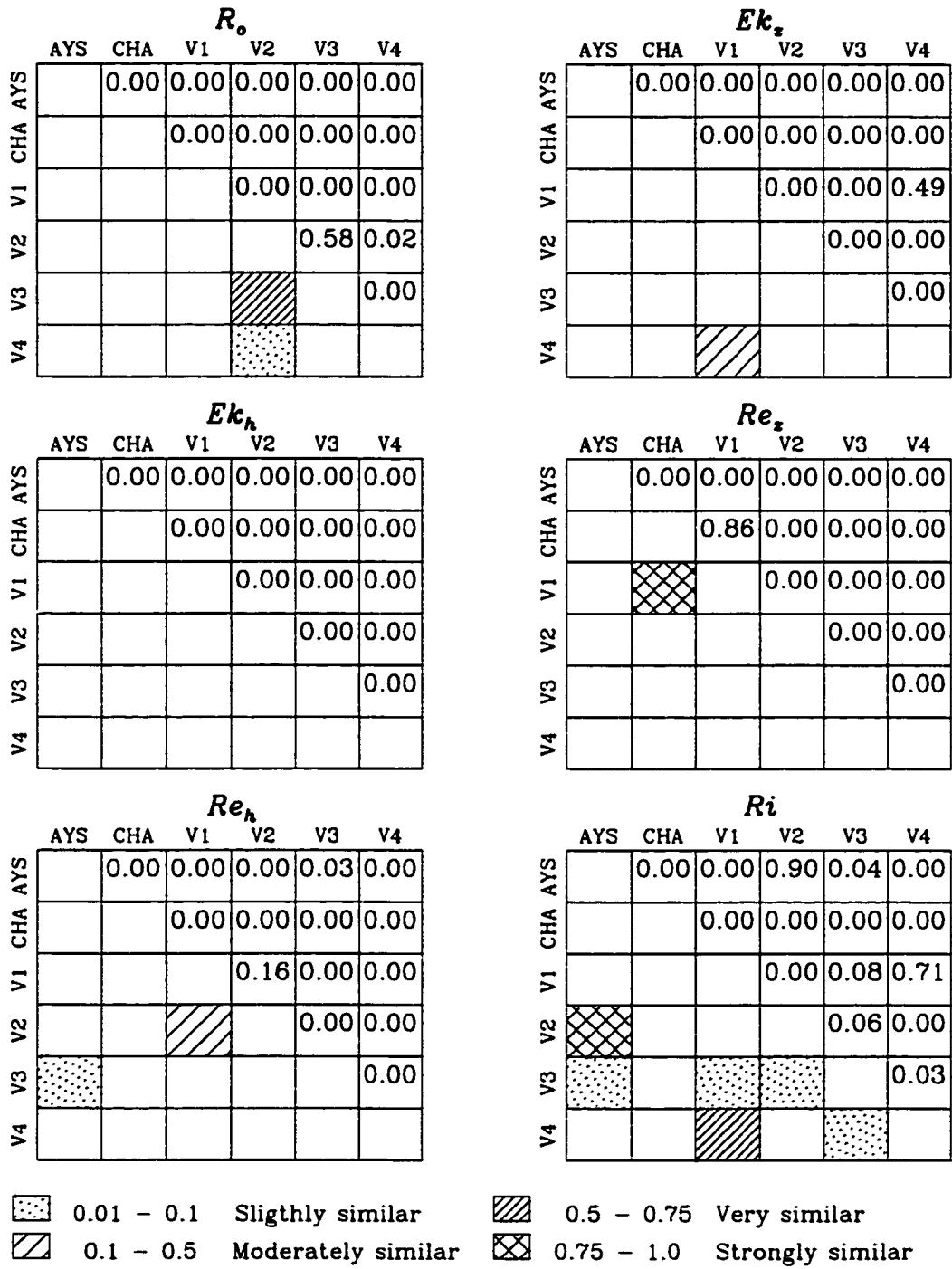
Figure 47. Matrices of similarity of variances using F-student test in the five nondimensional numbers. Values correspond to the probability that variances be equals in the range 0 to 1, 1 indicating equal variances.

means. The paired systems that exhibited similarities between both mean and variances were Ventisquero 1 and Ventisquero 4 (vertical Ekman number and Richardson number), Ventisquero 1 and Ventisquero 2 (horizontal Reynolds number), and Aysen and Ventisquero 3 (horizontal Reynolds number). Similarities were stronger among these systems as they were not only similar in their means, but also in their variances. Again, the Richardson number exhibited the larger number of similarities of variances between transects, making similar Aysen with Ventisqueros 2 and 3.

The tidal range to depth ratio also exhibited similarities between systems (Figure 48). In the case of the means, they were similar between Ventisquero 1 and Ventisquero 2, very close to each other, and between Ventisquero 2 and Ventisquero 3, on both sides of the pass. This is not surprising as these transects have similar tidal ranges and comparable depths. The first pair of transects even showed similarity between the variances. But similarities between Ventisquero 1 and Ventisquero 2 were also observed in their means of the Reynolds number (vertical and horizontal) in Figure 46, which revealed a stronger similitude. Providing a diagnostic about the importance of the nonlinearities, the tidal range to depth ratio, a parameter based on a geometric characteristic, has proven to be a useful tool to confirm dynamic similarities of the classic nondimensional groups.

5.5 Discussion

Dimensionless numbers and geometric parameters

In this subsection I explore the relationship between the dimensionless numbers and some specific geometric parameters.

In terms of the magnitudes of the dimensionless numbers observed in this study,

Tidal range to depth ratio

Similarity of means

	AYS	CHA	V1	V2	V3	V4
AYS		0.00	0.00	0.00	0.00	0.00
CHA			0.00	0.00	0.00	0.00
V1				0.17	0.00	0.00
V2			////		0.01	0.00
V3				:::		0.00
V4						

Similarity of Variances

	AYS	CHA	V1	V2	V3	V4
AYS		0.00	0.43	0.00	0.20	0.00
CHA			0.00	0.00	0.00	0.00
V1	////			0.01	0.08	0.00
V2			:::		0.00	0.00
V3	////		:::			0.08
V4					:::	

::: 0.01 – 0.1 Sligthly similar
/// 0.1 – 0.5 Moderately similar
/// 0.5 – 0.75 Very similar
XX 0.75 – 1.0 Strongly similar

Figure 48. Matrices of similarity of mean and variances of the tidal range to depth ratio, using t-student test and F-student test,respectively. Values correspond to the probability that means or variances be equals in the range 0 to 1, 1 indicating equal means or variances.

Reynolds numbers (Figures 42 and 43) cover a wide range of values ranging from 0 to greater than 100, as in the case of Ventisquero 1. Critical Reynolds numbers for flow passing over an obstacle have been accepted as follows: below $Re=5$ the flow is basically potential flow; steady recirculating eddies exist for a range of Reynolds number between about 5 and 40 [*Van Dyke*, 1982]; and for values over 60 instabilities begin to be observed, leading to vortex shedding [*Pedlosky*, 1987, p. 309, *Dennis and Middleton*, 1994]. In modelling a western boundary layer, *Ierley and Young* [1991] found that the idealized flow becomes unstable between 20 and 100. The idea of an obstacle in the path of the flow applies for the six sections under study (a pinnacle for Chacao, a seamount for Aysen and the contraction for Ventisquero), then the critical values indicated may be taken as a reference for the analysis. Ventisquero 3 and 4 exhibit the highest ranges in Reynolds number, consistent with the presence of residual eddies in that region. These are the only two sections where the means of the Reynolds number were over 5, the limit for recirculations to be generated. Nevertheless, all the cross-sections had a region in their distributions where the flow was unstable (over 40-60).

Rossby number is also an indicator of the tendency of the flow to rotate [*Shearman et al.*, 2000]. Chacao Channel shows higher mean and range values than Ventisquero 4, then we would expect vorticity in both regions (Figure 39). But Chacao has also strong frictional effects, which makes this less suitable for eddy formation in the residual flow. *Chapman and Haidvogel* [1992] investigated the formation of Taylor caps over a seamount. They found that independent of the fractional height of the seamount, Taylor columns cannot be formed if the Rossby number exceeds 0.25. Thus, these authors

provide a good example of an application of a nondimensional number (Rossby number) combined with a geometric parameter (fractional height). Thus, it follows that a combination in the application of Rossby and Reynolds number, plus a particular geometric parameter, seems to be appropriate to understand the generation of residual eddies in any system.

Chapman and Haidvogel [1992] also classify seamounts according to their fractional height as tall seamounts ($\delta > 0.7$), mid-size seamounts ($0.4 < \delta < 0.7$), and short seamounts ($\delta < 0.4$). According to the data presented in table II, Chacao and Aysen sections have tall seamounts and sections 3 and 4 of Ventisquero exhibit short seamount. The aspect ratio is also large in Chacao and Aysen.

So far I have presented evidence that relates the tidal range to depth ratio with dimensionless numbers, the Reynolds number with a topographic obstacle, and the Rossby number with fractional height. Further investigations are required to link the geometric characteristics with the dynamics of two systems that exhibit dynamic similarity.

Dynamics and similarities between means

In this subsection I explore the similarities among the means of the dimensionless numbers and the dynamics of the different systems.

In analyzing dynamic similarities among natural systems, I have been able to obtain evidence for similarity in the means of at least 24 combinations of dimensionless numbers and systems (Figure 46). In terms of the three major regions (Aysen, Chacao and Ventisquero), I found similarities of the means in at least one dimensionless number

between the three possible combinations: Aysen and Chacao, Aysen and Ventisquero, and Chacao and Ventisquero.

Figure 46 shows that in the six dimensionless numbers Ventisquero 3 and 4 exhibited some level of similarity. This is not surprising as both transects were located close to each other, then the forces in competence on both sections were expected to be also similar. More revealing are the similarities that confirm the dominant terms in the momentum balance presented in the three previous sections of this study. In figure 46, a first example is provided by Aysen Fjord, which is not similar to any other system, except in those numbers where the effect of the earth's rotation was not considered (Vertical and horizontal Reynolds number). This confirm the importance of the Coriolis term in the momentum balance in Aysen Fjord early reported in section 2 of this study. Making comparisons among Ventisquero 1 and Ventisquero 3 and 4, three sections representative of Ventisquero Sound, I found that they are similar just in those dimensionless numbers where advection is not considered (Vertical and horizontal Ekman number, and Richardson number), confirming that advection was dominant in Ventisquero Sound. A third example is provided by Chacao Channel, a system where the effects of the earth's rotation were less important and Horizontal friction was the dominant term. It made this system different to other systems in the numbers where Coriolis accelerations and Horizontal friction were involved (Rossby, Ekman and horizontal Reynolds numbers). Instead, Chacao was similar just in one case, with Aysen Fjord, where their corresponding ratios of advection to vertical friction (Vertical Reynolds number) were similar. In this last case, resemblance occurs between a system

dominated by nonlinearities (Chacao) and a system where quasigeostrophy dominates (Aysen).

In summary, the nondimensional analysis demonstrated that, in spite of the geographical characteristics, some similarities can be established between the dynamics of different flows in natural systems. Complete similarity involving the six nondimensional numbers, nevertheless, was just observed between Ventisquero 3 and Ventisquero 4. Further investigations may be addressed to elucidate in more detail the relationships between the dynamic similarities and the geometric characteristic of the sections.

CONCLUSIONS

Current measurements and density profiles obtained in the three regions provided the basis for the analysis of the research questions indicated in section 1. The conclusions have been grouped in five main topics: 1) Subtidal flows, 2) Topographic effects, 3) Transverse dynamics, 4) Tidal current amplitudes and the dynamics, 5) The across and along-fjord dimensions, and 6) Dynamic similarity.

Subtidal flows

The mean flow in Aysen Fjord showed a three layer structure that was consistent with up-fjord wind-induced exchange: a thin (< 8m) weak outflow close to the surface due to river discharge; a layer of inflow (down-wind) underneath attributed to the effect of wind-stress; and a deep compensatory outflow due to the barotropic pressure gradient set up by the wind. In Chacao Channel, the mean flow exhibited weak vertical structure because of strong vertical mixing. The predominant lateral structure consisted of mean outflow (toward the ocean) in the channels, and mean inflow (toward Gulf of Ancud) over the pinnacle and the sides of the channel. This lateral structure pattern was consistent with the mean flow pattern expected from tidal rectification, as robust overtides were generated throughout the transect. In the case of Ventisquero Sound, the mean flow in the northern side of the pass showed a tendency of the flow to rotate anticlockwise with increasing depth. South of the pass, mean surface outflow and mean bottom inflow (at 20 m) developed near the western side of the fjord. Within the pass, the sill represented a boundary between mean inflows and outflows.

Topographic effects

The bank in Aysen Fjord showed salient effects in the across-channel distribution of subtidal flow by shifting the location of strongest near-surface inflow and strongest mid-depth outflow to the channels, by masking the three layer vertical structure, by shifting the flow direction away from the bank, by inducing recirculation at its top, and by causing a bifurcation of the flow below the pycnocline. In Chacao Channel, the pinnacle in the center of the cross-section contributed to flow divergence, vorticity, and enhancement of the variations of the lateral flow $(\partial v/\partial y)$ and lateral shears of the along-channel flow $(\partial u/\partial y)$, respectively. In Ventisquero Sound, the sill/contraction combination induced different patterns of the residual circulation on both sides of the pass, and there were also evidences of increasing of the magnitudes of the tidal flows toward the north, reaching a maximum over the sill, and then decreased northward owing to continuity conservation of volume. Consequently, the bottom topography and coastline geometry were key factors in modifying the circulation and in determining nonlinearities in the flow.

Transverse dynamics

In Aysen Fjord, the effects of the earth rotation were important to maintain the across-fjord momentum balance quasigeostrophic. The wind stress made vertical friction important, and the sidewall effects (from the coast and the bank) made horizontal friction and advection important. In Chacao Channel, the effects of the earth rotation were less important. The balance was dominated by the effect of the pinnacle, which induced strong lateral gradients of the flow $(\partial v/\partial y)$, making nonlinearities dominant in this system. Horizontal friction, a customarily neglected term in estuarine studies, was the dominant

term. The balance was between advection and diffusion. In Ventisquero Sound, the effects of the earth rotation were comparable to vertical and horizontal friction, but the contraction of the coast and the sill made advective accelerations dominant in the momentum balance.

Tidal current amplitudes and the dynamics

The locations of the strongest tidal current amplitudes in the sections were compared with the dominant terms in the corresponding systems. In Ventisquero Sound, where advection was dominant in the momentum balance, the strongest tidal currents concentrated over the shoals. In Chacao Channel, the strongest tidal currents were observed in the channels, as friction was the dominant term. In Aysen Fjord, there were evidences that advective accelerations were important to the momentum balance, as the strongest tidal current amplitudes were located over the narrowest and shallowest region. It follows that only on the basis of the distribution of the tidal current amplitudes, a first diagnostic of the momentum balance in the system can be suggested. Advection would be the dominant term in systems where strongest tidal amplitudes are located over the shoals, and friction be dominant where strongest tidal amplitudes are located in the channels.

The across and along-fjord dimensions

As indicated in the corresponding sections, the magnitudes of the residual flows exhibited proportions of the across to the along-fjord dimension that could not be neglected. In Aysen, they were in a ratio of about 1:5, in Chacao about 1:2, and in Ventisquero about 1:1. Comparable magnitudes in Ventisquero could be attributed to the

dominance of advection. The distributions also showed consistence from one component to the other, as the highest values of the along-fjord distribution were located in the same regions of the highest across-fjord values.

In terms of the magnitudes of the terms in the momentum balance, the across-fjord to along-fjord ratio was in the range of 0.7 to 1 in Aysen Fjord, for the advective and frictional (vertical and horizontal) terms, but it was about 4 for the Coriolis term. In Chacao Channel, they were 0.5, 0.08, 0.25, and 0.1 for the advective, Coriolis, vertical friction and horizontal friction terms, respectively. In Ventisquero Sound, the ratio ranged between 0.7 and 1 for all the terms in the four transects. It follows that the differences between the terms in the two dimensions were notable just in Chacao Channel, a system strongly dominated by nonlinearities. For the other two systems they were comparable. Therefore, magnitudes of the mean flows and terms in the momentum balance were comparable in most of the cases, highlighting the importance of the across-fjord dimension.

Dynamic similarity

In spite of the differences in the momentum balance, across-variability of the subtidal flows, and topographic effects in every case indicated above, it was possible to establish some dynamic similarities among the systems. Evidences of similarity were found in 24 combinations of nondimensional groups, from which three exhibited similarities in their means and variances of different dimensionless groups at the same time. They were Aysen - Ventisquero 3, Ventisquero 1 - Ventisquero 2, and Ventisquero 1 - Ventisquero 4. There were also similarities between distant places, and differences between two

sections that were close to each other. Similarities among the means confirmed in most

cases the dominant terms in the momentum balance previously established. The results

obtained suggest that if the cross-sections exhibited similarity in the six nondimensional

numbers (as in the case of Ventisquero 3 and 4) they could be considered as dynamically

similar. If that occurs, the competing forces are similar between the two systems. But as

indicated in the introduction of Section 5, the geometric similarity is also desirable when

comparing two natural systems. Further investigations are necessary to establish the most

appropriate parameters based in the geometric characteristic of the cross-sections. A list

of these parameters was presented in Table II, and a relationship between some of them

with specific nondimensional numbers was discussed. Therefore, dynamic similarity in

the six dimensionless numbers, along with geometric similarity based in some specific(s)

parameter(s), or in a combination of them, would provide the basis to establish complete

similarity between two natural systems. The three systems studied here were therefore

dynamically different as also established by the estimates of the dynamic terms.

REFERENCES

Bowden, K.H. and P. Hamilton, Some experiments with a numerical model of circulation and mixing in a tidal estuary. *Estuarine Coastal and Shelf Science*, 3, 281-301, 1975.

Cameron W.M. On the transverse forces in a British Columbia Inlet. *Trans. Roy. Soc. Can.* 45, 1-9, 1951.

Csanady, G. T., Lateral momentum flux in boundary currents, *Journal of Physical Oceanography*, 5, 705-717, 1975.

Chapman D. C. and D. Haidvogel, Formation of Taylor caps over a tall isolated seamount in a stratified ocean. *Geophysical and Astrophysical Fluid Dynamics*, 64, 31-65, 1992

Cushman-Roisin B., *Introduction to geophysical fluid dynamics*, Prentice Hall, 320 pp., 1994.

Defant, A., *Physical Oceanography*, *Vol. 2*. Pergamon Press, 598 pp., 1961.

Dennis, T. and J. H. Middleton, Effects of viscosity and bottom friction on recirculating flows. *Journal of Geophysical Research*, 99(C5), 10183-10192, 1994.

Dyer, K. Lateral circulation effects in estuaries, in *Estuaries, Geophysics and the environment*, pp 22-29. National Academy of Siences, Washington, D.C., 1977.

Dyer, K. *Estuaries, a physical introduction*. Ed. John Wiley & Sons, 2nd edition, 195 pp.,1997.

Elliot, A. Observations of the meteorologically induced circulation in the Potomac Estuary. *Estuarine and Coastal Marine Sciences*, 6,285-299, 1978.

Farmer, D.M. The influence of wind on the surface layer of a stratified inlet: Part II. Analysis. *Journal of Physical Oceanography*, 6, 941-952, 1976.

Farmer, D. M. T. R. Osborn. The influence of wind on the surface layer of a stratified inlet: Part I. Observations. *Journal of Physical Oceanography*, 6, 931-940, 1976.

Farmer, D.M. and H. J. Freeland. The physical oceanography of fjords. *Progress in oceanography*, 12, 147-219, 1983.

Farmer, D., E. D'Asaro, M. Trevorrow and G. Dairiki, Three-dimensional structure in a tidal convergence front. *Continental Shelf Research*, 15(13) : 1649-1673, 1995.

Farmer, D.M. and L. Armi. The generation and trapping of solitary waves over topography. *Sience*, 283, 188-190, 1999.

Fierro J., J. Belmar, S. Rosales and J. Blanco. Caracterización del régimen de mareas en canales interiores en las vecindades de la constricción de Meninea. *Resúmenes Ampliados Crucero Cimar-Fiordo 4*. Ed. Comité Oceanográfico Nacional, Chile. 76 pp. 1999.

Freeland H., D. Farmer and C. Levings. *Fjord Oceanography*. Plenum Press. NATO conference series vol. 4, 115 pp., 1980.

Friedrichs, C. and O. Madsen, Nonlinear diffusion of the tidal signal in frictionally dominated embayments. *Journal of Geophysical Research*, 97 (C4): 5637-5650, 1992.

Friedrichs, C. and D. Aubrey, Tidal propagation in strongly convergent channels. *Journal of Geophysical Research*, 99(C2), 3321-3336, 1994.

Gade H.G. Deep water exchanges in a sill fjord: a stochastic process. *Journal of Physical Oceanography* 3,213-219, 1973

Gade H. G. and A. Edwards. Deep-water renewal in fjords. In: *Fjord Oceanography* . Edited by H. Freeland, D. Farmer and C. Levings. NATO conference series vol.4, pp. 453-489. Plenum Press, 1980.

Geyer, W.R., J. Trowbridge, and M. Bowen, The dynamics of a partially mixed estuary. *Journal of Physical Oceanography* 30: 2035-2048, 2000.

Giese, B. S. and D. A. Jay. Modelling tidal energetics of the Columbia River estuary. *Estuarine, Coastal and Shelf Science*, 29, 549-571, 1989.

Gill, A. E., *Atmosphere-Ocean Dynamics*, 622 pp., Academic Press, San Diego, Calif.,1982

Green, M., Spectral estimates of bed shear stress at subcritical Reynolds numbers in a tidal boundary layer. *Journal of Physical Oceanography*, 22, 903-917,1992.

Grubert, J. P., Interfacial mixing in stratified channel flows. *Journal of Hydraulic Engineering*, 115 (7), 887-905, 1989.

Hansen, D. V. and M. Rattray, Jr., Gravitational circulation in straits and estuaries, *Journal of Marine Research*, 23, 104-122, 1965.

Ianniello, J., Tidally induced residual currents in estuaries of constant breadth and depth. *Journal of Marine Research*, 35, 755-786, 1977.

Ianniello, J., Tidally induced residual currents in estuaries of variable breadth and depth. *Journal of Physical Oceanography*, 9, 962-974, 1979.

Ianniello, J., Comments on tidally induced residual currents in estuaries: Dynamics and near bottom flow characteristics. *Journal of Physical Oceanography*, 11, 126-134, 1981.

Ierley, G. R. and W. R. Young, Viscous instabilities in the western boundary layer, *Journal of Physical Oceanography*, 21, 1323-1332, 1991.

Janowitz, G. S. and L. J. Pietrafesa, The effects of alongshore variation in bottom topography on a boundary current - (topographically induce upwelling). *Continental Shelf Research*, 1 (2), 123-141, 1982.

Jones, B. and A.J. Elliot, The parametrization of lateral and bottom friction in depth integrated numerical models. *Journal of Marine Environmental Engineering* 3, 1-13, 1996.

Joyce, T. On in situ "calibration" of shipboard ADCPs. *Journal of Atmopheric and Oceanic Technology*, 6, 169-172, 1989.

Kjerfve, B., Velocity averaging in estuaries characterized by a large tidal range to depth ratio. *Estuarine, Coastal and Shelf Science*, 3, 311-323, 1975.

Kjerfve, B., Bathymetry as an indicator of net circulation in well mixed estuaries. *Limnology and Oceanography*, 23 (4), 816-821, 1978.

Kjerfve, B., L. H. Stevenson, J. A. Proehl, T. Chrzanowski, and W. M. Kitchens, Estimation of material fluxes in an estuarine cross section: A critical analysis of spatial measurement density and errors. *Limnology and Oceanography*, 26 (2), 325-335, 1981.

Klinck, J., J. O'Brien and H. Svendsen. A simple model of fjord and coastal circulation interaction. *Journal of Physical Oceanography*, 11, 1612-1626, 1981.

Krauss, W. and B. Brugge. Wind-produced water exchange between the deep basins of the Baltic Sea. *Journal of Physical Oceanography*, 21, 373-384, 1991.

Kundu, P. K. , *Fluid Dynamics*, Academic Press, 638 pp., 1990

Le Provost, C. and M. Forferino, Tidal Spectroscopy of the English Channel with a numerical model. *Journal of Physical Oceanography*, 15, 1009-1031, 1985.

Li, C. and J. O'Donnell, Tidally driven residual circulation in shallow estuaries with lateral depth variation. *Journal of Geophysical Research*, 102 (C13): 27,915-27,929, 1997.

Li, C., A. Valle-Levinson, K. C. Wong and K. Lwiza, Separating baroclinic flow from tidally induced flow in estuaries. *Journal of Geophysical Research*, 103 (C5), 10,405-10,417, 1998.

Li, C. and A. Valle-Levinson. A two dimensional analytic model for a narrow estuary of arbitrary lateral depth variation: The intratidal motion. *Journal of Geophysical Research*, Vol. 104, C10, 23525-23543., 1999.

LeBlond, P. H., Tides and their interaction with other oceanographic phenomena in shallow water (Review). In: B. B. Parker (ed.), *Tidal Hydrodynamics*. J. Wiley and Sons, New York. P. 357-378, 1991.

Lwiza, K. M. M., D. G. Bowers, and J. H. Simpson. Residual and tidal flow at a tidal mixing front in the North Sea. *Continental Shelf Research*, 11(11), 1379-1395, 1991.

Miles, J. W., On the stability of heterogeneous shear flows. *Journal of Fluid Mechanics*, 10, 496-508, 1961.

Muñoz P., S. Avaria and H. Sievers. Presencia de dinoflagelados tóxicos del género *Dinophysis* en el Seno Aysén, Chile. *Revista de Biología Marina* 27(2):187-212, 1992.

Murty, T. S., F. G. Barber and J. D. Taylor, Role of advective terms in tidally generated residual circulation. *Limnology and Oceanography*, 25 (3), 529-533, 1980.

Niemeyer, H. and P. Cereceda. *Hidrografía*. In: Geografía de Chile. Vol.8. Edited by Instituto Geográfico Militar 320 pp.1984.

Ott, M. W. and C. Garrett, Frictional estuarine flow in Juan de Fuca Strait, with implications for secondary circulation. *Journal of Geophysical Research*, 103 (C8), 15657 - 15666, 1998.

Park, M-J, Transient tidal vorticity in coastal seas. Ph.D Thesis, State University of New York at Stony Brook, NY, 105 pages, 1990.

Parker, B. B., The relative importance of the various nonlinear mechanisms in a wide range of tidal interactions. In: B. B. Parker (ed.), *Tidal Hydrodynamics*. J. Wiley and Sons, New York. P. 237-268, 1991.

Pattiaratchi C., A. James and M. Collins, Island wakes and headland eddies: a comparison between remotely sensed data and laboratory experiments. *Journal of Geophysical Research*, 92 (C1), 783-794, 1986.

Pedlosky, J., *Geophysical Fluid dynamics*. Springer-Verlag, 710 p., 1987

Pond S. and G. Pickard, *Introductory dynamical oceanography*, Butterworth-Heinemann, 2nd Ed., 329 pp., 1998.

Pickard G. Some physical oceanographic features of inlets of Chile. *Journal of the Fisheries Research Board of Canada*, 29, 1077-1106, 1971.

Pickard G. and K. Rodgers. Current measurements in Knight Inlet, British Columbia. *Journal of the Fisheries Research Board of Canada*, 16, 635-678, 1959.

Pingree, R. D. and L. Maddock, The M_4 tide in the English Channel derived form a non-linear numerical model of the M_2 tide. *Deep Sea Research*, 25, 53-63, 1978.

Pingree, R. D. and L. Maddock, The effects of bottom friction and earth's rotation on an island's wake. *Journal of Marine Biological Association U.K.*, 60, 499-508, 1980.

Pritchard, D. W., The dynamic structure of a coastal plain estuary, *Journal of Marine Research*, 15,33-42, 1956.

Redfield, A.C., *Introduction to the tides*. Woods Hole, MA: Marine Science International. 340 p., 1980.

Savenije, H., Analytical expression for tidal damping in alluvial estuaries. *Journal of Hydraulic Engineering*, 124 (6), 615-618, 1998.

Scott, F. C., A numerical study of the interaction of tidal oscillations and non-linearities in an estuary. *Estuarine, Coastal and Shelf Science*, 39, 477-496, 1994.

Seim, H. and M. Gregg, Detailed observations of a naturally occurring shear instability, *Journal of Geophysical Research*, 99(C5), 10049-10073, 1994.

Shearman, R. K., J. A. Barth, J. S. Allen and R. L. Haney, diagnosis of the three-dimensional circulation in mesoscale features with large Rossby number. *Journal of Physical Oceanography*, 30 (11), 2687-2709, 2000.

SHOA, *Nautical Chart 7210*, Canal Chacao. Hydrographic and Oceanographic Service of Chilean Navy (SHOA). 5ᵃ Ed., 1993a.

SHOA. *Nautical chart 8290*, Seno Aysen. Edited by Hydrographic and Oceanographic Service of Chilean Navy (SHOA). 1ᵃ Ed. 1993b.

SHOA, *Nautical Chart 802*, Canales Puyuguapi y Jacaf. Hydrographic and Oceanographic Service of Chilean Navy (SHOA). 1ᵃ Ed., corrected until 1994.

SHOA, Derrotero de la costa de Chile. Pub. 3001. Hydrographic and Oceanographic Service of Chilean Navy (SHOA). 8ᵃ Ed. Updated July 1996. Vol I and II, 1995

Silva N., H. Sievers and R. Prado. Características oceanográficas y una proposición de circulación para algunos canales de la costa de Chile entre 41°20' S y 46°40' S. *Revista de Biología Marina (Valparaíso)*, 30(2), 207-254, 1995.

Silva N., C. Calvete and H. Sievers. Características oceanográficas físicas y químicas de canales australes chilenos entre Puerto Montt y Laguna San Rafael, (Crucero Cimar-Fiordo 1). *Ciencia y Tecnología del Mar*, 20, 23-106, 1997.

Skyllingstad, E.D. and D.W. Denbo, The role of internal gravity waves in the equatorial system, *Journal of Physical Oceanography*, 24(10), 2093-2210, 1994.

Smith, R., Combined effects of buoyancy and tides upon longitudinal dispersion. In: *Bouyancy effects on coastal and estuarine dynamics. Coastal and estuarine studies, AGU series*. Ed. D. Aubrey and C. Friedrichs. Volume 53, 319-329, 1996.

Speer, P. E., D. Aubrey and C. Friedrichs, Nonlinear hydrodynamics of shallow tidal inlet/bay systems. In: B. B. Parker (ed.), *Tidal Hydrodynamics*. J. Wiley and Sons, New York. P. 321-339, 1991.

Sternberg, R. W. Friction factors in tidal channels with differing bed roughness. *Marine Geology*, 6, 243-260, 1968.

Stigebrandt, A. On the effect of barotropic current fluctuations on the two-layer transport capacity of a constriction. *Journal of Physical Oceanography*, 7, 118-122, 1977.

Svendsen, H. Exchange processes above sill level between fjords and coastal water. In: *Fjord oceanography.*, Edited by Freeland, H. J.; Farmer, D. M.; Levings,C. D. Plenum press, p. 355-361, NATO Conf. Ser.4 : Mar. Sci., 1980.

Svendsen, H. and R.Thompson. Wind driven circulation in a fjord. *Journal of Physical Oceanography*, 8,703-712, 1978.

Tee, K. T., Tide-induced residual current, a 2-D nonlinear numerical tidal model. *Journal of Marine Research*, 34: 603-628, 1976.

Tennekes H. and J. L. Lumley, *A first course in turbulence*, MIT Press, 300 pp., 1972

Trump, C.L. and G. Marmorino, Calibrating a gyrocompass using ADCP and DGPS data. *Journal of Atmospheric and Oceanic Technology*, 14 : 211-214, 1997.

Tully, J. P. On structure, entrainment and transport in estuarine embayments. *Journal of Marine Research* 17, 523-535, 1958.

Valle-Levinson, A., and K. M. Lwiza, 1997, Bathymetric influences on the lower Chesapeake Bay hydrography *Journal of Marine Systems*, 12, 221-236, 1997.

Valle-Levinson, A. and L. Atkinson. Spatial gradients in the flow over an estuarine channel. *Estuaries*, 8 (2a), 179-193, 1999.

Valle-Levinson, A., F. Jara, C. Molinet and D. Soto. Observations of intratidal variability of flows over a sill/contraction combination in a Chilean fjord. *Journal of Geophysical Research*, vol . 106 (c4): 7051-7064, 2001a.

Valle-Levinson, A., C. Lascara and W. Boicourt. On the linkages among density, flow, and bathymetry gradients at the entrance to the Chesapeake Bay. Submitted to *Journal of Geophysical Research*, 2001b.

Van Dyke, M., *An album of fluid motion*, Parabolic Press, California, 7th printing, 1998.

Walters, R. and F. Werner, Nonlinear generation of overtides, compound tides, and residuals. In: B. B. Parker (ed.), *Tidal Hydrodynamics*. J. Wiley and Sons, New York. P. 297-320, 1991.

Wells, J.T., Dynamics of coastal fluid muds in low-moderate-, and high-tide-range environments. Proceedings of the Symposium on the Dynamics of Turbid Coastal Environments., *Canadian Journal of Fisheries and Aquatic Science*, vol. 40, pp. 130-142, suppl.1, 1983.

White, W., An oceanic wake in the equatorial undercurrent downstream from the Galapagos Archipelago. *Journal of Physical Oceanography*, 3, 156-161, 1973.

Wolanski E., J. Imberger and M. L. Heron, Island wakes in shallow coastal waters. *Journal of Geophysical Research*, 89 (C6), 10553-10569, 1984.

Wong, K. On the nature of transverse variability in a coastal plain estuary. *Journal of Geophysical Research*, vol 99, c7, 14209-14222, 1994.

VITA

Mario A. Cáceres

PERSONAL DATA

I was born on 13 May 1957 in Santiago, Chile to Mario Cáceres and Luisa Muñoz.
I married María Teresa Sánchez Román on 11 February 1984.

EDUCATION

B.S. from Naval Polytechnical Academy, Av. Jorge Montt s/n, Viña del Mar, Chile (1982).
M.S. in Oceanography from University of Concepción, Av. Chacabuco and E. Larenas, Concepción, Chile (1989).

MEMBERSHIP

American Geophysical Union
Phi-Kappa-Phi